2014

Seismic attribute-assisted structure analysis of the Mackay dome transpressional system, Bighorn basin, southern Montana: Evidence for reservoir compartmentalization

Abigail Lauryn Morris
West Virginia University

Seismic attribute-assisted structure analysis of the Mackay dome transpressional system, Bighorn basin, southern Montana: Evidence for reservoir compartmentalization.

Abigail Lauryn Morris

Thesis submitted
to the Eberly College of Arts and Sciences
at West Virginia University

in partial fulfillment of requirements for the degree of

Master in Science in
Geology

Dengliang Gao, Ph.D., Chair
Timothy Carr, Ph.D.
Jim Templin, M.S.

Department of Geology and Geography

Morgantown, West Virginia
2014

Keywords: Seismic Attributes, 3D Seismic, Bighorn basin, Reservoir compartmentalization, Faults

ABSTRACT

Seismic attribute-assisted structure analysis of the Mackay dome transpressional system, Bighorn basin, southern Montana: Evidence for reservoir compartmentalization.

Abigail Morris

The Mackay dome field is found in southern Montana, in the northern most section of the Bighorn basin. It is characterized by a transpressional positive flower structure that lies above the left lateral Nye-Bowler lineament. The main reservoir is the Cretaceous Greybull sandstone, which is sourced by the lower Permian Phosphoria. The reservoir has been divided into two main compartments, but complicated faulting could divide it into a more segmented reservoir. The seismic attributes most extreme curvature, variance, and ant tracking were applied to the Greybull reservoir in order to delineate bounding and segmenting faults of the reservoir. These attributes identified minor faults that divide the reservoir into five fault block compartments, more than the two previously discovered. Detailed investigation indicates various sets of faults and fractures with distinct mode, orientation, intensity, and scale that should affect the migration potential and sealing capacity of oil and gas. By looking at lateral amplitude changes, the nature of the seal, static or dynamic, can be inferred. Our seismic attribute-assisted structure analysis is instrumental in evaluating reservoir geometry and continuity that can be used to determine whether the compartment is a good target for drilling wells.

Acknowledgements

I would first like to thank my thesis advisor, Dengliang Gao, for his support, encouragement and guidance throughout graduate school. I'd also like to thank my committee member, Dr. Carr for getting me started and keeping me on track.

Thank you to Energy Corporation of America for providing the seismic data and well logs. I would like to give a special thanks to my committee member Jim Templin for his knowledge of the study area, as well as Doug Parker for assistance with setting up the project. I'd also like to thank Pete Sullivan for his interest and support. Lastly I would like to thank the URS for funding (to Dengliang Gao) under: URS 2013 Outstanding NETL/RUA Research Award (400U.OUTSTANDIRD).

Table of Contents

Seismic attribute-assisted structure analysis of the Mackay dome transpressional system, Bighorn basin, southern Montana: Evidence for reservoir compartmentalization

List of Figures

1. Introduction

a. Objectives and Approach

The focus of this study is to better delineate structural grain and geometry within the Mackay dome field, including the spatial and temporal relationship between faults and folds. The Mackay dome field consists of a complex transpressional system, which provides excellent trapping geometries. The intense deformation that created this dome has created numerous faults, some minor, and some that cut across the entire structure. Major faults are important for understanding deformational history, including unravelling the paleostress field. However, mapping minor faults can be extremely important for discovering compartmentalized reservoirs as well as avoiding drilling hazards.

Seismic attribute analysis can assist in detecting major faulting patterns throughout the entire structure, as well as smaller scaled faults within reservoirs, seals, and other areas of interest. Large scale fault mapping will help to determine the structure's deformational history, which can provide information about migration and trapping timing, Smaller scale faults may serve as barriers or leakage pathways within the reservoir, depending on their structural style and displacement.

Compartmentalized reservoirs can be either harmful or beneficial in drilling successful wells. The Mackay dome is broken into smaller compartments, separated by both static and dynamic seals. It is crucial to know the nature of the seals between compartments, so fluid and pressure changes while extracting hydrocarbons can be better predicted. Targeting multiple compartments may seem costly, but identifying their extent and sealing nature can be beneficial

for reducing costs while drilling and increasing production. Two main compartments within the Greybull reservoir have been identified, the western and eastern lobes, but the discovery of additional faults could break this reservoir into more than two lobes. Identifying faults through the use of seismic attribute analysis can allow for better well path planning and increase production.

2. Geologic Setting

a. Structural Setting

The Mackay dome lies on the Nye-Bowler lineament, which is an anticlinal trend in the northern part of the basin that overlies a basement left lateral shear zone (Figure 1a). The Nye-Bowler lineament trends northwest-southeast in this area, and there are known high angle thrust faults previously mapped that trend roughly northeast-southwest, at an oblique angle to the strike-slip displacement. The Nye-Bowler lineament separates the Bighorn basin from the Reed Point syncline to the north, as well as the Crazy Mountains basin (Finn et al., 2010). Successful petroleum prospects along the Nye-Bowler lineament include the Golden dome and Dry Creek gas fields (Finn et al., 2010). The Mackay dome study area is just northeast of the Beartooth Mountains, which formed during the Laramide orogeny as Precambrian-cored uplift (Finn et al., 2010).

b. Tectonic History

i. Laramide Orogeny

The Laramide orogeny occurred during the Late Cretaceous to Early Eocene, approximately 75-35 Ma and was a period of crustal instability in the Western Cordillera of the present day United States (Bird, 1998 and Finn et al., 2010). It involved the reactivation of

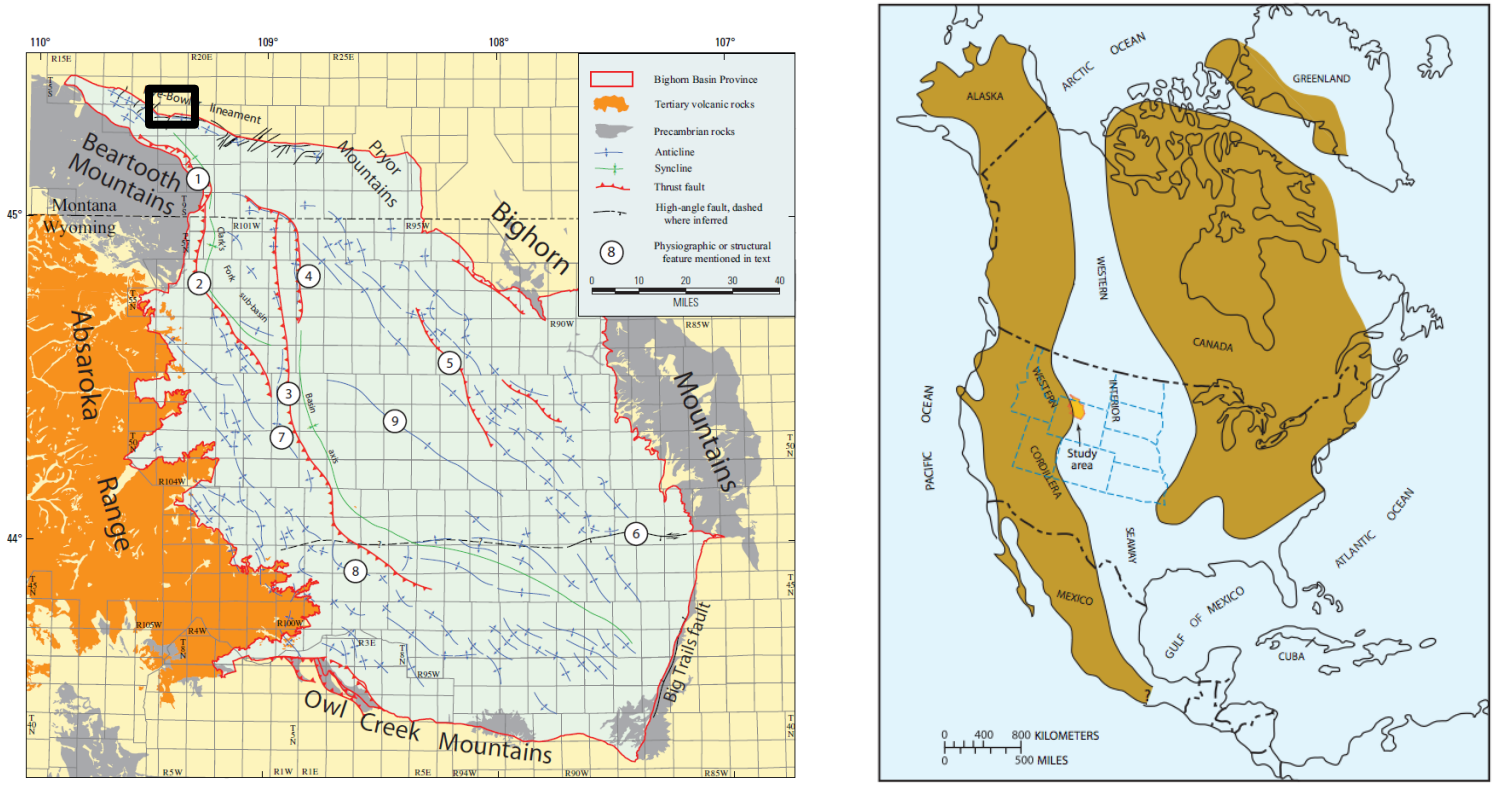

Figure 1. A.) Location of Mackay dome within the Bighorn basin. Bighorn basin extent is shown in blue. (From Finn et al., 2010)

B.) Maximum extent of the Western Interior seaway

PreCambrian normal faults into high angle reverse faults. The Laramide orogeny is associated with thick skinned tectonics, with deformation initiating in the deep basement rock in response to contraction from thrust loading to the West. These basement cored uplifts are responsible for the mountain ranges that surround the basin's perimeter, including the Beartooth range to the northwest, Owl Creek mountains to the south, and Bighorn mountains to the east. The mountains are flanked by steeply dipping, highly deformed Cambrian to Paleocene aged sedimentary rocks (Finn et. al., 2010). These Laramide structures shed a constant supply of sediment into the Bighorn basin.

ii. Sevier Orogeny

The timing of the Sevier orogeny partially coincided with the Laramide orogeny, from about 119 to 50 Ma (Bird, 1998). The Sevier orogeny is associated with thin skinned tectonics, and involved displacement of sedimentary layers along weak bedding planes for tens of kilometers to the east (Bird, 1998). This orogeny had the strongest impact in the center of its wedge, which occurred in southwest Wyoming and northeast Utah. There were three main episodes of thrusting, the Crawford thrusting ca. 89-84 Ma, Absaroka thrusting, ca. 84-75 Ma, and the Hogsback thrusting, ca. 56-50 Ma (Decelles and Mitra, 1995). These thrusts become younger as the wedge propagates eastward. To the north, in southeastern Idaho and Central Wyoming, the Paris, Meade, Absaroka, Darby, and Prospect thrusts occurred as episodic thrusts, again propagating to the East with the advancement of the wedge (Figure 2). The Sevier orogeny can be identified by low angle thrusts that occur along weak bedding planes, and generally trend west-east.

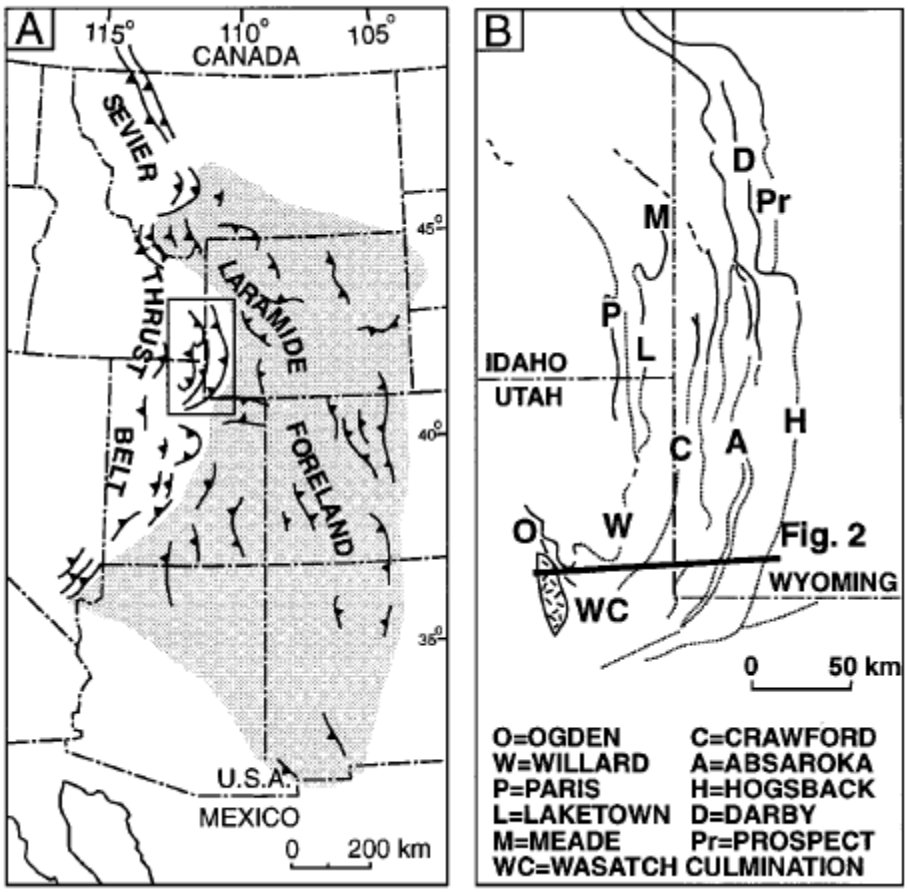

Figure 2. Major Sevier thrusts (from Bird, 1998).

c. Depositional Setting

The Bighorn basin is a foreland basin that developed during the Cretaceous on the eastern margin of the western cordilleran front. It is an elongated north-south trending basin, that was deposited in an epicontental sea, the Western Interior seaway, which stretched from the Gulf of Mexico to the Arctic ocean at its greatest extent (Figure 1b). The uplift and resulting erosion of the western Cordilleran uplands provided a constant shed of sediment into the basin. Changes in sediment supply as well as relative sea level rise and fall are responsible for the deposition of non-marine, marginal marine, and marine deposits. The basin was filled by the end of the

Cretaceous, and the upper moist strata record the onset of the Laramide orogeny (Kauffman, 1977).

d. Stratigraphy

i. Potential Source Rocks

There are three potential source rocks in the stratigraphy of the Northern Bighorn basin, The Mowry shale, Thermopolis shale, and Phosphoria mudrock. The Mowry and Thermopolis shales are present in the logs for this dome, but the deeper Permian Phosphoria shale is not penetrated by wells. Figure 3 shows a standard stratigraphic column for the petroleum system in this study area.

The Mowry shale is the uppermost source rock, deposited in the Upper Cretaceous. It consists of two distinct units, the upper siliceous part, and the lower Shell Creek shale. The lower unit consists of thin, fissile clay-rich beds. It ranges in thickness from 160 to 400 feet. The upper part of the Mowry consists of a dark brown, organic-rich, hard, brittle, silica rich shale due to the presence of tan bentonite beds, with a thickness of 240 to 400 feet. According to Finn (2010), the Mowry shale is intermediate, between a Type-II and Type-II kerogen rock, meaning it can be a source for both oil and gas.

The Thermopolis shale lies beneath the Muddy sandstone and Mowry shale (Figure 3). It is a dark grey to black marine shale or siltstone that is 125 to 230 feet thick. The Thermopolis shale is a Type-III kerogen, providing a gas source to this petroleum system (Finn 2010).

The Phosphoria Formation is Permian aged rock is an organic carbon rich, phosphorus rich mudstone. It is a shallow marine rock that was deposited in an area of upwelling, which

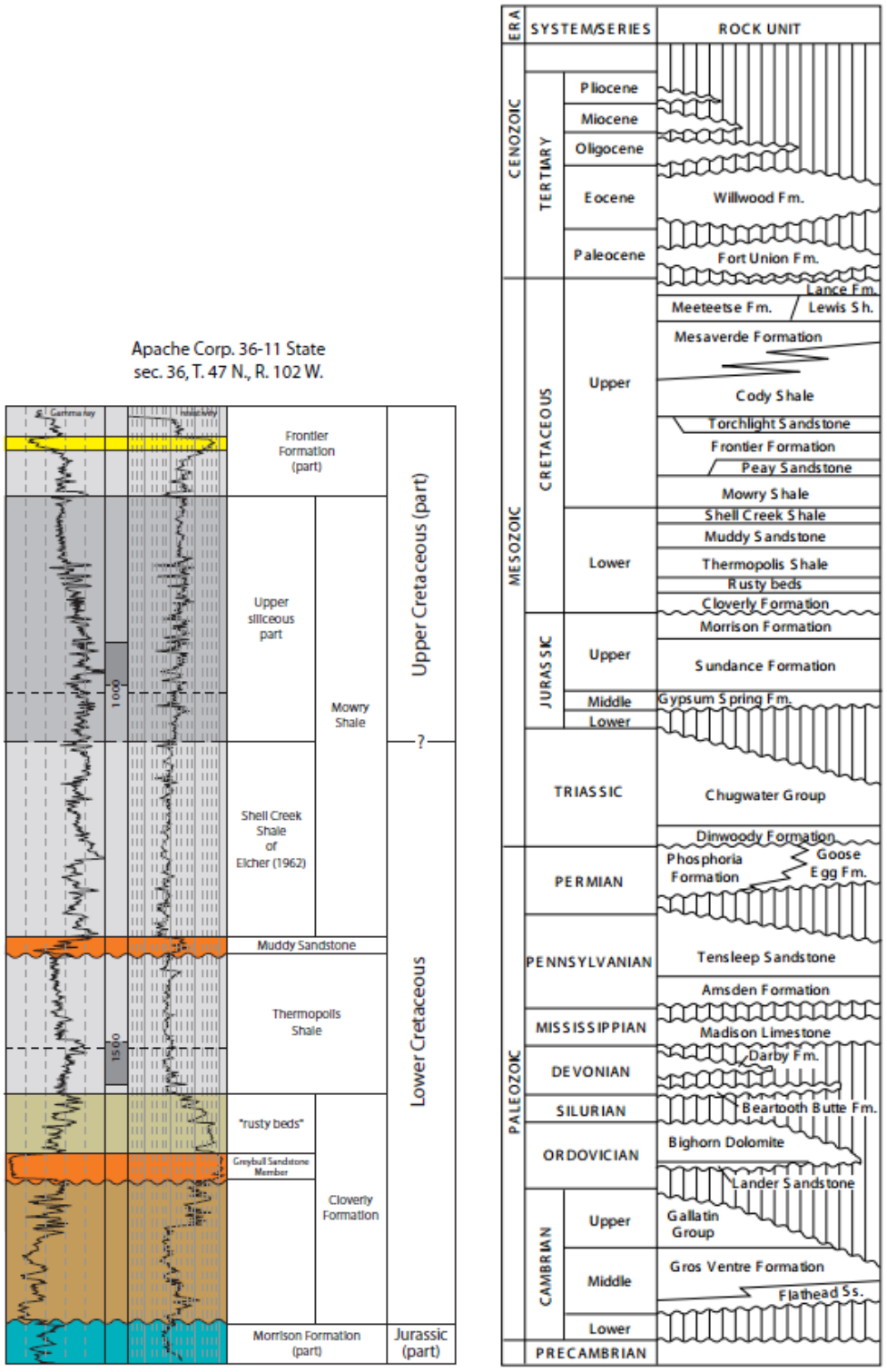

Figure 3. Stratigraphic columns for area of interest. Bottom from Fox and Dolton, 1995.

provided a unique environment for the high accumulation of sapropel on the seafloor. It is believed to be about 2 km deep in Southwestern Montana (Maughan, 1975).

ii. Potential Reservoir Rocks

There are three potential reservoir rocks in the stratigraphy of the Mackay dome field. The Frontier formation is from the Upper Cretaceous and represents the shallowest potential reservoir. The Greybull sandstone acts as the primary reservoir historically, and was deposited in the Lower Cretaceous. Lastly, the Lakota sandstone is the deepest reservoir, and is from the Lower Cretaceous.

The Frontier Formation is a marginal marine unit that consists of shale, siltstone, and sandstone. There are at least six sandstone units within the formation that serve as good reservoirs for the capture of hydrocarbons from the lower Mowry and Thermopolis shales. The Frontier sands are deltaic or shoreface deposits which range in thickness from 450 to 1075 total feet (Finn et al, 2010).

The most productive reservoir in this field, and therefore is the focus of this study is the Greybull sandstone. It sometimes is included in the Cloverly Formation, and overlies the Kootenai Formation (Lopez 2000). The Kootenai Formation consists of floodplain and lacustrine deposits, and is a purple claystone (Finn et al., 2010). The Greybull sandstone is a fluvial sandstone, consisting of fine to medium grained cross-bedded, well rounded quartz (Lopez, 2010). It is incised into the lower Kootenai formation, and varies in thickness from 0 to 200 feet. It is a productive reservoir that is believed to be sourced by the lower Permian Phosphoria shale (Fox and Dolton, 1995).

The deepest potential reservoir is the Lakota Sandstone. It lies beneath he Kootenai formation, and just above the Jurassic Morrison Formation (Figure 3). According to the log data provided, the sandstone can be up to 100 feet thick, similar to the Greybull sandstone. It is also believed to be sourced from the Permian Phosphoria formation.

e. Transpressional Structures

Wrench tectonics have historically provided good traps for the capture of large quantities of oil and gas. Oblique fault block rotation on either side of a fault may cause convergence or divergence along a strike-slip zone (Wilcox et al., 1973). Positive flower structures are an expression of transpressional deformation in the subsurface. Transpressional deformation is a combination of strike slip as well as coaxial strain with shortening perpendicular to the main fault. Transpression may occur along a bend in the main strike-slip fault, but the zone does not consist of pure strike-slip displacement (Fossen, 2010). Reflection seismic imaging has provided a means to study strike slip features in better detail. Often times, strike slip fault are difficult to detect in seismic data not only because they may not show vertical displacement, but also because they are nearly vertical. Strike slip faults can be identified by looking for restraining and releasing bends, where vertical displacement is caused by normal and reverse faulting. These bends are characterized by the widening upward of these normal and reverse faults, creating a flower structure, (Figure 4). The increase of faulting towards the surface in flower structures may be mechanical, as it becomes easier to deform the rock as the load above it lessens (Fossen, 2010).

The Mackay dome is a positive flower structure, caused by the deep, left lateral Nye-Bowler lineament deforming the weaker sedimentary rocks above it. The flower structure can clearly be

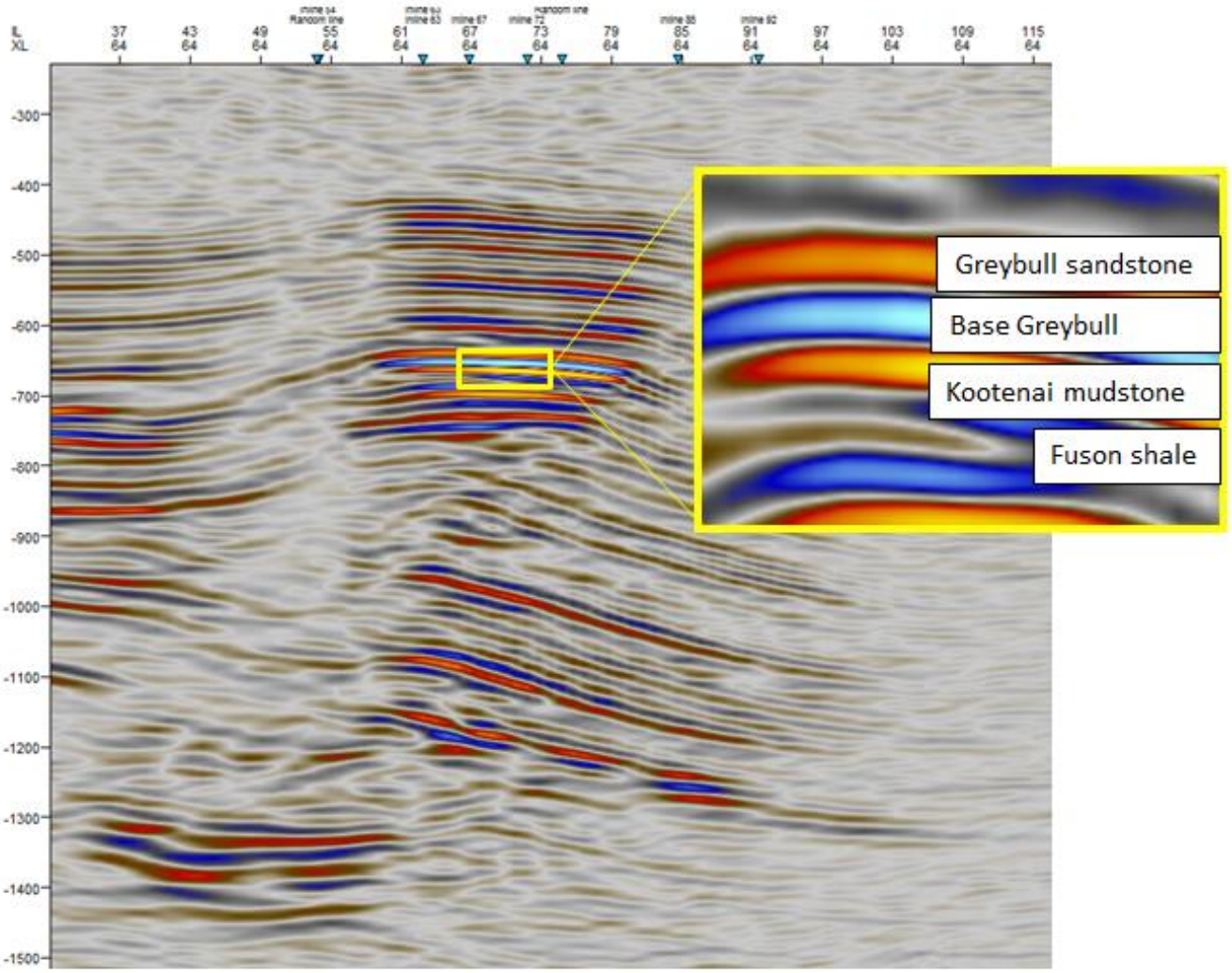

Figure 4. Display of Crossline 64 with area of interest highlighted. The four horizons picked included the Dakota siltstone, Greybull sandstone, Kootenai mudstone, and Fuson shale. Cross section of flower structure shows center of structure thrusted upward by bounding transpressional faults.

seen in cross section in the seismic data collected (Figure 4). It is bound on both sides by areas of low amplitude response, which is where the transpressional faults are located. The center of the flower shows a high amplitude area which represents the reservoir area of interest. This flower structure is caused by transpression along a bend within the main strike slip fault, which causes the rocks to buckle and be pushed upward in order to accommodate the stress from deformation.

f. Reservoir Compartmentalization

The Mackay dome field is a compartmentalized reservoir. It consists of two main lobes, the western and eastern lobes. Because of the complexity of the transpressional system, tilted and rotated fault blocks can provide numerous traps for hydrocarbon accumulation that may or may not be in translation with one another. Reservoir compartments may consist of two different types of boundaries, 'static' seals and 'dynamic' seals. 'Static' seals have the capability of isolating hydrocarbon accumulation throughout geologic time and are completely sealed. 'Dynamic' seals may be temporary or have a very low permeability, and do not hold petroleum deposits forever (Jolley et al., 2010).

Knowing the type of reservoir compartments can help with production. If they are contained by 'dynamic' seals, then draining one compartment can affect the pressure and fluid properties of another compartment. 'Static' seals are ideal because each compartment will act as its own pressurized environment, independent of the drilling in nearby targets. In order to better understand the nature of the seals, faults need to be analyzed for leakage potential. Log analysis for different compartments yielding different results could give clues to whether or not there is

interaction across the entire reservoir. However, determining the nature of these seals is difficult and not always conclusive.

3. Previous Work

An enhanced oil recovery reservoir study was completed in 2009, which outlined the structure of the field as well as plans for increasing hydrocarbon extraction. The study characterized the field into two separate domes, the western and eastern lobes, separated by a major normal fault trending north-northeast. The western lobe contains just heavy oil, and there is a gas cap present in the eastern lobe. Because the reservoir is at about 3700 feet depth, steam injection to enhance heavy oil recovery has been determined unfavorable. This study proposes using gas from the Eastern lobe to lower viscosity of the heavy oil in the Western oil for enhanced recovery.

The presence of the gas cap was discovered from W.R.Mackay well, which produced only oil. This well is 30 feet higher than the oil producing well, Foot Hills 13-13, so the gas cap was found to be less than 30 feet thick, assuming constant porosity and lithology characteristics. However, there is limited well data, particularly on the western side of the western lobe, and eastern side of the eastern lobe. Wells are concentrated towards the center of the dome, so it is uncertain what lithology characteristics are present in the edges of the structure. By analyzing seismic attributes along surfaces within the reservoir, lithologic trends may be inferred.

4. Dataset

Data was provided to West Virginia University by Energy Corporation of America (ECA). A 3D seismic survey was provided, and will be main focus of this study, which is approximately 6 square miles. The inlines trend northwest-southeast and are approximately 3 miles long. The

crosslines trend southwest-northeast and are approximately 2 miles long. They are spaced 82.5 feet away from each other. LAS and raster digital log files were also provided. They contained six curves with gamma ray logs, eleven spontaneous potential (SP) logs, caliper logs, two density logs, four resistivity suite logs, and two sonic logs. There are also tops picked for six of the wells. They reach approximately 4000 feet deep. One of the wells is a horizontal well used to penetrate a greater extent of the reservoir. Figures 5 is a display of the log curves provided.

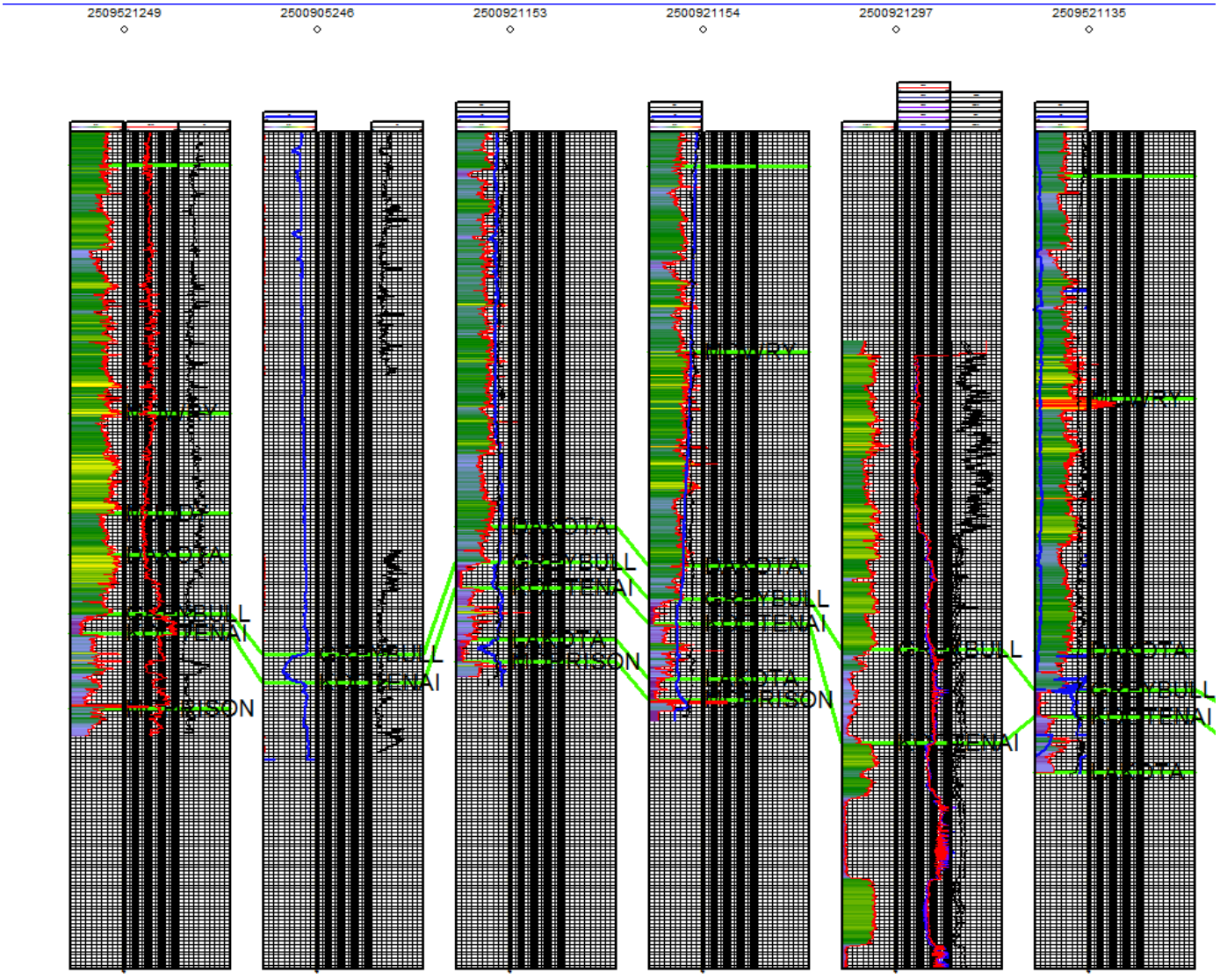

Figure 5. Select well logs with log data displayed. Track one shows gamma ray (shaded) and SP (blue). Track two shows resistivity curves and track three shows density and sonic curves.

Figure 5 shows the six logs with more complete data, including gamma ray, SP, resistivity, density, and sonic logs. Core data was also provided for two wells, including porosity and permeability data, as well as XRF/mineralogy data for one of the cores. Production reports dating back to the 1950s were provided, as well as a recent reservoir study report completed for ECA. The reservoir study report contained background information on the drilling program as well as some volumetric estimates based on reservoir geometry and well data.

The vertical resolution of the seismic data was calculated from the sonic log for the Greybull interval in the well 25096521275, ECA_Federal_#1H. The average velocity was estimated from the log to be about 80 ms/ft, or about 12,500 ft/sec (Figure 6). Tau was found by generating a wavelet in Kingdom SMT for the well Federal#1H, where the tuning time was found to be .0013, or tau/2 (Figure 7). The vertical resolution was then calculated from the following equation:

$$minumum\ resolvable\ thickness = velocity * \frac{\tau}{4} = 12{,}500\ {}^{ft}/_{sec} * .oo65\ sec = 81.25\ feet$$

The minimum resolvable thickness was found to be 81.25 feet. This means that beds thinner than 81.25 cannot be resolved seismically. Because the Greybull is thicker than this in all of the logs, the Greybull surface is seismically accurate and isopach sand thickness maps can be created reliably from seismic data.

5. Methods

a. Seismic Well Tie

Sonic and density logs from the well ECA_Federal_#1-H (API 2509521275) were used to generate a synthetic seismogram using Petrel's Seismic well tie plugin. This allows log data to

be converted into time so that information such as formation tops can be translated into the seismic data time domain. The sonic and density logs, interval velocity, and correlation coefficients as well as results from the seismic well tie are shown in Figure 8. The synthetic seismogram did not match the real seismic data perfectly, so it had to be stretched and shifted.

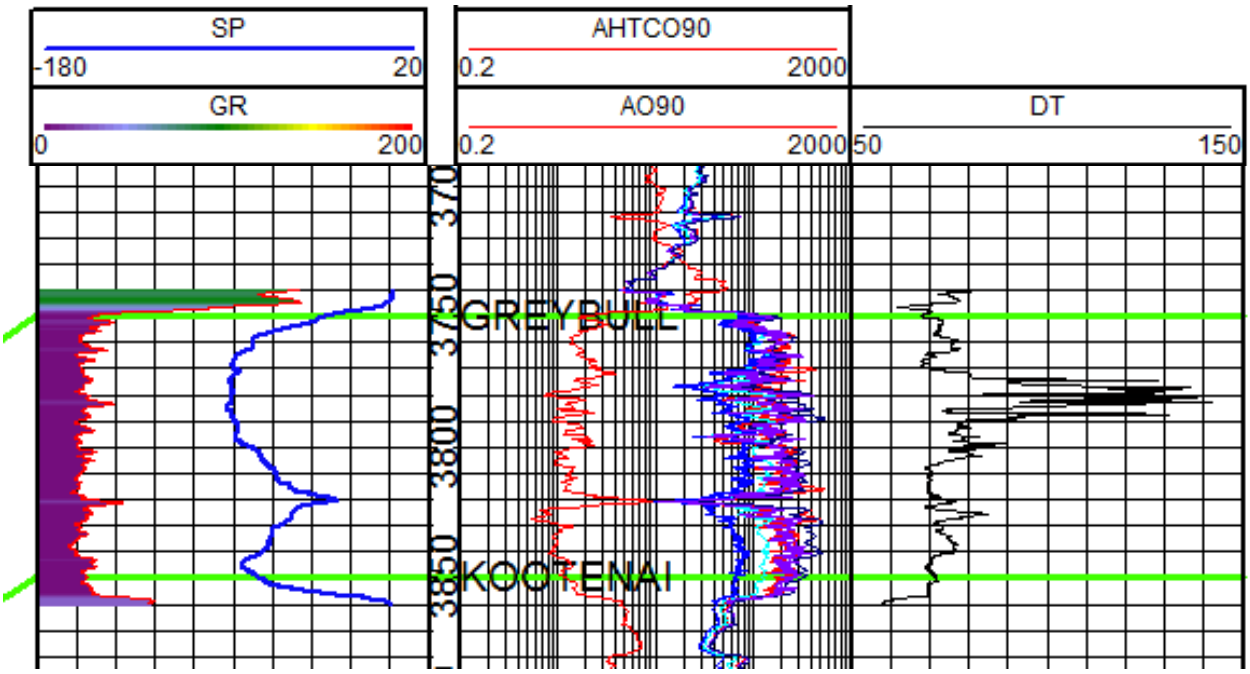

Figure 6. Greybull interval showing DT curve used for determining an average velocity of 80 ft/ms.

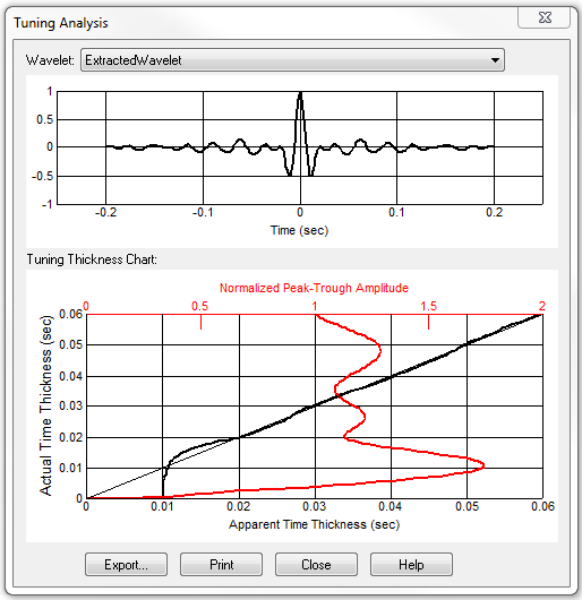

Figure 7. Wavelet displayed with Normalized peak to trough amplitude for determination of Tau.

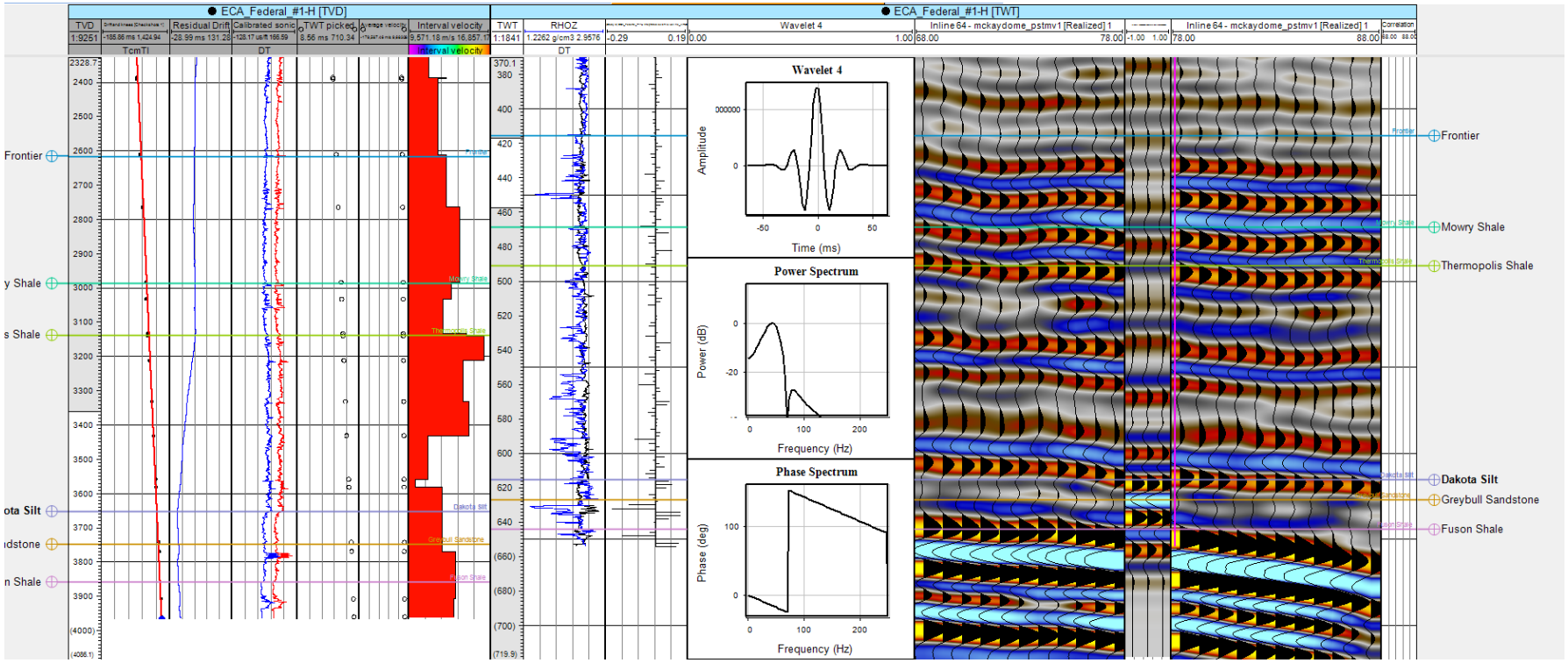

Figure 8. Seismic well tie created in Petrel before shifting. Tops for Frontier sandstone, Mowry shale, Thermopolis shale, Dakota siltstone, Greybull sandstone, and Fuson shale are identified.

b. Seismic Attribute Analysis

Surfaces were mapped for the Greybull sandstone, base of Greybull sandstone, Kootenai mudstone, and Fuson shale (upper member of the Lakota formation). Figure 4 shows an inline of the seismic data with these horizons identified. These horizons were identified using the well seismic tie. Faults were mapped along the seismic volume's inline and crossline. In order to better evaluate the structure of the Mackay dome, a seismic attribute analysis was performed using the structural attributes curvature, variance, and ant tracking. To look at thickness of the reservoir, the spectral decomposition attribute was used and compared to isopach thickness maps as well as well log formation thicknesses.

i. Curvature

Curvature is a seismic attribute that is useful in characterizing fractures in a dataset. Curvature can be described as the lateral change of the radius of curvature, R, along a curve in the data's structure (Chopra and Marfurt, 2010). Curvature can be expressed as positive or negative. Positive curvature has a K-value greater than 0, and represents concave downward structures such as anticlines and domes. Negative curvature has a K value less than 0, and is representative of concave upward structures such as synclines and basins. Completely flat structures have a K-value of zero.

Curvature is scale-dependent, meaning it can detect different sized features based on its evaluation step of Δx and Δy. By altering the radius of curvature, different sized faults or fractures can be detected. Along faults, movement can cause bending from friction or drag along the fault block boundaries. The type of bending will be reflected in the curvature attribute as

positive or negative. Knowing the type of curvature can help to determine the structural style of the faults, whether they are normal or reverse.

For the Mackay dome study area, most extreme curvature is used to delineate major faults, which may control where hydrocarbons accumulate. Fault blocks can act as reservoir compartments for the storage of hydrocarbons, if they are tight sealing faults. Weaker leaking faults may act as potential migration pathways. Curvature can be used to finding compressional faults related to thrusting. For the faults in this study area, most should be compressional due to regional thrusting. However, local extension would be expected in the top of the dome, where there has been local extension due to buckling of reservoir formation. There may also be extensional faults associated with en echelon tension oblique to strike slip faulting or rotation.

ii. Variance

Variance is useful in place of coherency . Variance is the trace by trace difference or variability in space, which is a reflectance of lateral or vertical change in acoustic impedance. Variance is most useful in detecting discontinuities in seismic datasets, such as faults. For this project, variance was used to delineate fault orientation within the structure. It can be compared to curvature results in order to look for consistency between the two fault detection methods.

iii. Ant Tracking

Ant tracking is an attribute that also serves as a fault detector. It is based on the natural tendency for ants to find the most efficient path from their home to their food (Cox, 2007). The ant tracking attribute detects faults in a seismic volume, while avoiding noise from the survey. Ant tracking attributes are applied to a seismic attribute volume, usually chaos or variance, which has been extracted from a structurally smoothed volume. For this project, ant tracking

will be applied to the curvature attribute volume in order to extract possible faults. The ant tracking volume generated was compared to the faults manually interpreted, as well as the curvature and variance attributes.

iv. Spectral Decomposition

Spectral decomposition is a stratigraphic attribute used to detect thickness. It utilizes a discrete Fourier transform function and seismic data to detect bedding thickness based on spectral band frequency size. The frequency, or size of the seismic wavelet is a function of bedding thickness. Spectral decomposition detects which frequency the wavelet fits best with and maps the trends spatially (Partyka et al., 1999). Because the Greybull sandstone is a fluvially derived reservoir, spectral decomposition can be used to detect facies changes. Channel sands and overbank deposits will have different spectral frequencies, and classifying these facies can help with targeting ideal sands for hydrocarbon accumulation.

c. Thickness Map

An isopach thickness map of the Greybull sandstone, as well as a total thickness map, was created in order to look at changes in the reservoir. This can help to identify thicker areas of rock with possibly more hydrocarbon reserve, net-sand thickness, or gross sand thickness. Faults will be overlain with the thickness map to see if the reservoir thickening is structurally or stratigraphically controlled. The results from this map will also be compared to the spectral decomposition maps and log data.

d. Log Analysis

In order to better understand the stratigraphy and hydrocarbon system of the Mackay dome study area, logs were evaluated to better understand lateral changes within the Greybull interval. Pickett plots were created for wells with sufficient log curves. This was used to estimate water and hydrocarbon saturation in the Greybull reservoir. These values were compared to production data to determine if there was still significant hydrocarbon in place. This could help determine whether different compartments in the reservoir are in translation with one another. Knowing the relationship of one compartment with its neighbor can help with identifying the nature of the seals between them.

In addition to Pickett plots, the resistivity of the water in the rock was determined. This is useful in determining a better depositional history of the reservoir formation. In order to get a better spatial understanding of the log analysis data, a map with the wells and significant faults was created with production data and calculated values. This map provides a good summary of the petroleum system and a means for easy comparison of different regions of the reservoir.

In order to look at water saturation within the reservoir in more detail, Archie's water saturation equation was applied and was calculated for the length of the log. In order to identify good pay within the reservoir interval, bulk volume water was also calculated. Bulk volume water can be calculated using the Sw log from Archie's equation and average porosity (φ) in the following relationship:

$$BVW = Sw * \varphi$$

The Bulk volume water values were plotted on the log in the same track as average decimal porosity. Wherever water saturation is 100%, there is no oil or gas in the rock, and the porosity curve and BVW curve will be the same. However, when water saturation is less than 100%, it will make the BVW curve be less than the porosity curve.

6. Results and Interpretations

a. Surface Maps

Because the focus of this project is on the Greybull sandstone reservoir, four surfaces were extracted near the reservoir, including the top and base of Greybull, the Kootenai formation, and the Fuson shale, and their surface structure maps are shown in figures 9, 10, 11, and 12, respectively. They are nearly identical with little variation in structure. Structural contours are displayed to show the good trapping geometry of the dome. There are two structural highs in this dome, the western and eastern lobes, shown by closed contours.

The amplitude pattern was also extracted along each of these surfaces from the seismic volume. The Greybull (Figure 13) and Kootenai (Figure 15) are high positive amplitude surfaces. The base of the Greybull (Figure 14) and the Fuson shale (Figure 16) are high negative amplitude surfaces. This section of the stratigraphy is represented by very high amplitude anomalies or bright spots, which are typically indicative of hydrocarbon presence, known as a direct hydrocarbon indicator (DHI). Major voids in these amplitude maps may be due to the presence of faults that lead to weak seismic response as linear fractures in the seismic data.

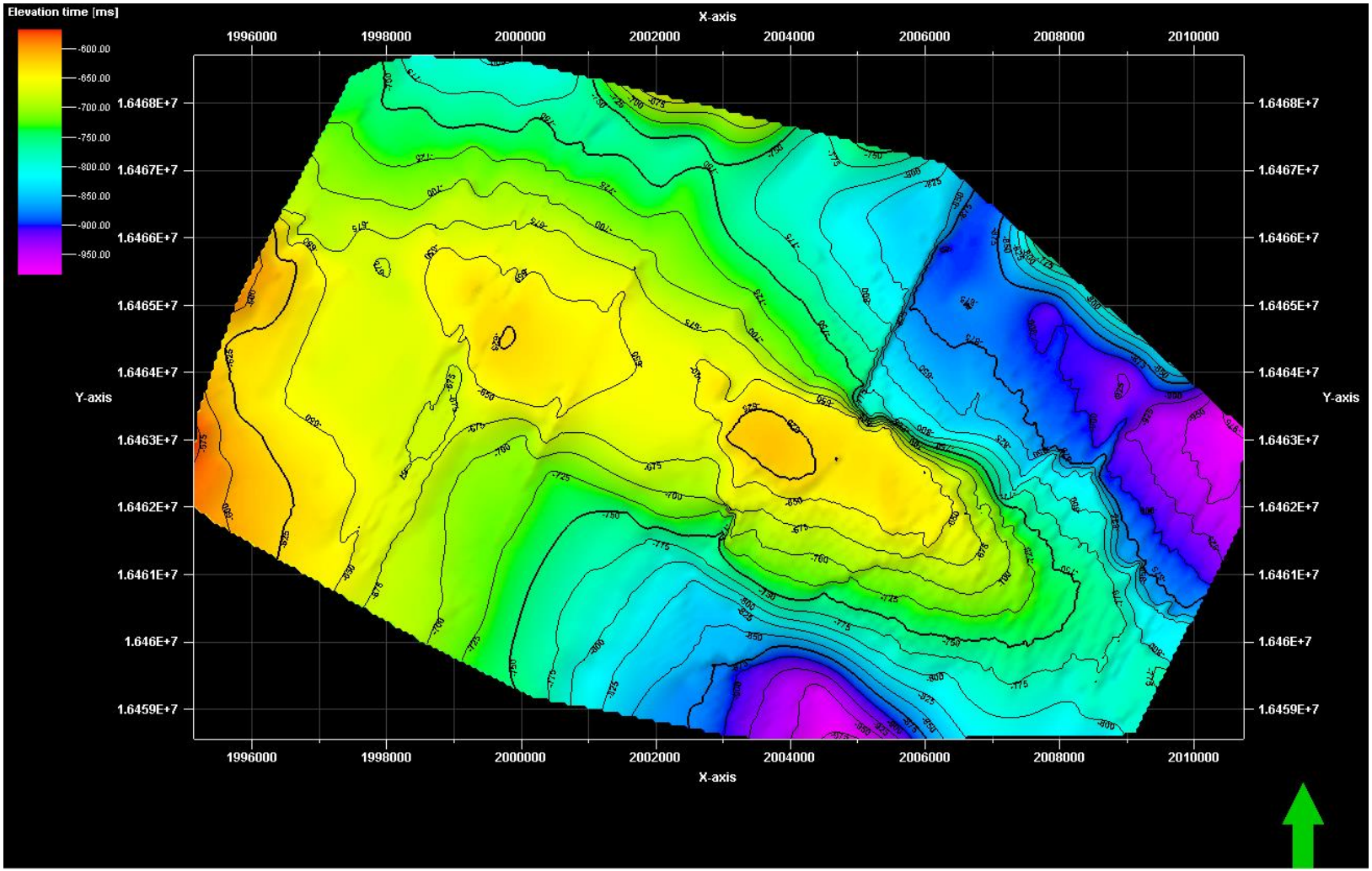

Figure 9. Greybull structure map.

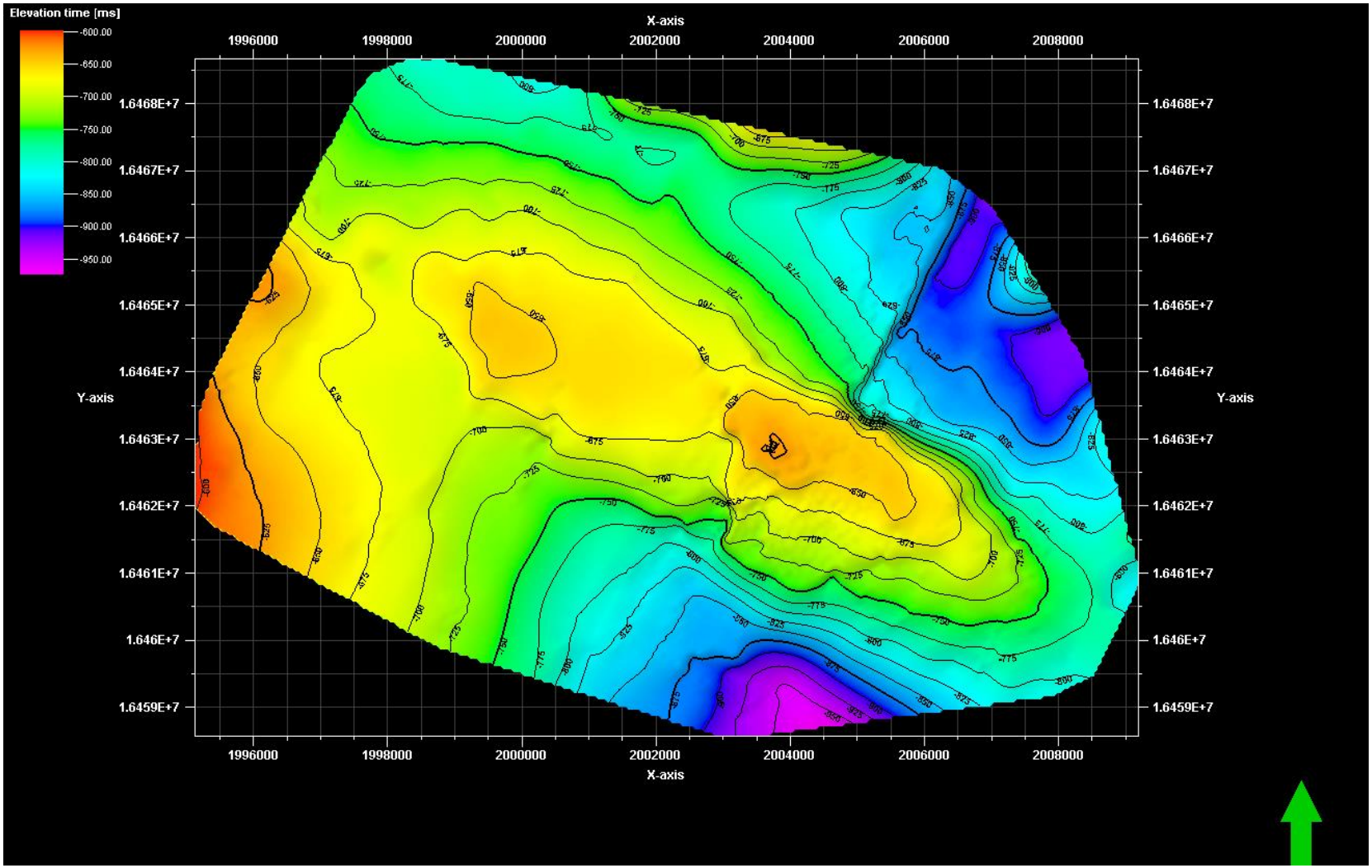

Figure 10. Base of Greybull structure map.

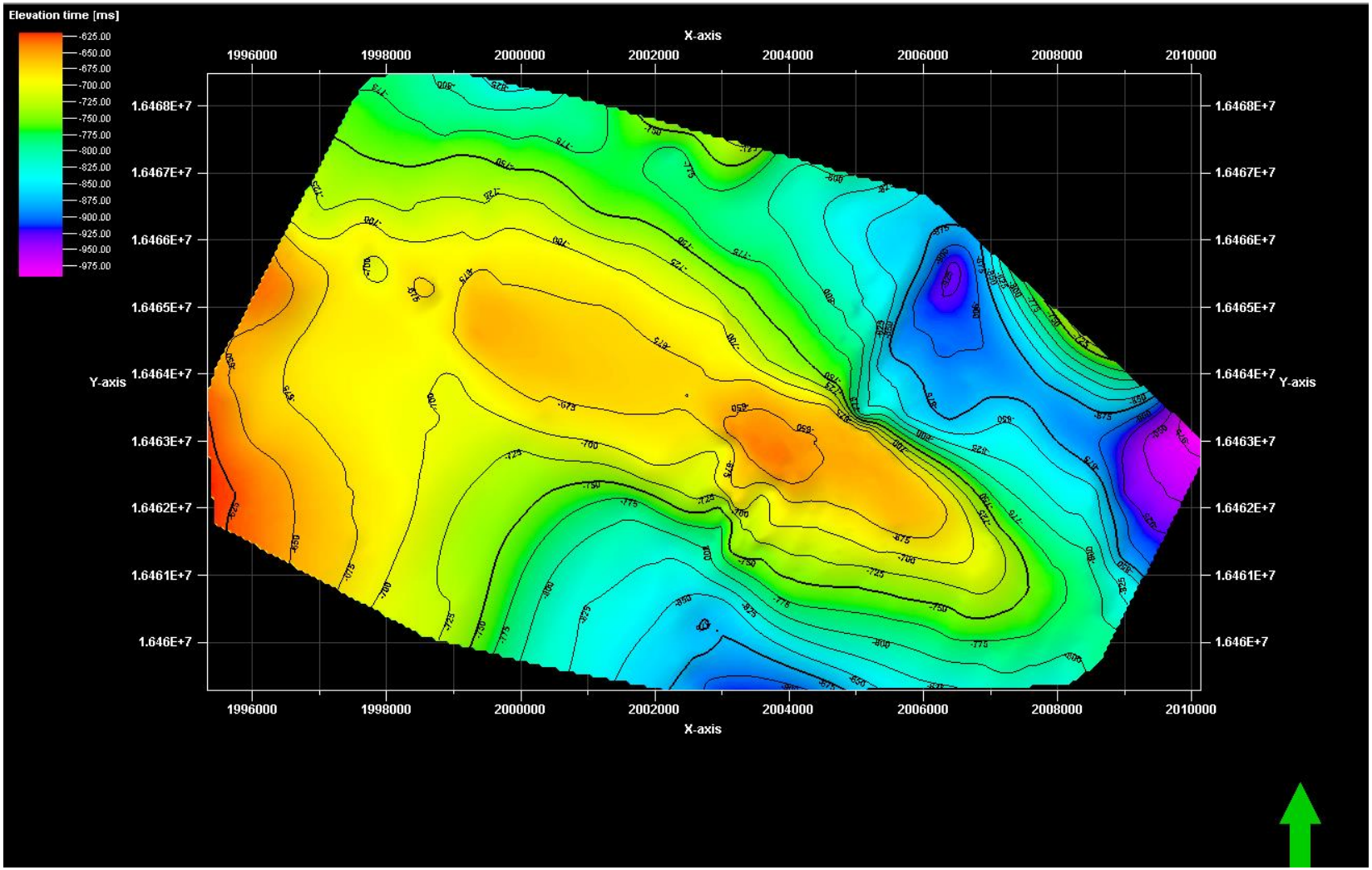

Figure 11. Kootenai structure map.

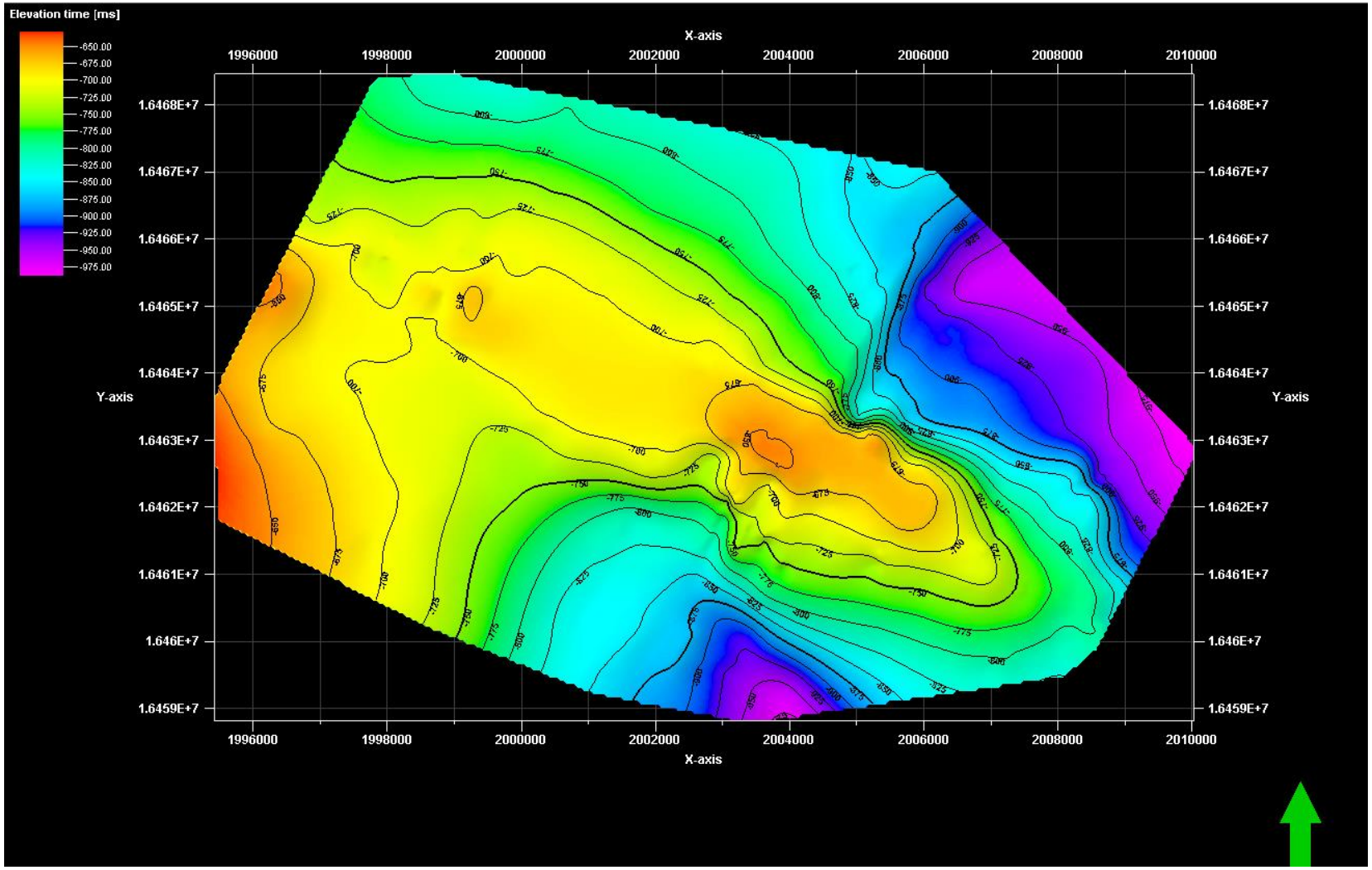

Figure 12. Fuson structure map.

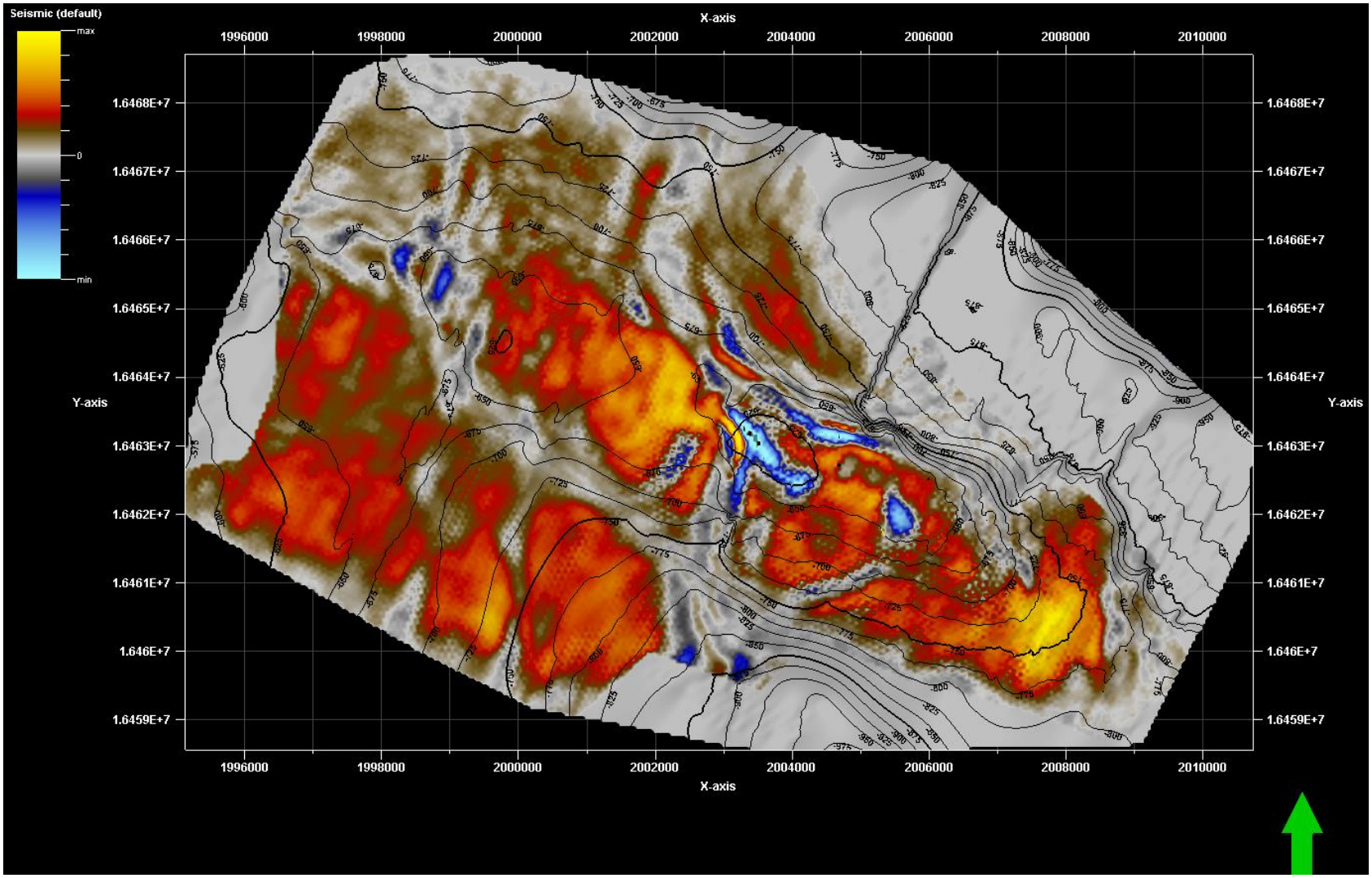

Figure 13. Greybull sandstone amplitude map.

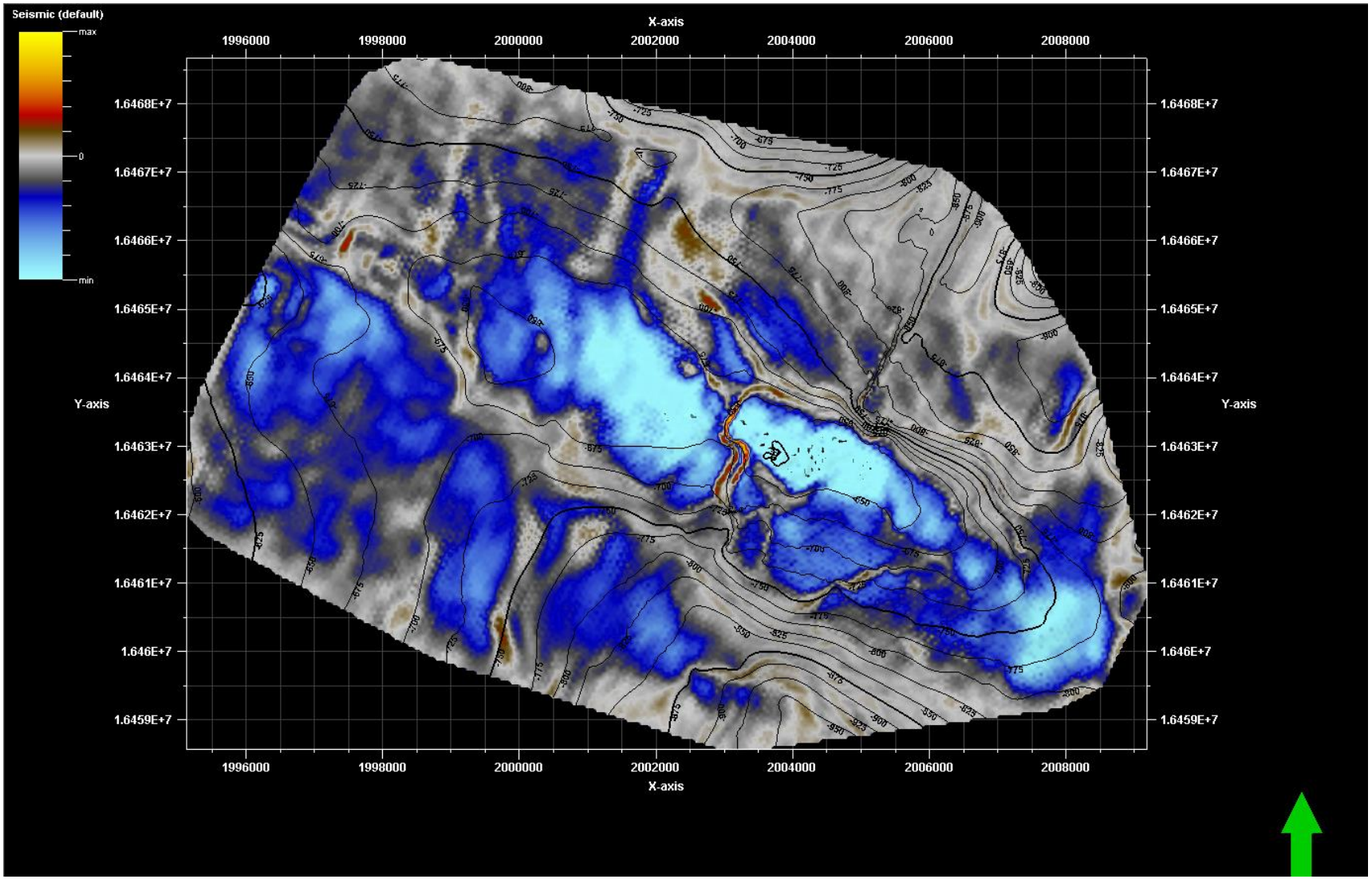

Figure 14. Base of Greybull amplitude map.

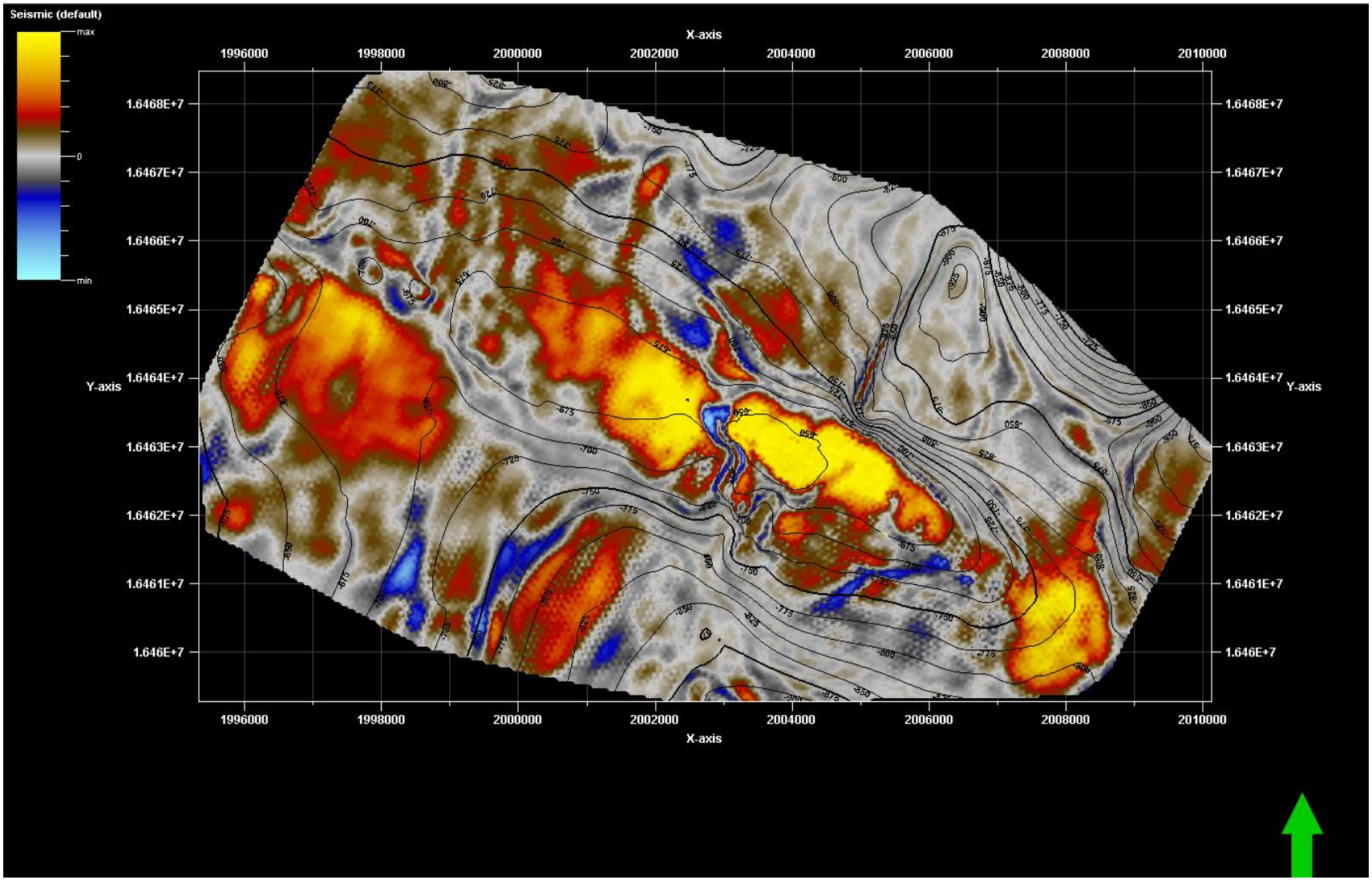

Figure 15. Kootenai mudstone amplitude map.

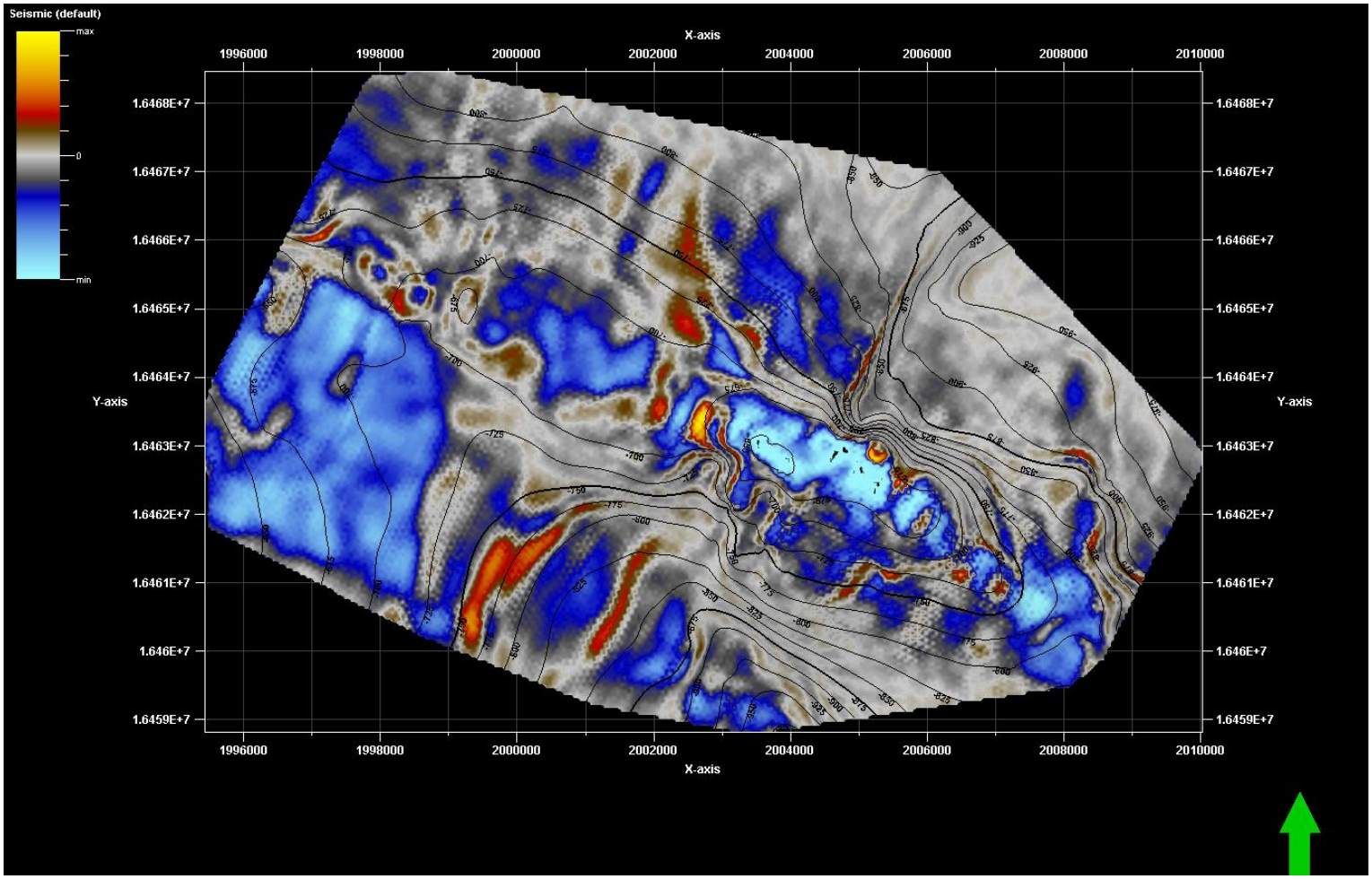

Figure 16. Fuson shale amplitude map.

a. Along Strike Variation in Structure

The Mackay dome changes its orientation along strike. Figure 17 shows a map view of four cross sections taken perpendicular to strike. The flanks of the flower structure steepen towards the center of the dome (cross sections 2 and 3). This shows that deformation is greatest towards the center of the structure, and more faults and fractures should be expected there. These fractures could be subseismic, and may not be seen in this dataset. However, the addition of fractures into the hydrocarbon system can either assist or hinder the total petroleum system. The fractures may increase permeability within the sandstone reservoir, allowing for the accumulation of a greater volume of hydrocarbons. However, if these fractures puncture the overlying seal, the Dakota siltstone, then it could be a potential migration pathway out of the reservoir. Lastly, if these fractures have been mineralized and sealed, it could actually reduce permeability and porosity, making it a poor reservoir.

Figure 17 also shows that the dip of the beds in this structure increase towards shallower depths. The flower structure is steepest at the top, and flattens with depth. This suggests that there is a potential detachment horizon along the base of the structure, so that strain does not build up and deform the overlying layers. Looking at the seismic data, a detachment horizon cannot be identified easily due to lower quality with depth and the lack of wells that penetrate past the Greybull petroleum system. This shallow, thin skinned sedimentary detachment is characteristic of the Sevier orogeny. However, it is known that the Nye Bowler lineament is a basement involved strike-slip fault that developed from the Laramide orogeny. This particular flower structure does not penetrate the basement rock and it is unknown how this structure connects with the main strike-slip fault of the Nye-Bowler lineament.

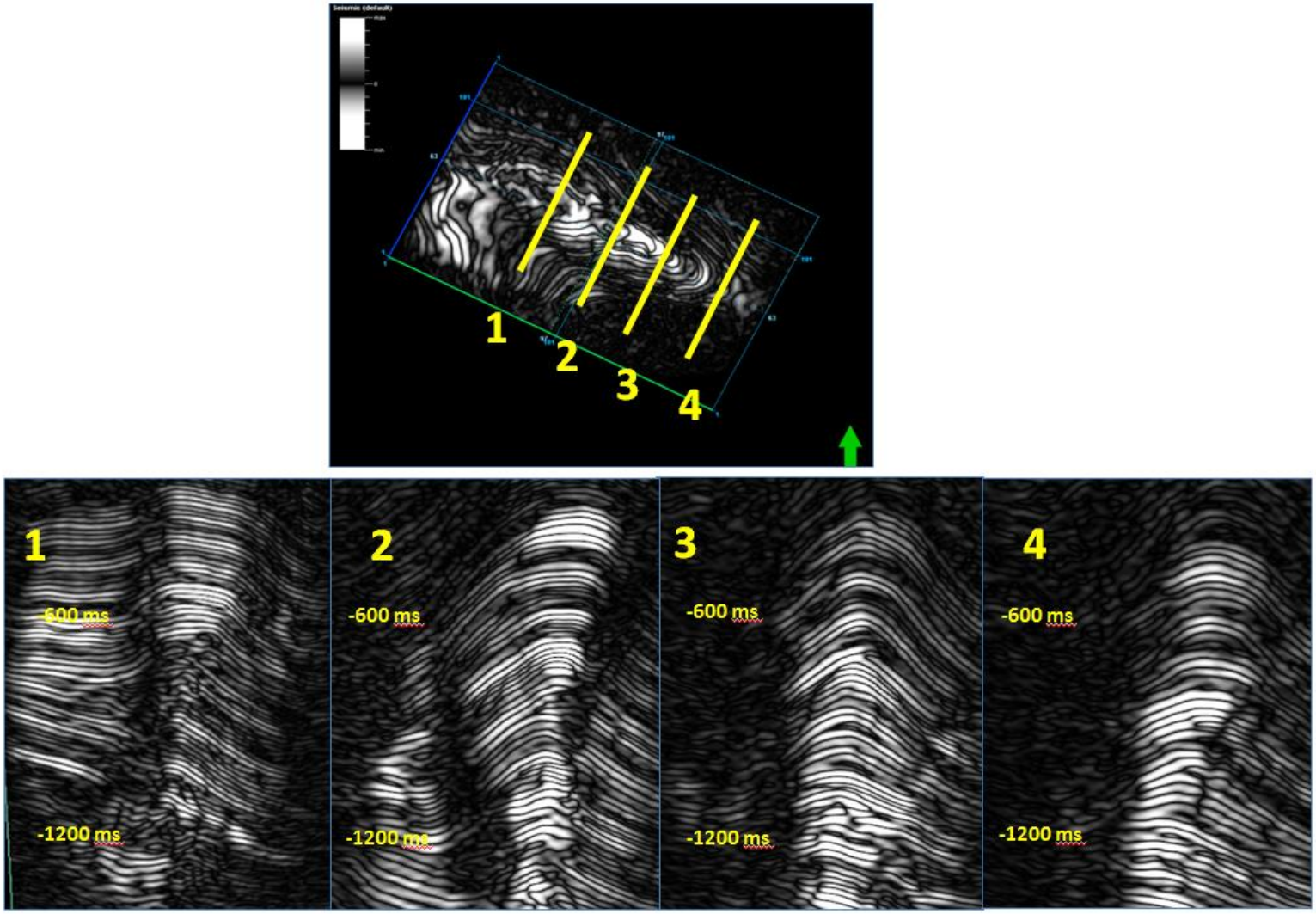

Figure 17. Cross sections 1-4 taken perpendicular to strike to show along strike variation in structure.

b. Fault Sets

From preliminary observations in time slices through the seismic data, three main fault sets were identified, Set 1, Set 2, and major strike slip faults. Figure 18 shows these three sets identified at a time slice at 538 ms. Set 1 consists of north-northwest trending faults, and set 2 consists of northeast trending faults. The major strike slip faults trend northwest, but are not completely parallel. Figure 18b shows this same time slice, with the curvature volume rather than amplitude. The same fault sets are clearly delineated in this attribute slice. There is an additional set 1 fault detected, and the boundary of these faults is much clearer.

An arbitrary cross section, roughly perpendicular to fault set 1 is shown in Figure 19. This image gives a better visualization of the true, rather than apparent, expression of structure geometry. The image has a vertical exaggeration of 10 to see the fault displacement and style more clearly. This cross section shows that the north-northwest fault set 1 consists of compressional features that dip to the west, which cause shortening in the roughly west-east direction. This shortening has caused certain fault blocks to thrust upwards over other blocks.

Figure 20 shows another arbitrary cross section drawn approximately perpendicular to Fault set 2. The center of this structure does show a structural high, with northwest and southeast sides dipping downward. Again, the deformation dominated by southeast dipping compressional faults, which are caused by northeast-southwest compression. Faulting style changes slightly in the Muddy sandstone interval, right above the Dakota siltstone reflector (Figure 20). This surface is very irregular, and may serve as an accommodation or detachment horizon for the upper and lower reservoir sections, the Frontier and Greybull sandstones, respectively.

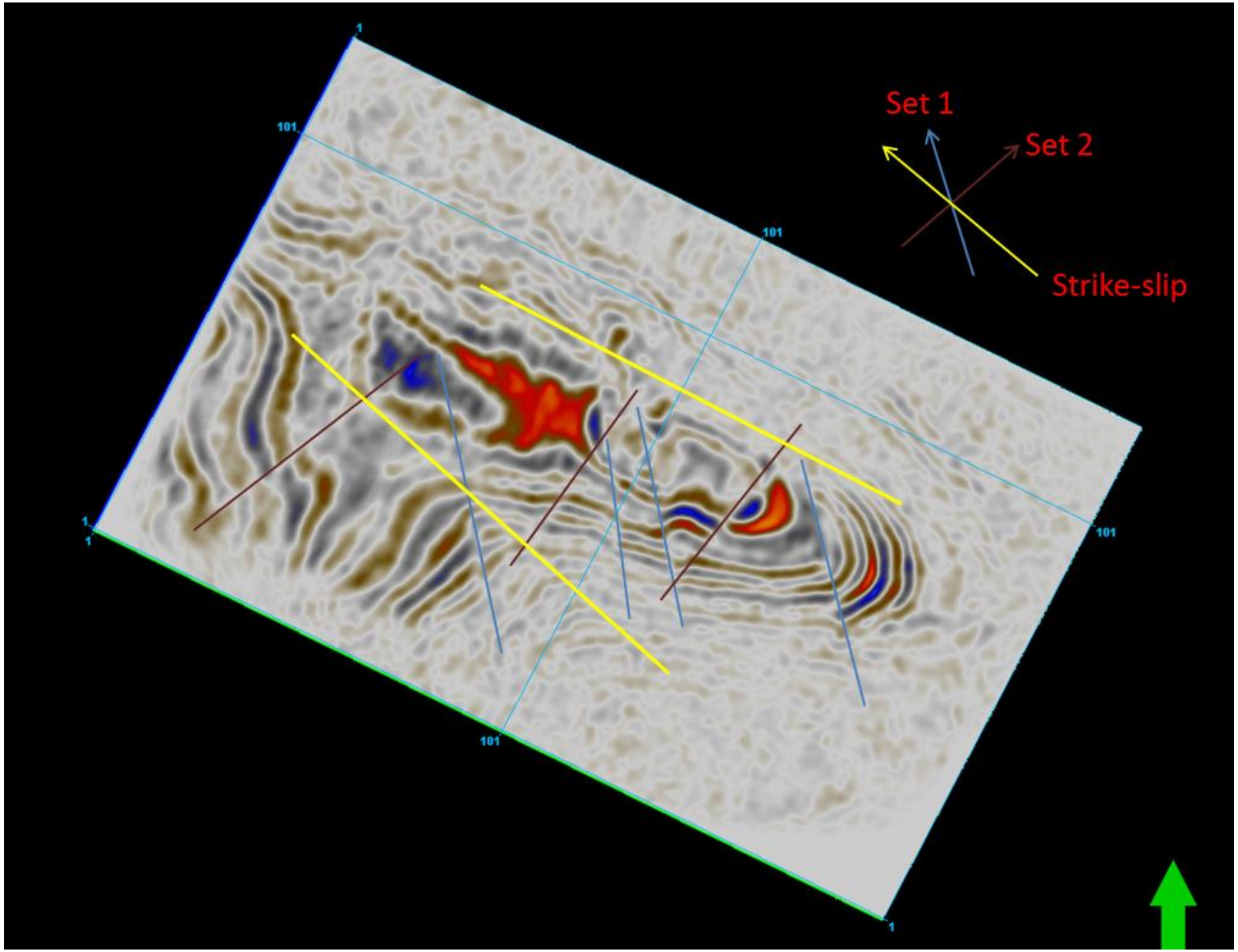

Figure 18a. Amplitude time slice at 538 ms showing three major fault sets.

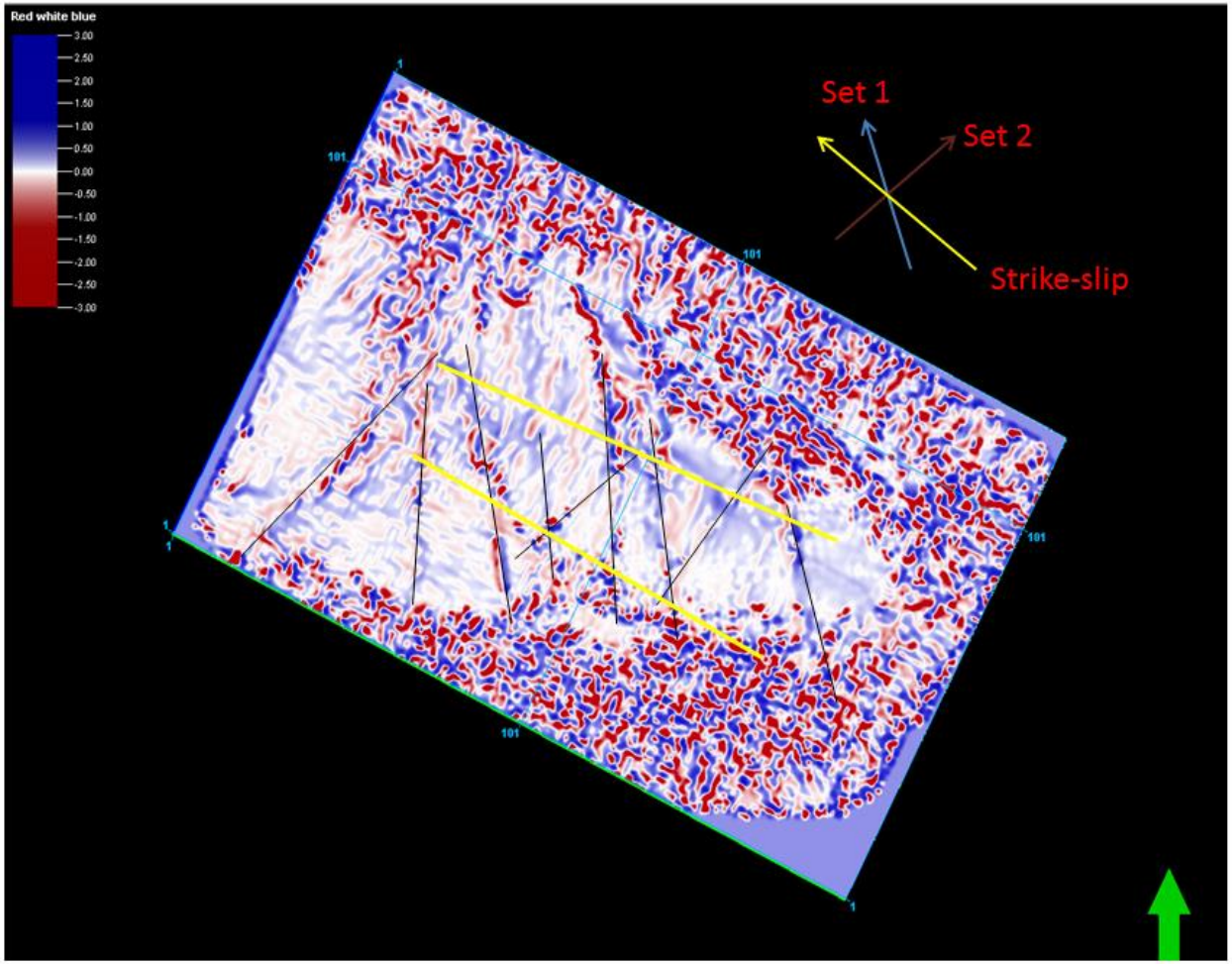

Figure 18b. Same time slice at 538 ms, with curvature attribute.

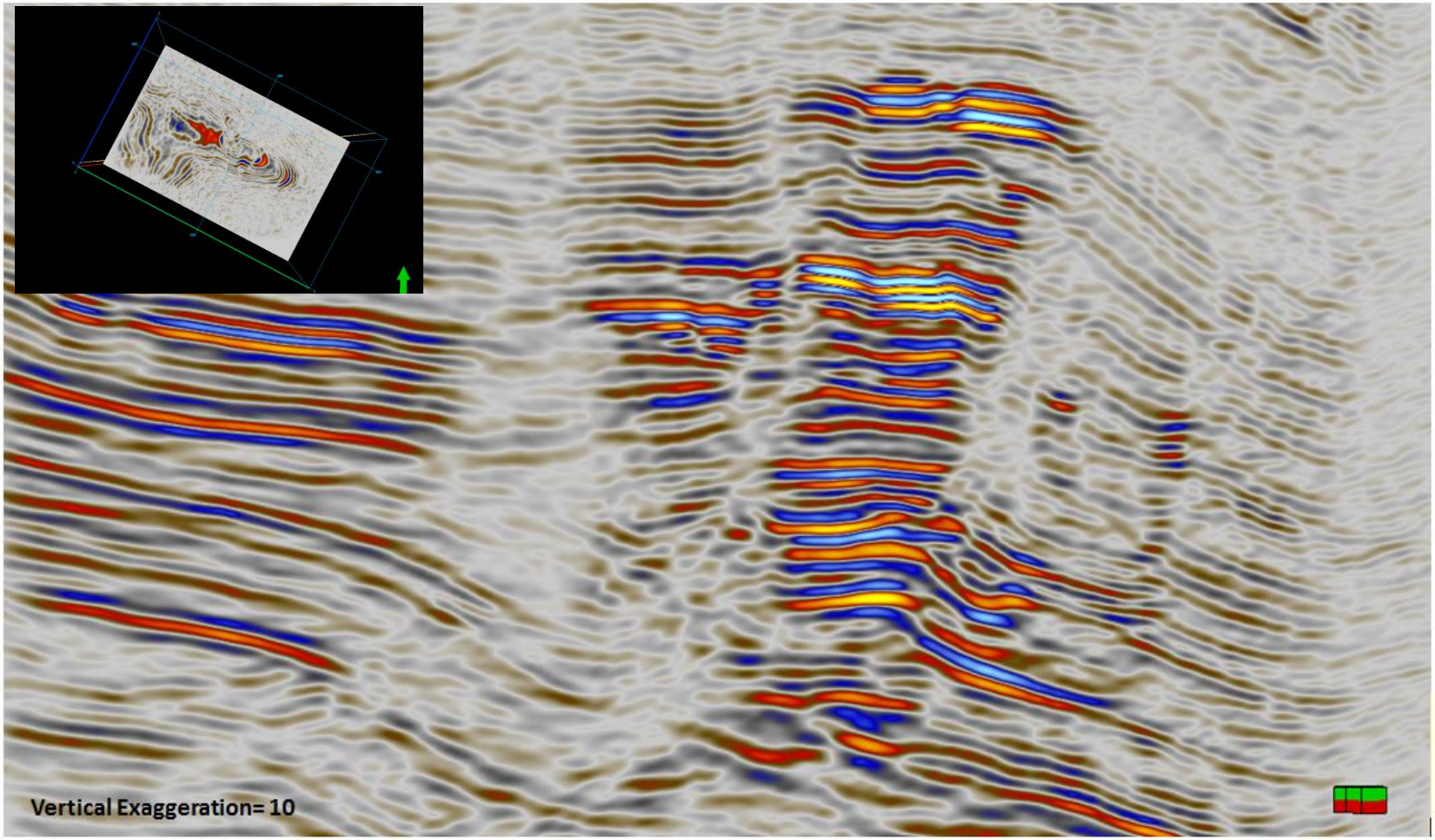

Figure 19. Cross section perpendicular to Joint set 1.

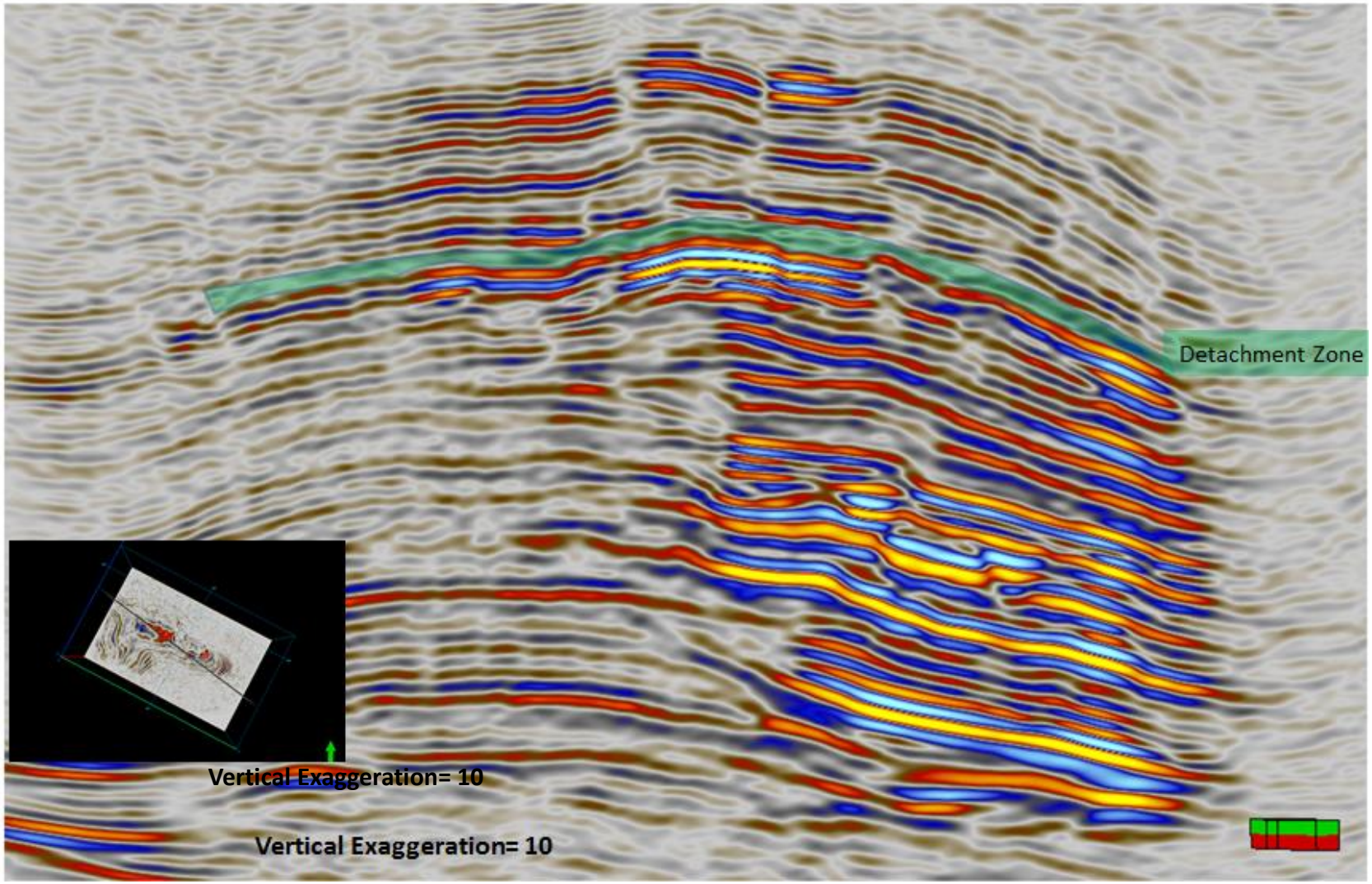

Figure 20. Perpendicular to Joint set 2. Possible detachment zone highlighted in green.

Although the strike slip faults have slightly different orientations, they both trend roughly northwest-southeast. These faults are major features that bound the flower structure, and serve as a physical boundary between the dome and surrounding structure. Figure 21 shows a cross section perpendicular to the southern strike-slip fault. This strike-slip fault is not a clear-cut fault, but rather is represented by a low resolution fault zone on the left side of the flower structure. The dip of the beds smoothly changes from the center of the flower outwards until this boundary is crossed. To the Southwest of this boundary, the dip of the beds shallows dramatically. This fault serves as a physical boundary between two deformation styles.

Two cross sections take along the fold axis of the flower structure are displayed next to one another in Figure 22. The first image shows a cross section displayed with a time slice that shows where the major strike slip fault lies. This cross section is just northeast of the major strike slip fault. It shows a plunging anticline that deepens to the southeast. There is good four way closure along this anticline. The second image shows a cross section taken southwest of the major strike slip fault. The anticline disappears and now there is a plunging monocline. This monocline does not have four way closure. The change in geometry as the fault is crossed shows a major change in structural style. Once this strike-slip boundary is crossed outside of the dome, four way trapping geometry disappears.

Figure 23 shows a cross section perpendicular to the northern strike slip fault, and again, this fault is represented by a low resolution deformation zone. There is a major change in bed dip as this barrier is crossed. Folds in the middle of the structure are part of a concave up anticline, but on the other side of the fault, the strata bend into a concave up syncline. This fault zone marks the boundary between an excellent and poor structural trap.

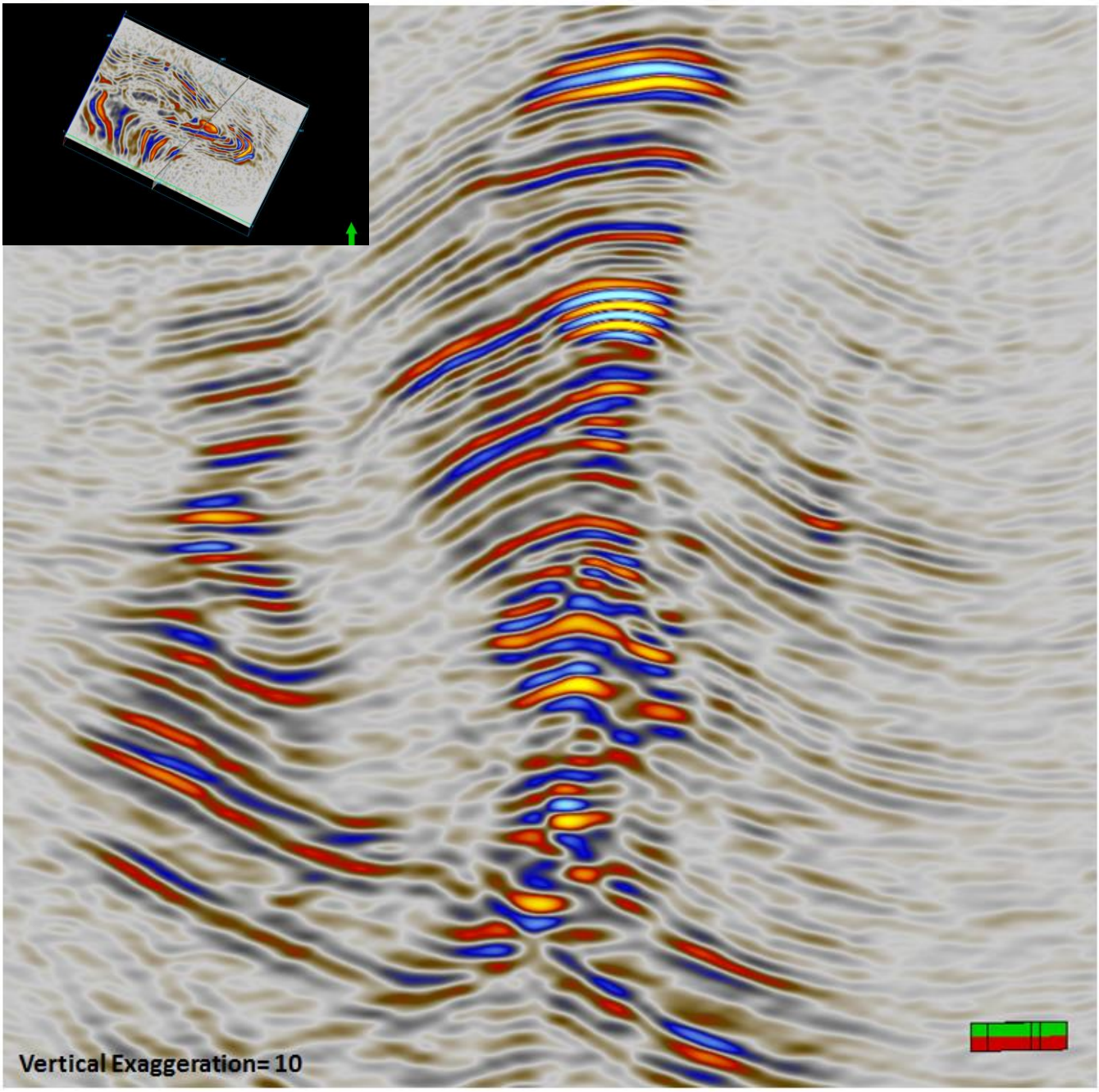

Figure 21. Cross section perpendicular to Southern strike-slip fault

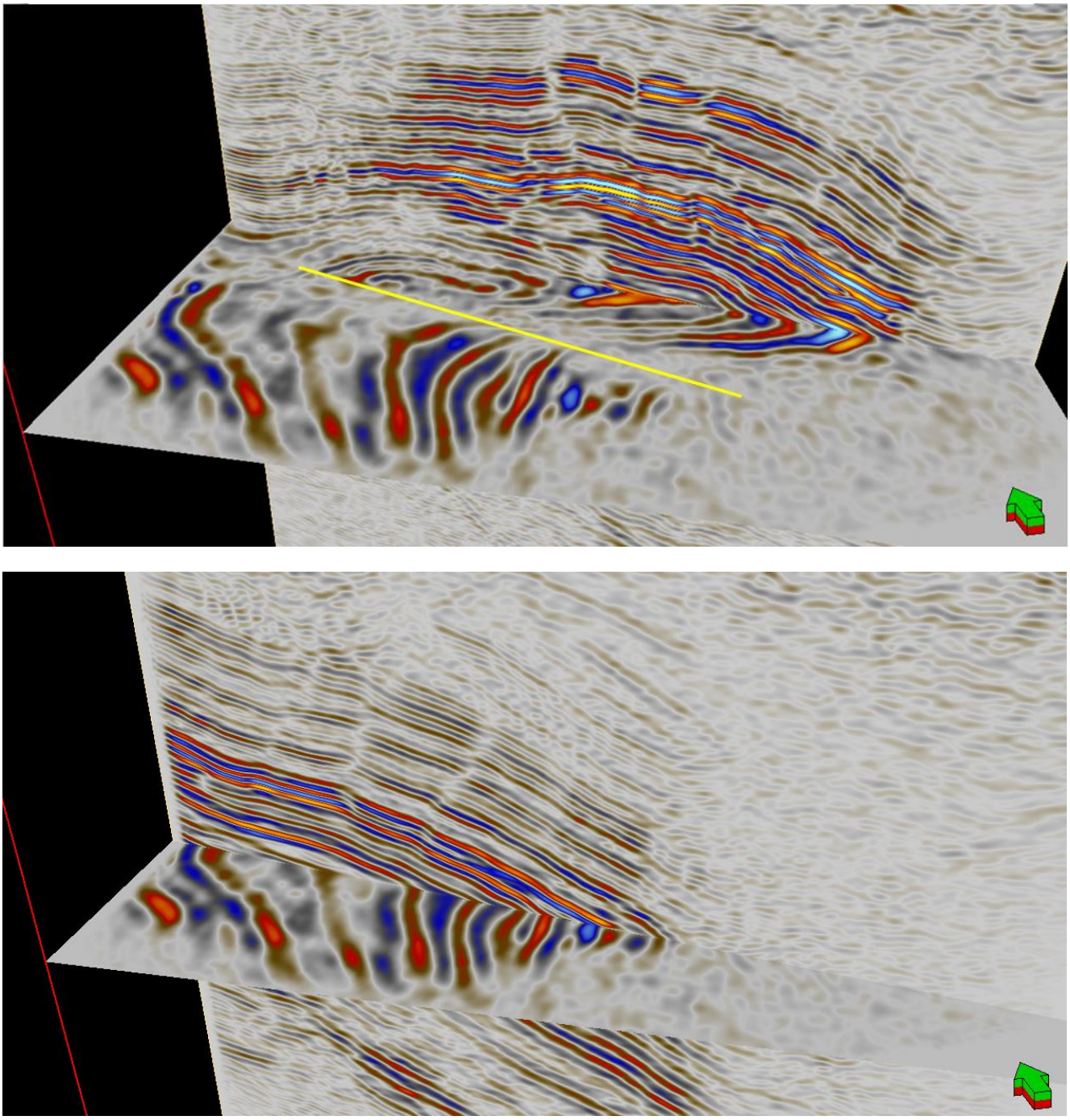

Figure 22. Cross sections taken along axis of plunging anticline. A.) Northeast of Southern strike-slip fault B.) Southwest of the same fault

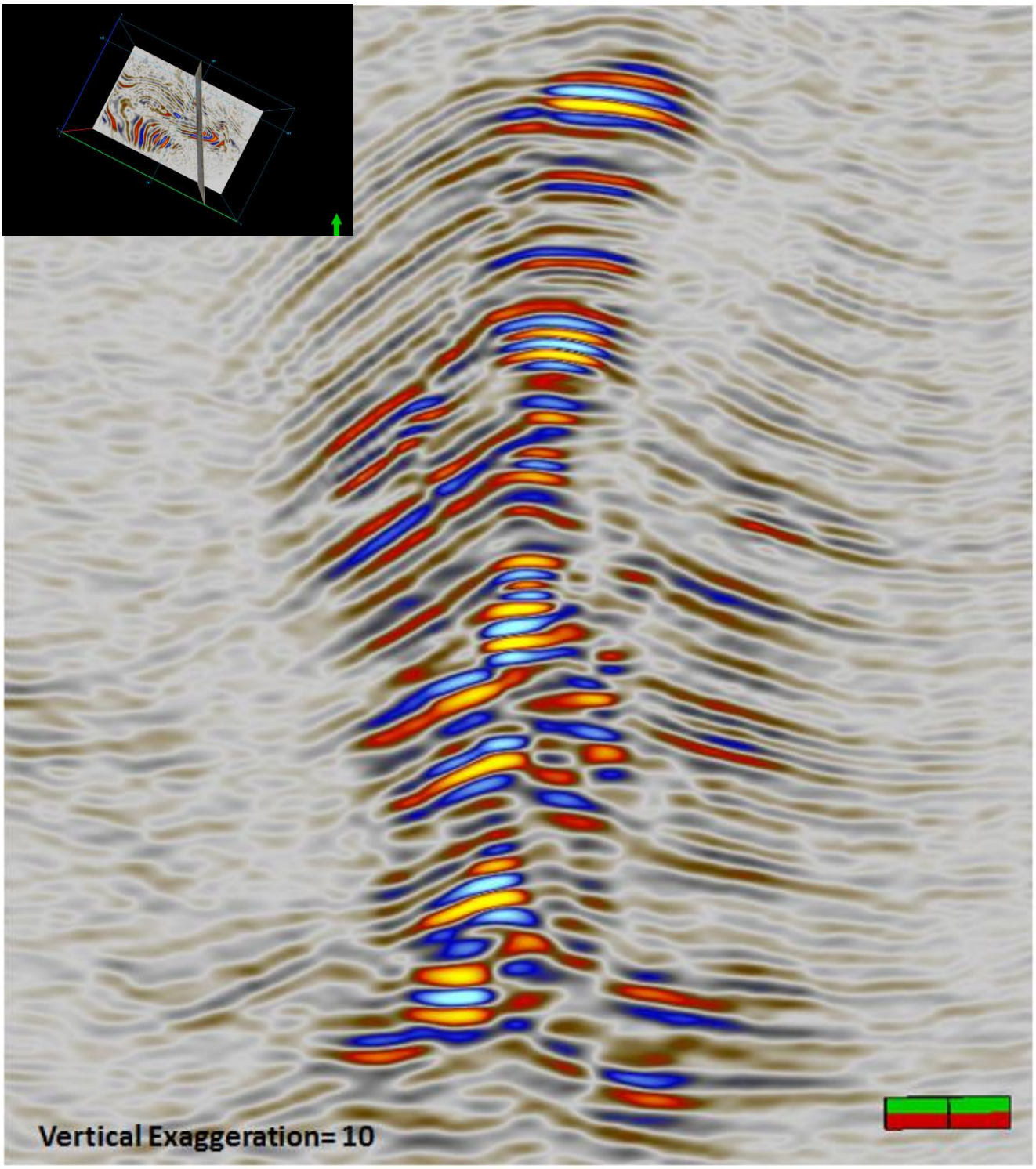

Figure 23. Perpendicular to Northern strike-slip fault.

c. Attribute Analysis

i. Curvature

Most extreme curvature with a step increment of 6 was extracted from the seismic volume, and then applied to each of the four surfaces. Figure 24 shows the Greybull sandstone with the most extreme curvature attribute extracted along its surface and structural contours displayed. There are major northwest-southeast trending faults which correlate with the steepest parts of the dome. These enclose the areas of hydrocarbon capture, and therefore will be referred to as bounding faults. Figure 25 shows the same map again with the major southern bounding fault picked. The image on the left shows an inline taken perpendicular to strike, outlined in map view on the left in yellow, which shows the same fault picked. In seismic, the fault does not show any major displacement as a thrust or normal fault. There is a change in bed dip as the fault is crossed, indicating a change in structural style. The fault trace is clearly visible, however, and suggests that these major bounding faults are associated with strike-slip motion. The next image, Figure 26, shows the northern bounding fault, which also suggests strike-slip motion. These two strike-slip faults are nearly parallel, but may verge to the northwest.

Another style of faulting detected by the curvature attribute is north-south trending faults that cut across the Mackay dome, segmenting it. Figure 27 shows the Greybull surface with curvature extracted again, and the major North-South bounding fault highlighted, which divides the Mackay dome into the western and eastern lobes. On the right is an image of a crossline, which is highlighted on the left in yellow, through this segmenting fault. This image shows the fault highlighted in blue, and gives a better idea of the structural style. This large segmenting fault, although part of a transpressional system, is a major normal fault. This normal fault has a footwall on the western lobe, which drops below the eastern lobe. It is

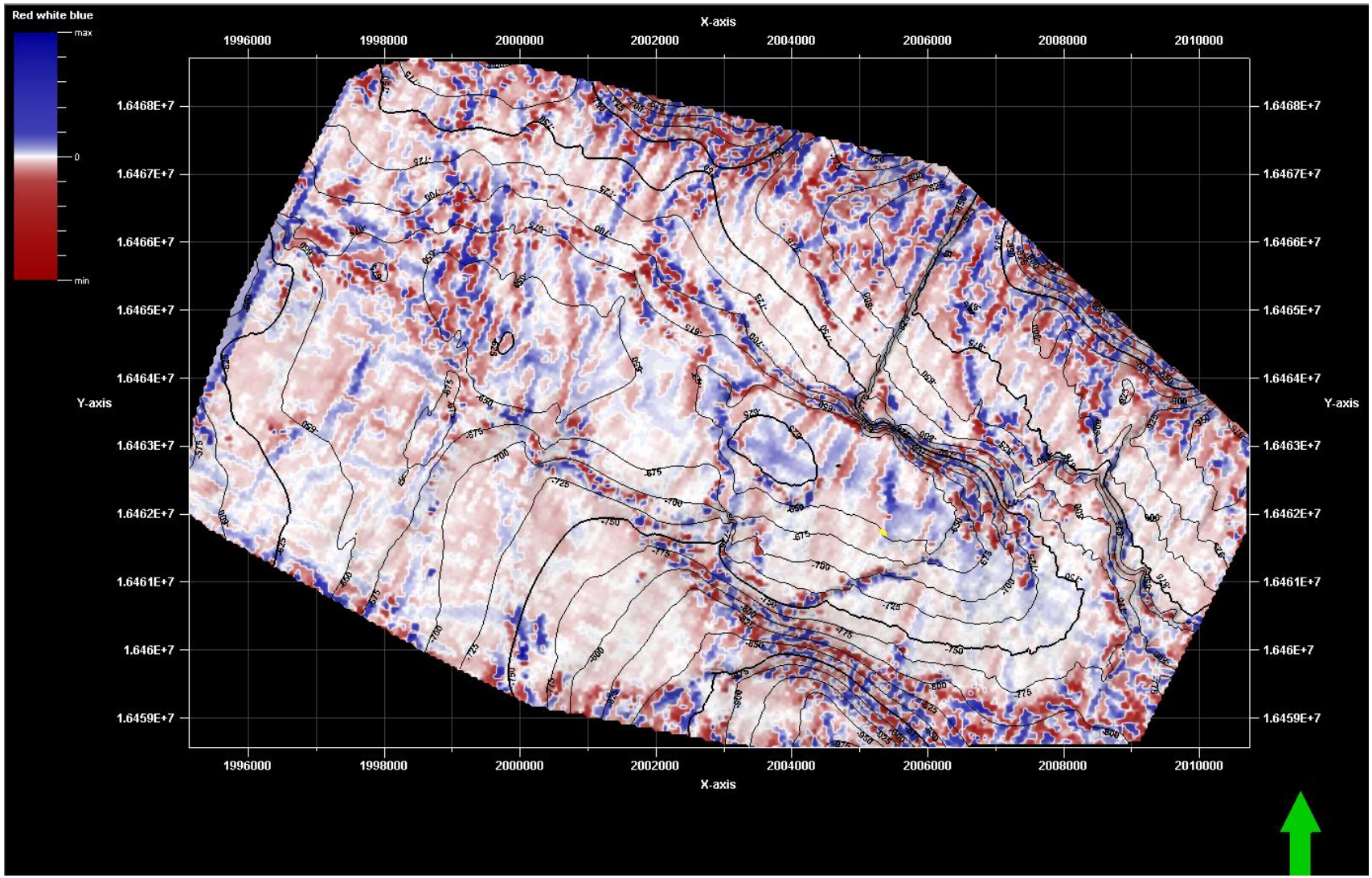

Figure 24. Most extreme curvature extracted along the Greybull sandstone surface.

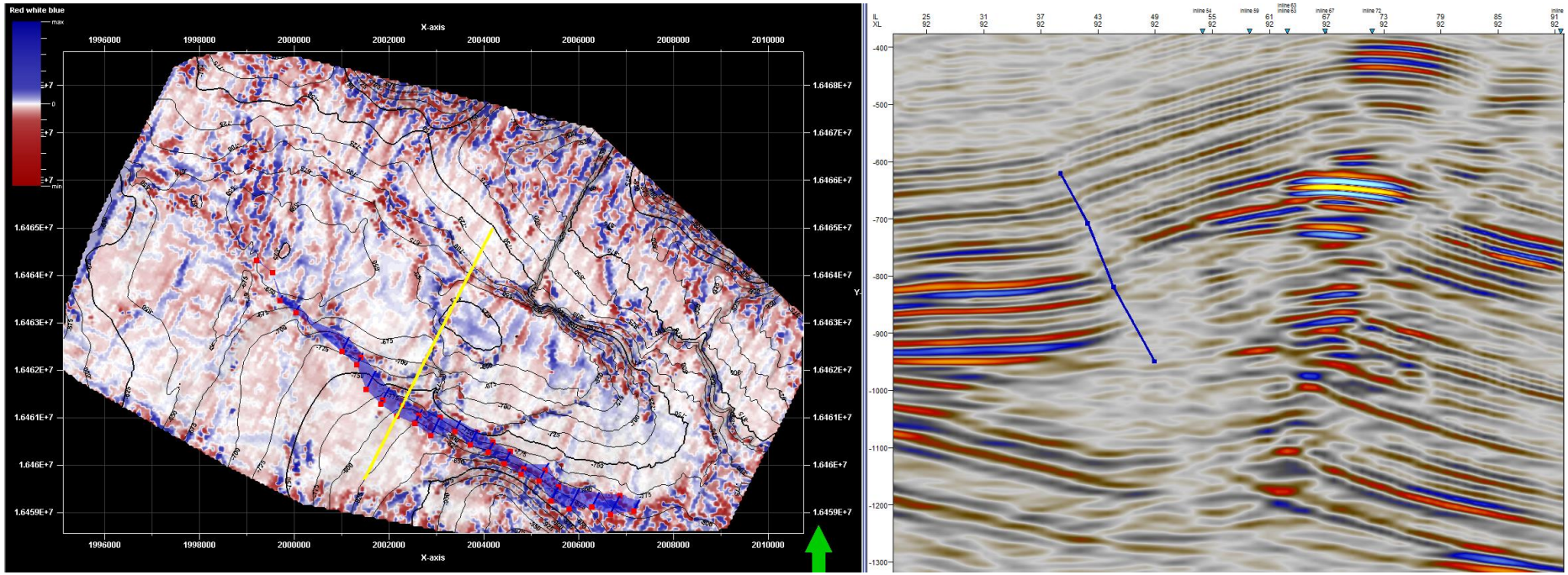

Figure 25. Greybull with curvature extracted and inline 63 showing nature of bounding fault.

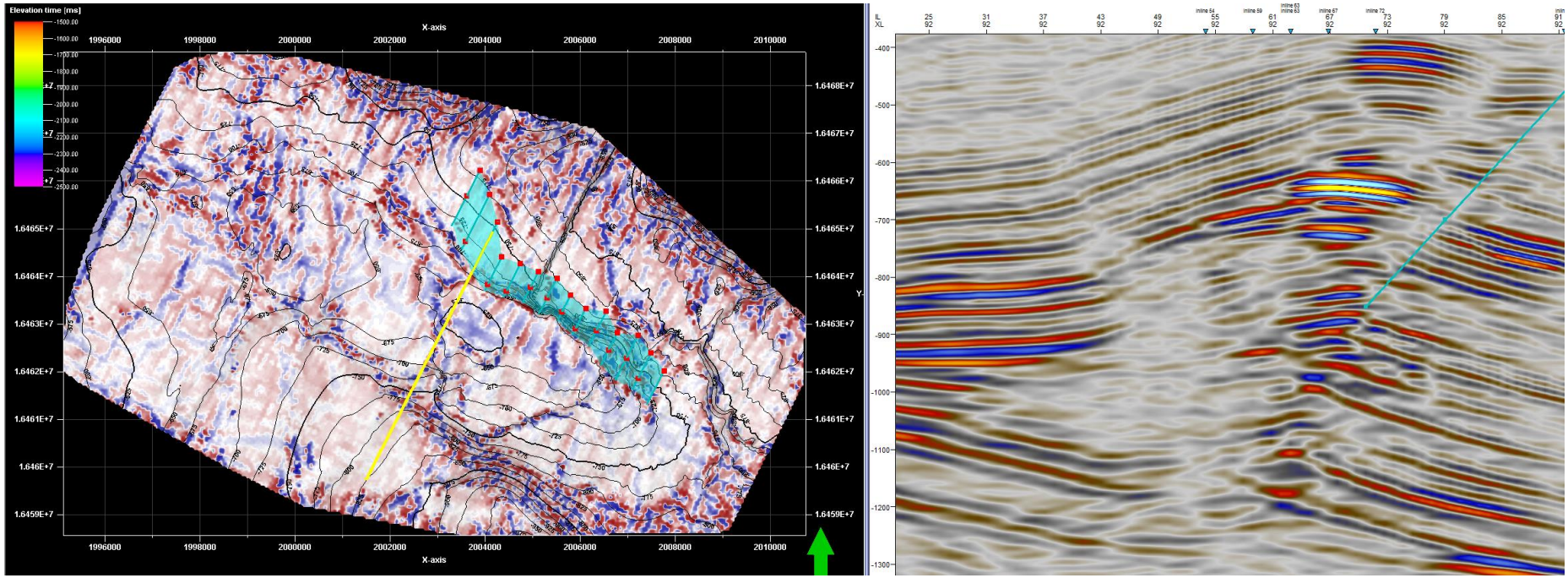

Figure 26. Northern bounding fault showing strike-slip motion.

important to note that this fault, although crucial in the reservoir interval, is a minor fault in this system. It has a throw of only a few hundred feet, and displaces only a portion of the strata.

This normal faulting may not be a result of transpression, but could have formed from a variety of reasons. It is towards the center of the anticline, and may represent a break related to bending of the rock in the west-east direction. It could also have formed at a different orientation, and during strike slip displacement, may have rotated to its present position. It is important when evaluating structure to look at major trends, and not characterize deformation based on observations in a small reservoir interval.

The last major faulting style shown in this curvature surface along the Greybull is northeast-southwest trending segmenting faults. Figure 28 shows one of these faults highlighted, with a crossline outlining this fault on the right. This fault is also a segmenting fault, but unlike the north-south fault, it is a thrust fault. The hanging wall is on the northwestern side, and thrusts over the southeast hanging wall. These faults are at an oblique angle to the extensional fault. Although this thrust trends northeast-southwest, it is slightly more eastern pointing than the major Set 2 faults previously observed. Again, this is a minor fault in the overall structure. It could have undergone rotating or be related to more local deformation. However, for this particular study, because the focus is on a small section of rock, mapping minor faults is still crucial for understanding compartment orientation. Although it may not be representative of major cross structure faults, it can provide boundaries or migration pathways within the reservoir.

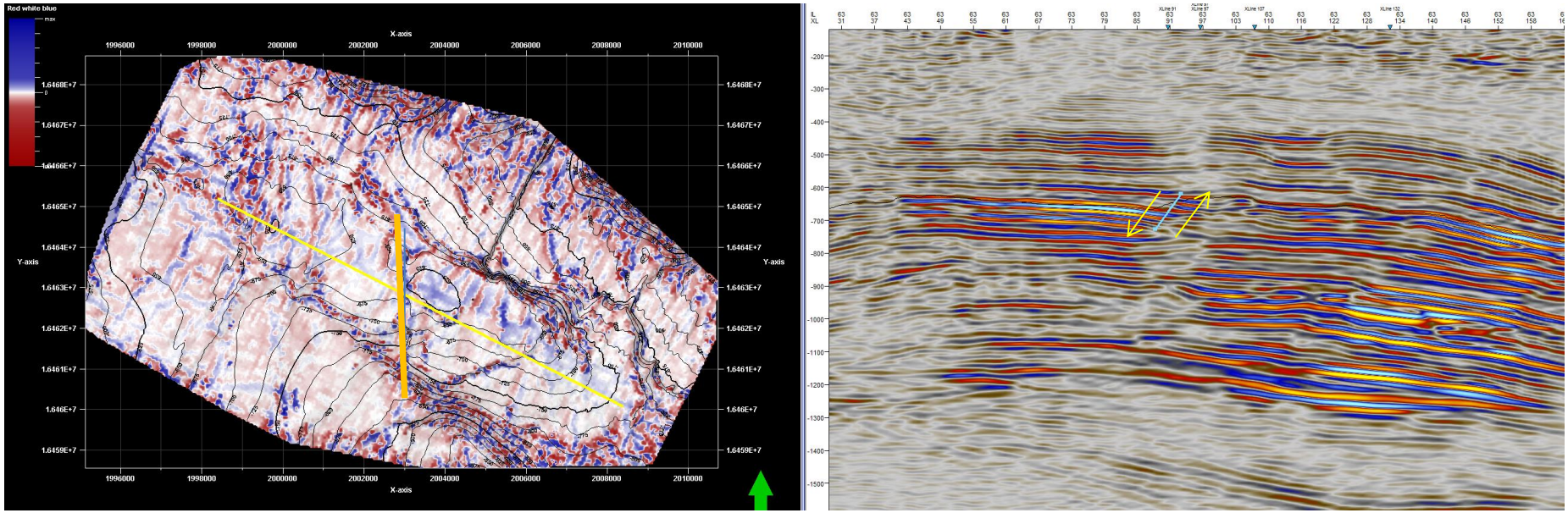

Figure 27. Segmenting normal fault outlined in map view on left and cross section on right.

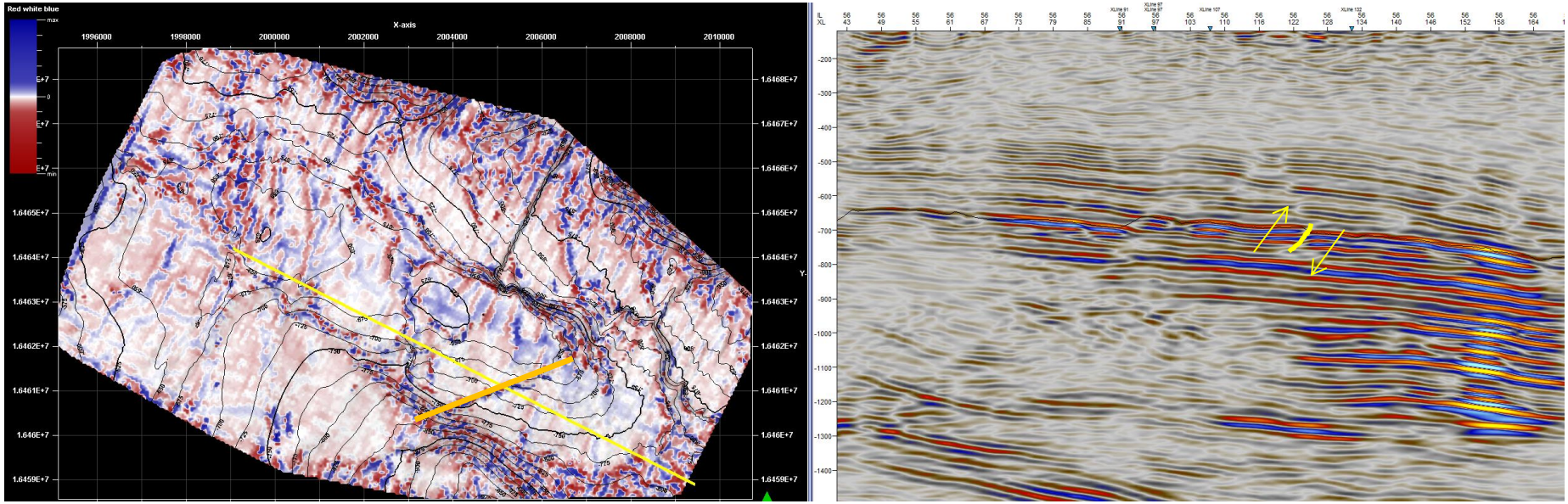

Figure 28. Segmenting thrust fault outlined in map view on left and cross section on right.

Figures 29, 30, and 31, show the base of Greybull, Kootenai, and Fuson surfaces with the most extreme curvature attribute extracted, respectively. The northern and southern bounding faults are clearly shown in all surfaces, and become closer to one another as depth increases. This is because the flower structure closes as depth increases. Again, these bounding faults are the strike-slip components of the transpressional system. In these three lower surfaces, the segmenting faults are not as clear as in the Greybull. By the lowest surface, both segmenting faults are nearly gone.

ii. Variance

In order to compare the results of the curvature attribute analysis, variance was also extracted from the seismic volume, then extracted along each of the four horizons (Figures 32-35). The north and south bounding faults are clear in all four horizons, and like in the curvature attribute, become closer towards the bottom of the structure. The north-south extensional segmenting fault is visible in all four horizons, but becomes more faint towards the bottom of the structure, particularly in Figure 35. The northeast trending thrust bounding fault is clear in Figure 32 and 33, but disappears in Figure 34 and 35. In the curvature surfaces, it was clear in the Greybull and base of Greybull, became faint in the Kootenai, and disappeared by the Fuson shale top. In cross section, this fault, although a major one in this reservoir system, does have a small trace vertically, appearing and disappearing quickly. It may not be a major fault in the overall structure of the flower, but is important to the petroleum system. Because the results from the curvature analysis agree with the variance analysis, these faults are real and present in the structure.

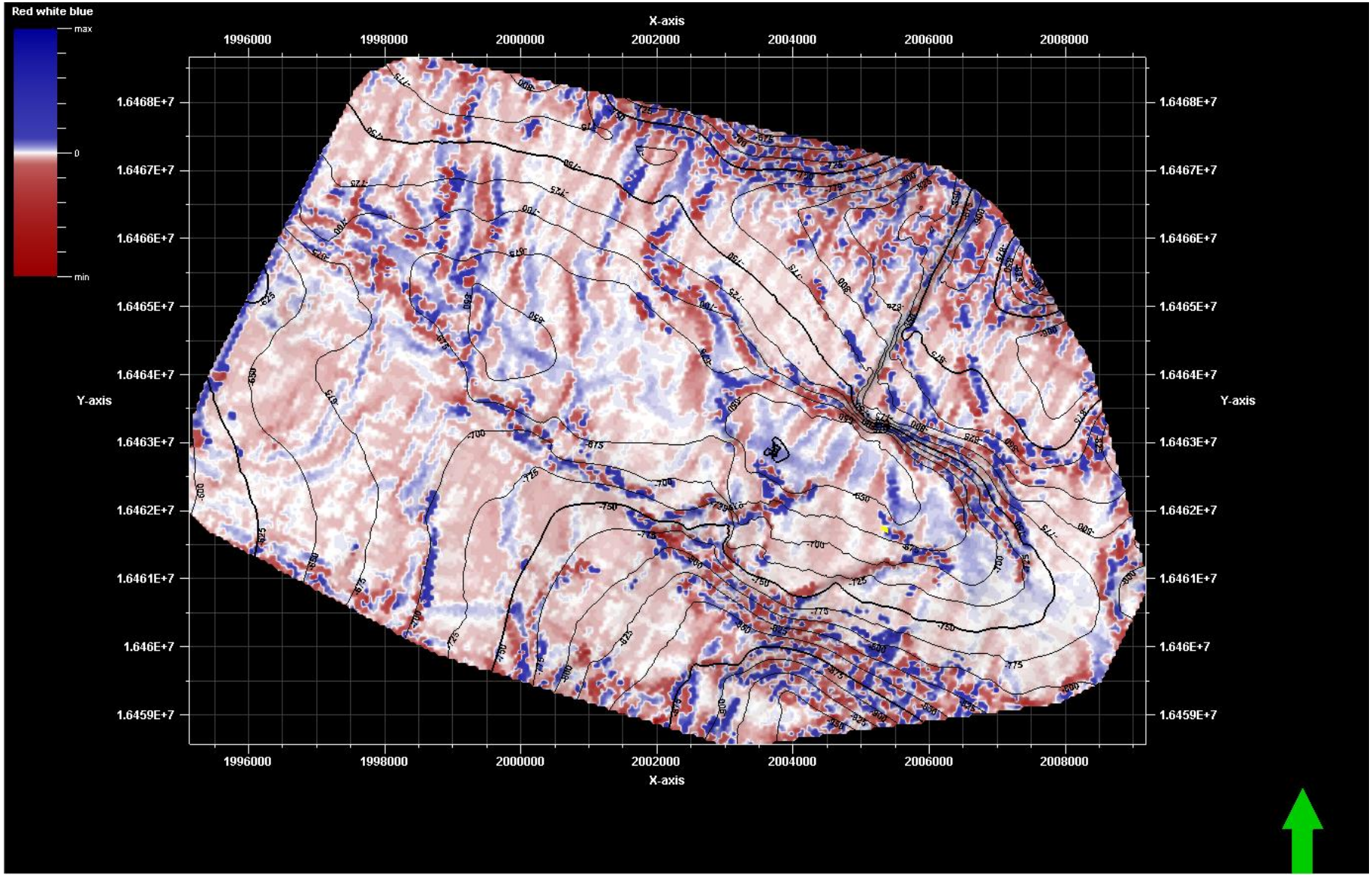

Figure 29. Most extreme curvature for Base of Greybull sandstone.

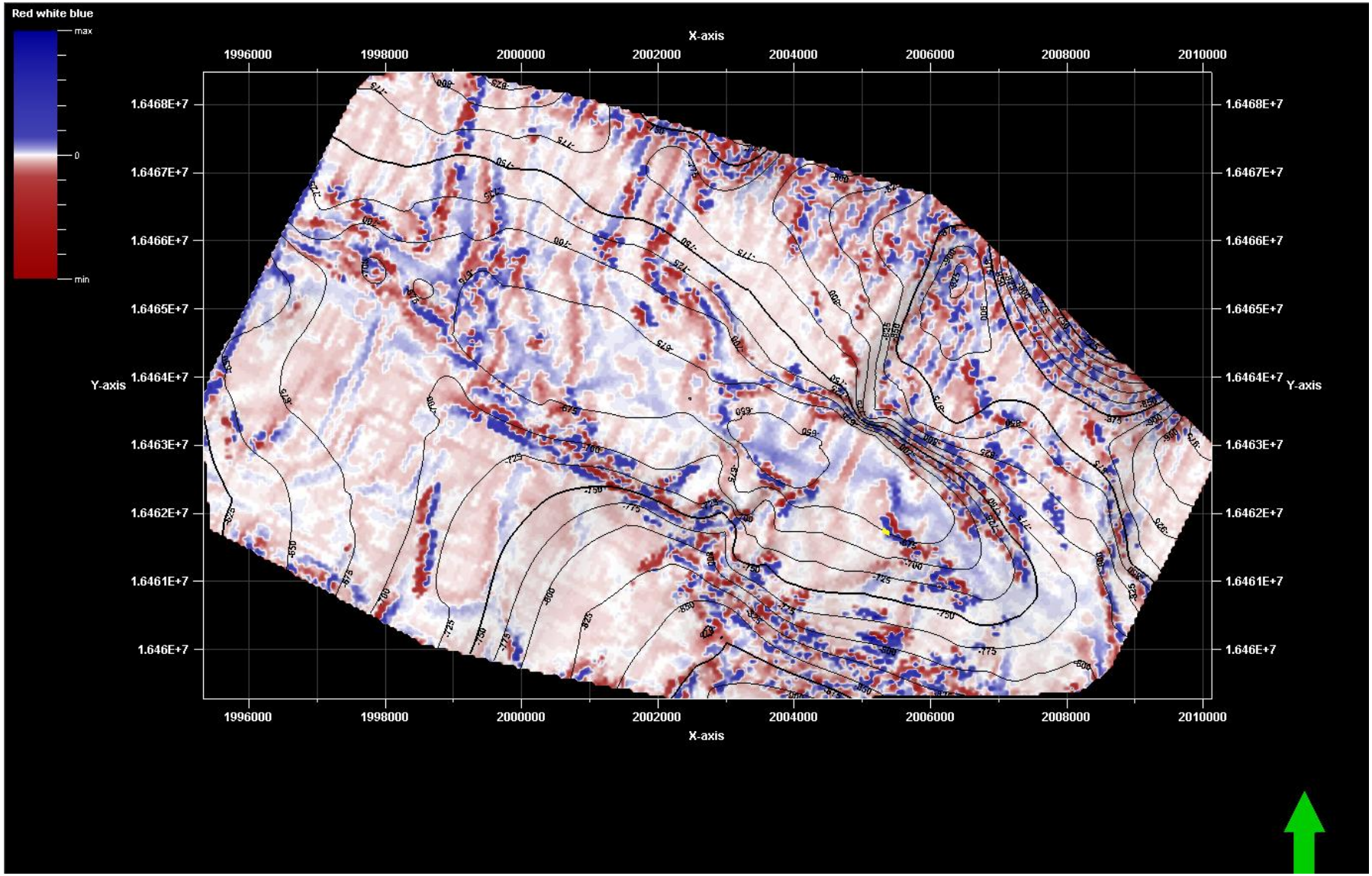

Figure 30. Most extreme curvature for Kootenai formation.

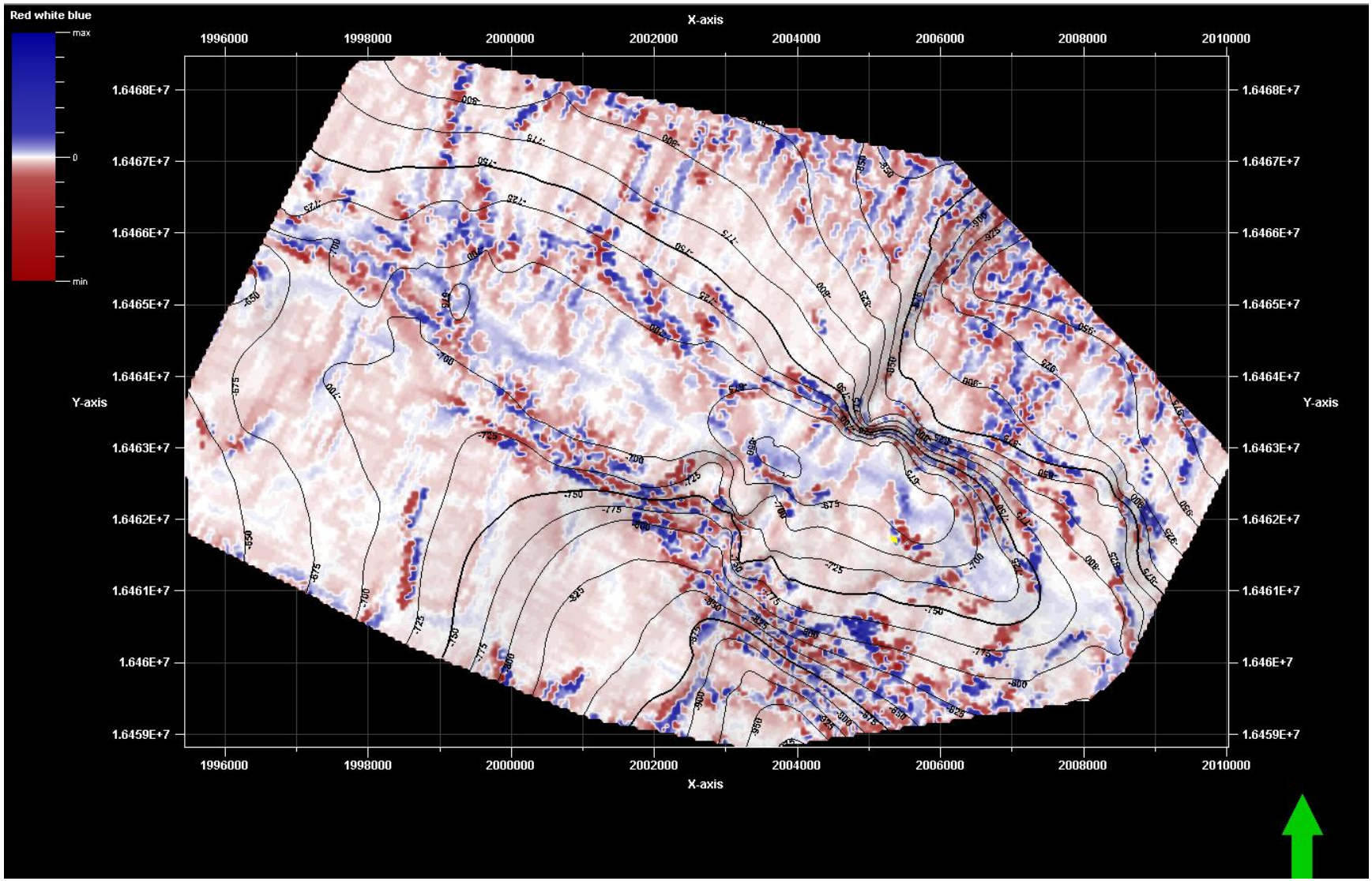

Figure 31. Most extreme curvature for Fuson Shale.

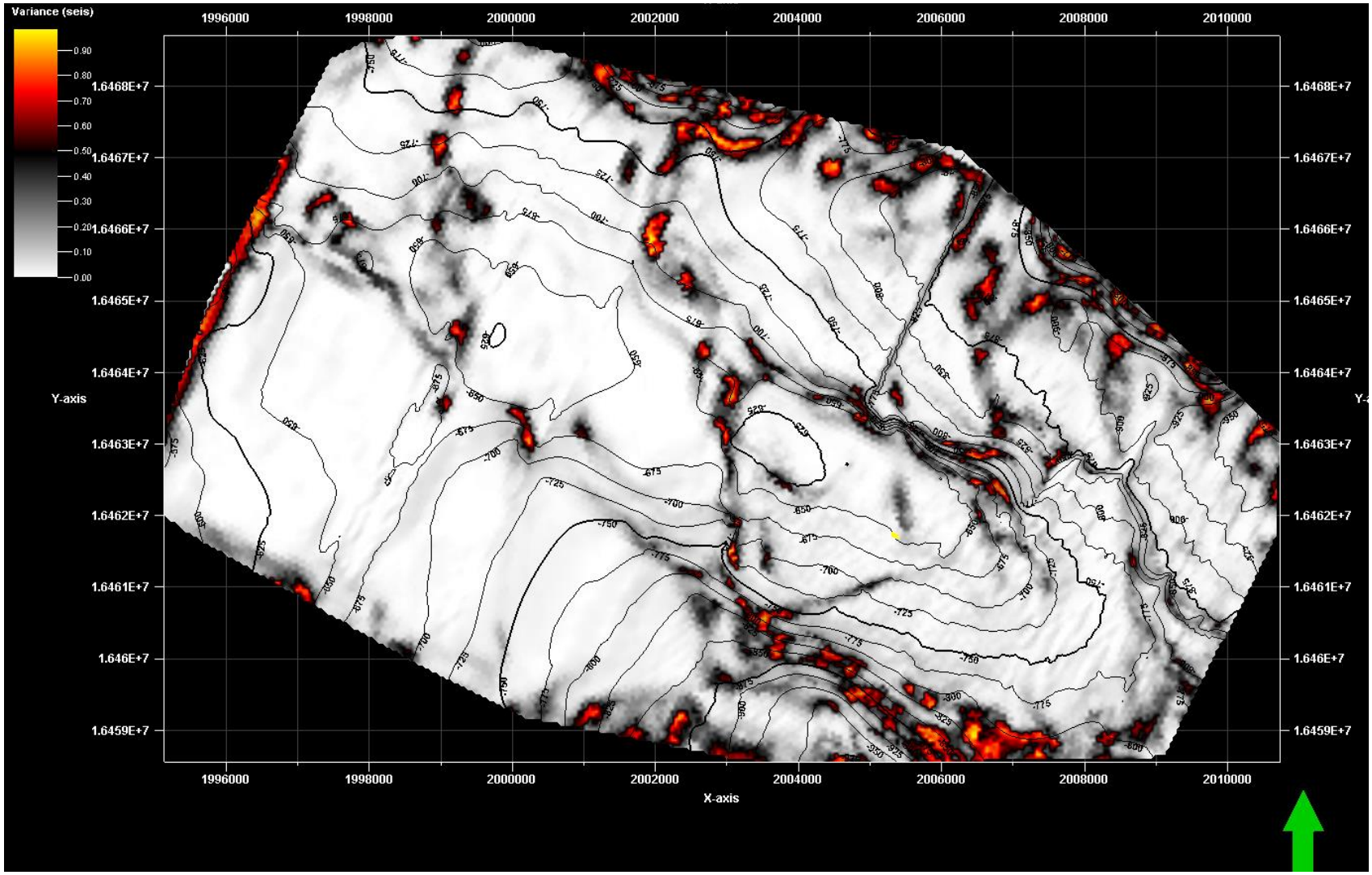

Figure 32. Variance extracted along the Greybull sandstone.

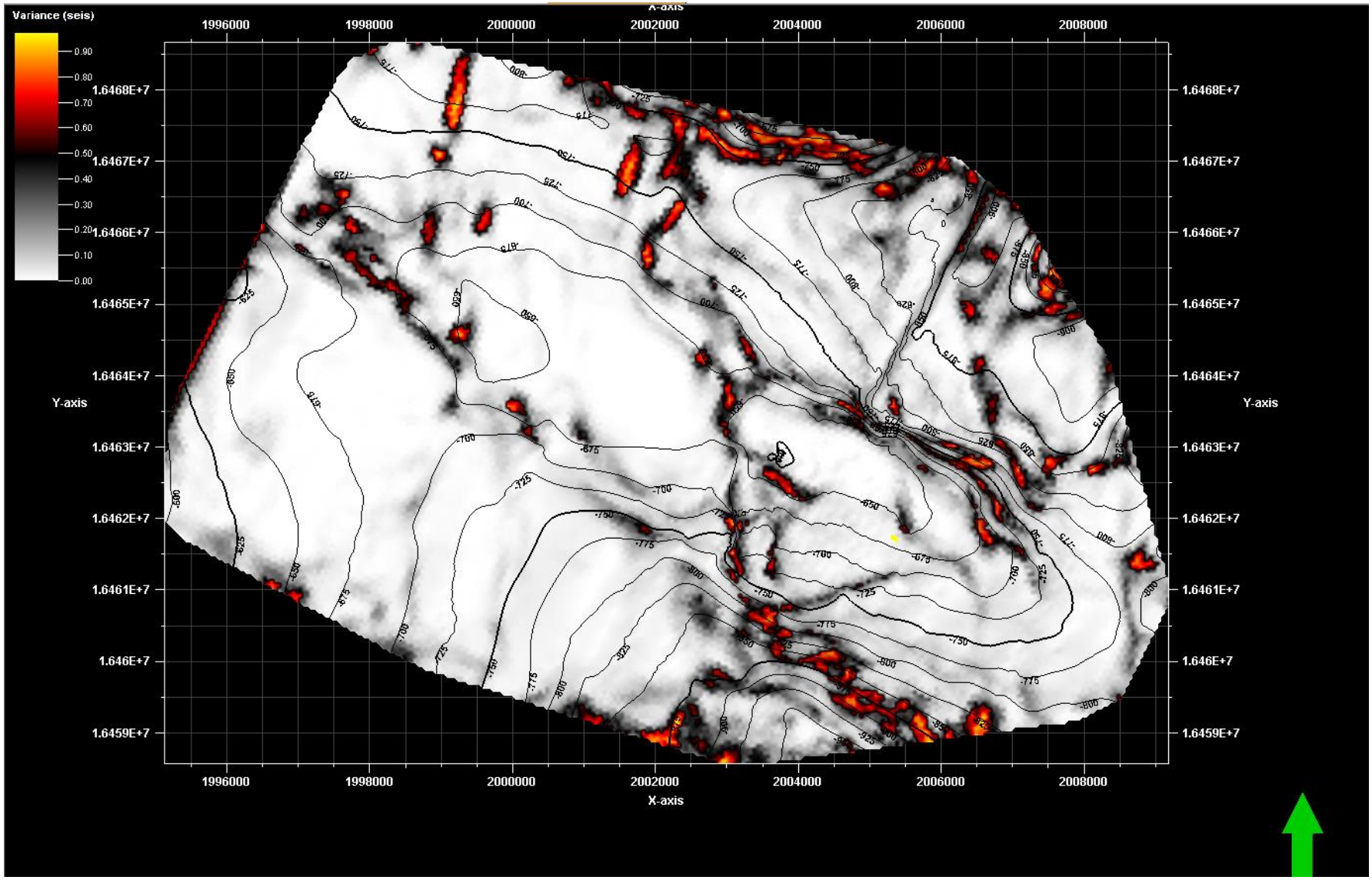

Figure 33. Variance extracted along the base of Greybull sandstone.

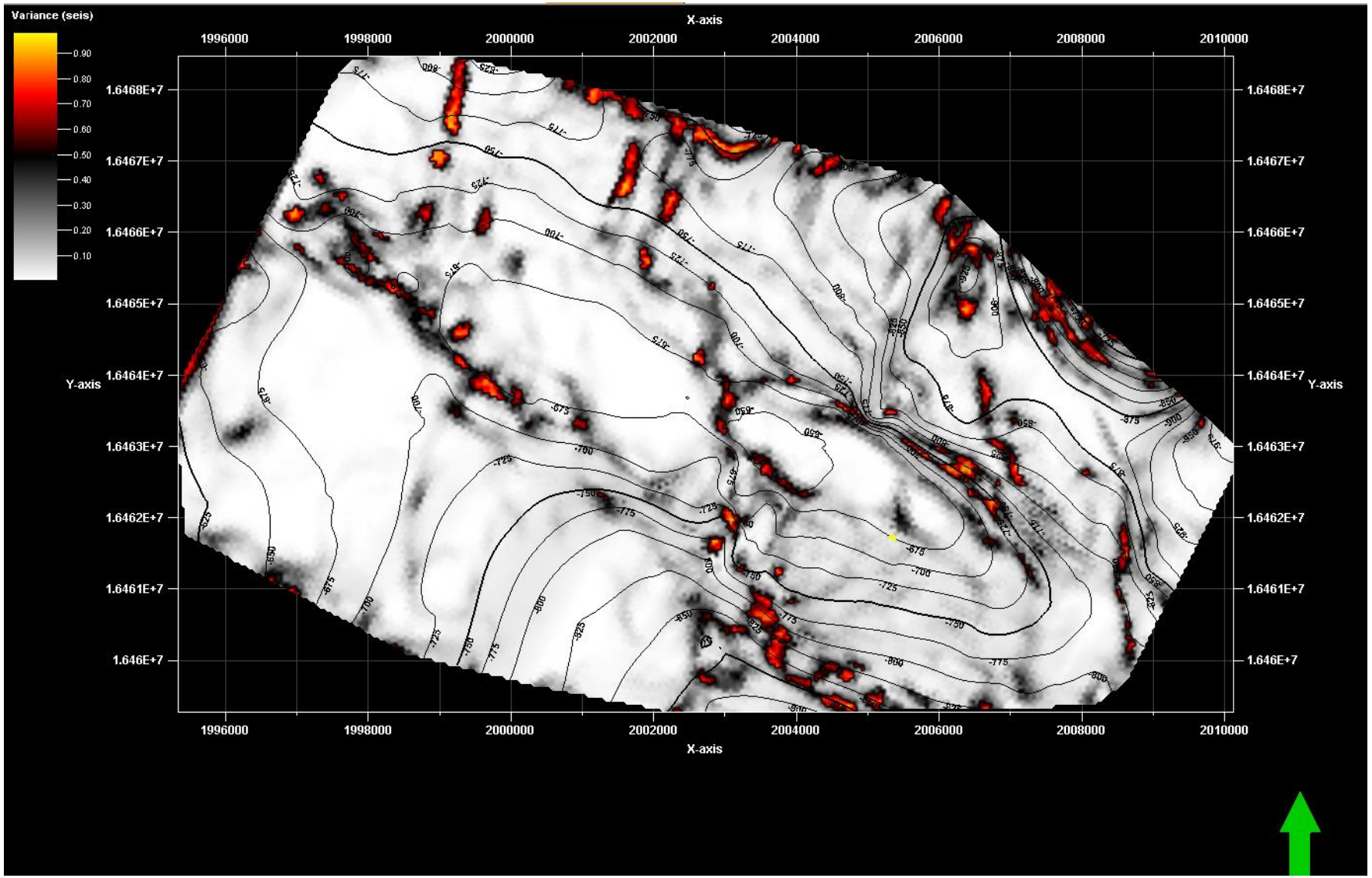

Figure 34. Variance extracted along the Kootenai formation.

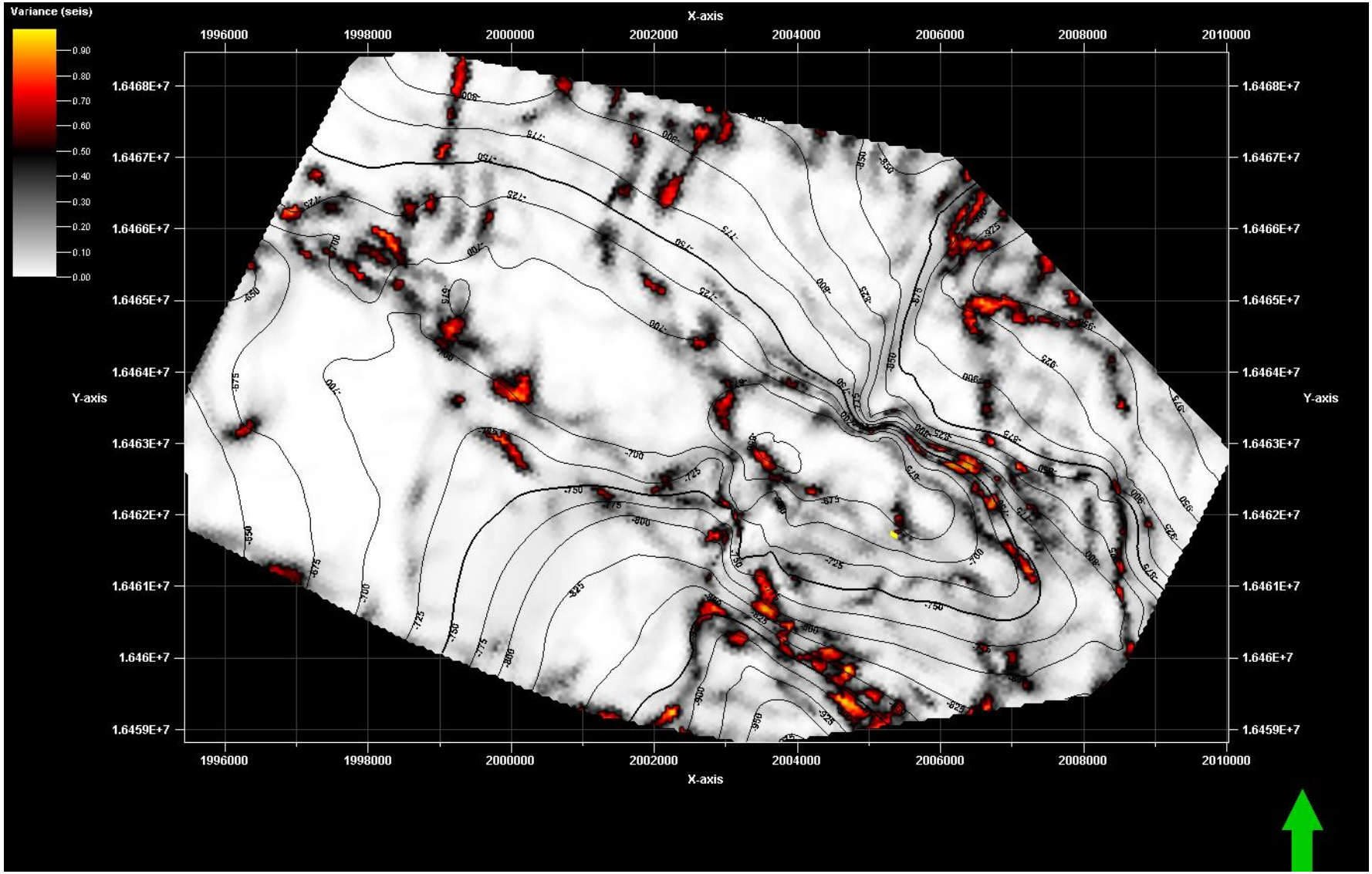

Figure 35. Variance extracted along the Fuson shale.

iii. Ant Tracking

The ant tracking attribute was applied to the most extreme curvature volume. Each of the four surfaces are shown with the attribute extracted along them (Figures 36-39). The Greybull surface shows the two bounding faults, and the segmenting faults. This attribute also highlights more faults that were not seen in the curvature and variance attributes. These could be subseismic faults, which may be discovered later while drilling wells, particularly horizontal wells while geosteering. Again, in the ant tracking attribute, the northeast trending segmenting thrust fault disappears by the Kootenai formation. The Greybull surface is more concentrated in ant tracks, which suggests it may have more deformation than the other three surfaces. This could be because the Greybull sandstone behaves differently mechanically than a shale. Sandstones will experience more brittle deformation compared to a shale which will deform in a more ductile manner.

iv. Thickness Maps

Figure 40 shows a thickness map created from the top of the Greybull surface to the surface immediately below it. Warmer colors represent thicker sections of reservoir, and cooler colors represent thinner sections. Contours are overlain, representing thickness to help with visual display. The reservoir is relatively homogenous in thickness, with a slightly thinner area of rock in the center. This may be depositional or structural. The next image in Figure 41 shows the thickness map overlying the variance surface. These surfaces are displayed together to see if thickness is structurally controlled. There is a little correlation between the area of thinning and major faults in the Greybull surface. However, some of the thickening does directly correlate

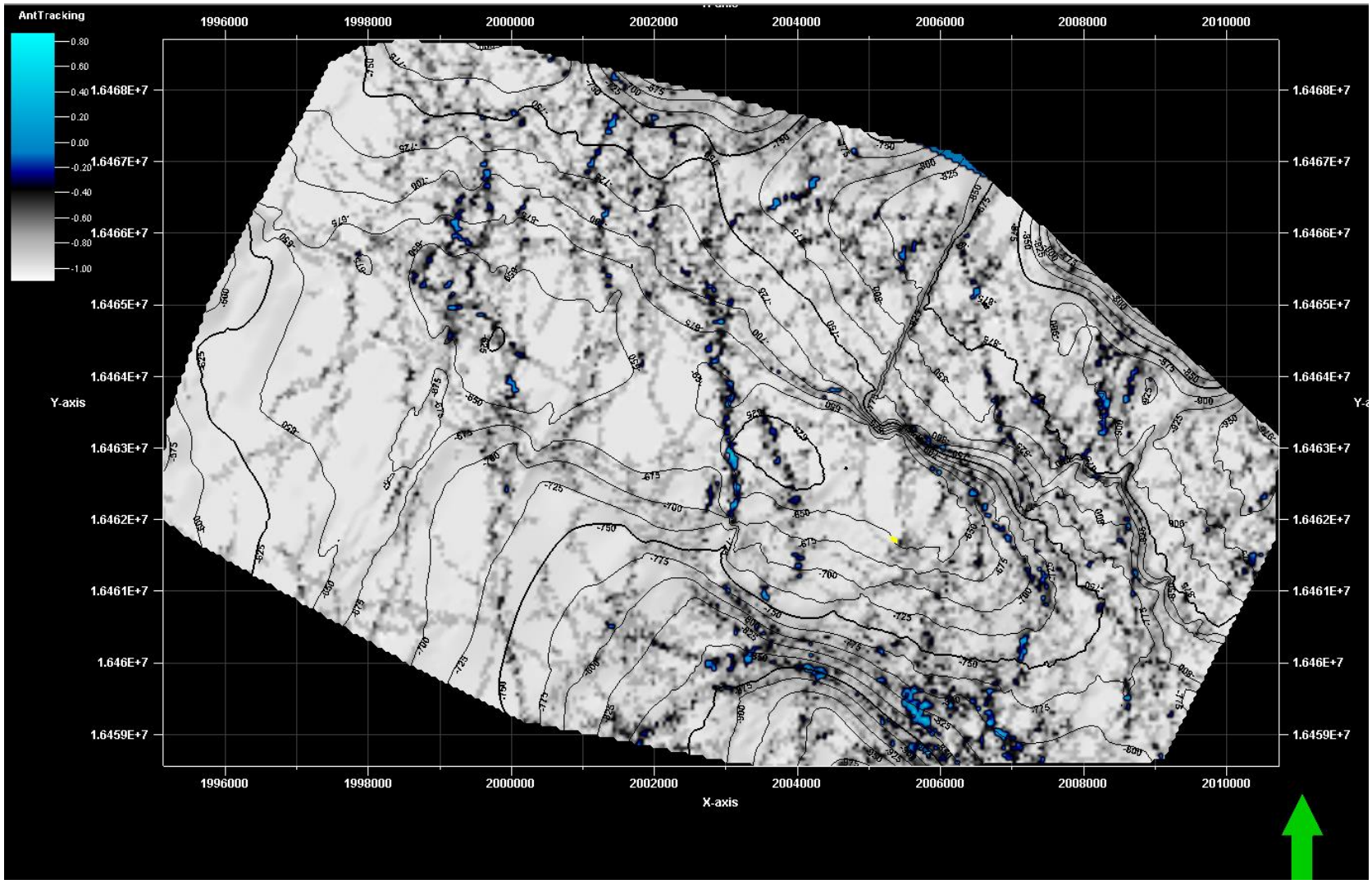

Figure 36. Curvature ant tracks extracted along the Greybull surface.

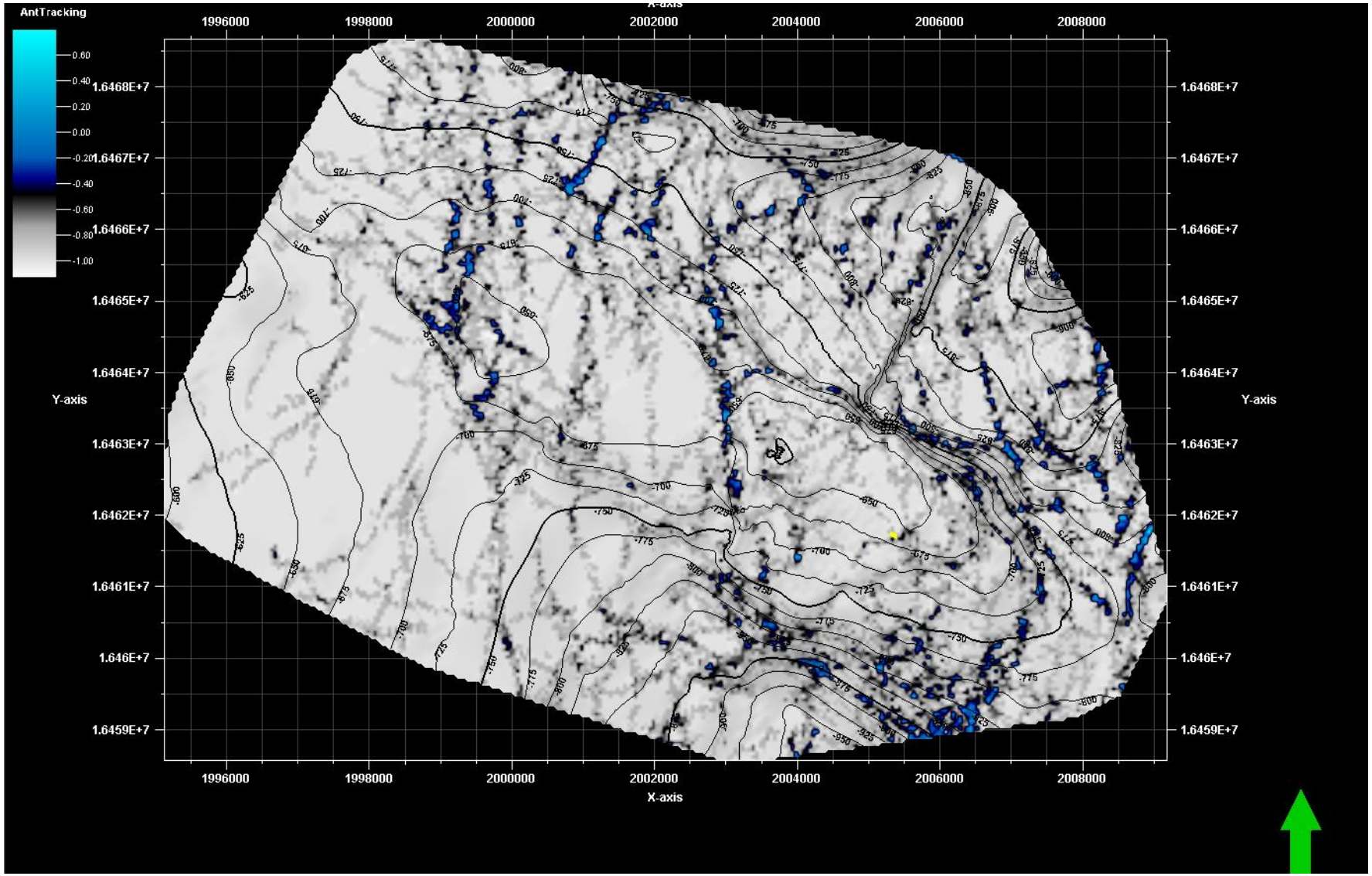

Figure 37. Curvature ant tracks extracted along the base of Greybull surface.

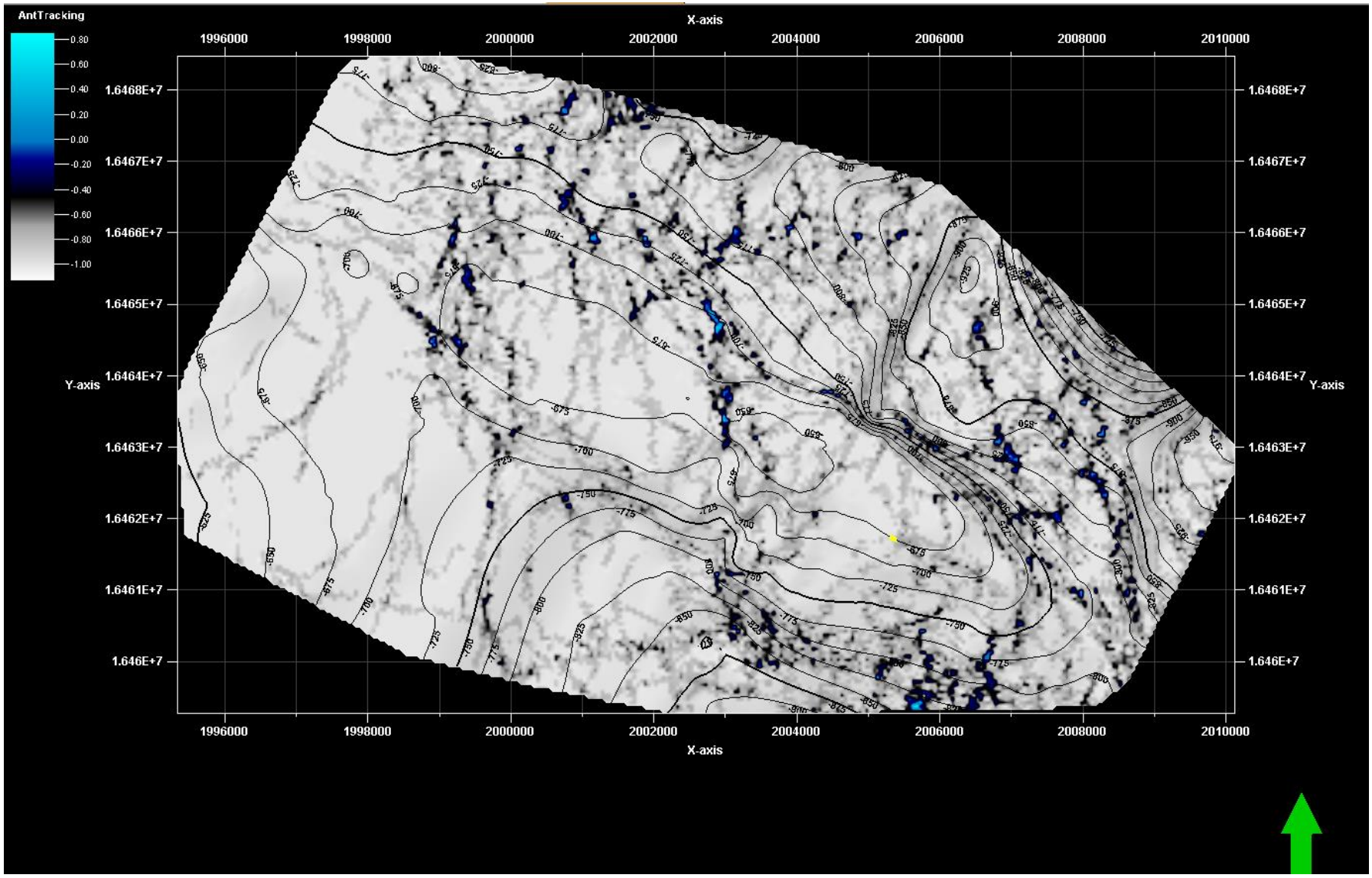

Figure 38. Curvature ant tracks extracted along the Kootenai surface.

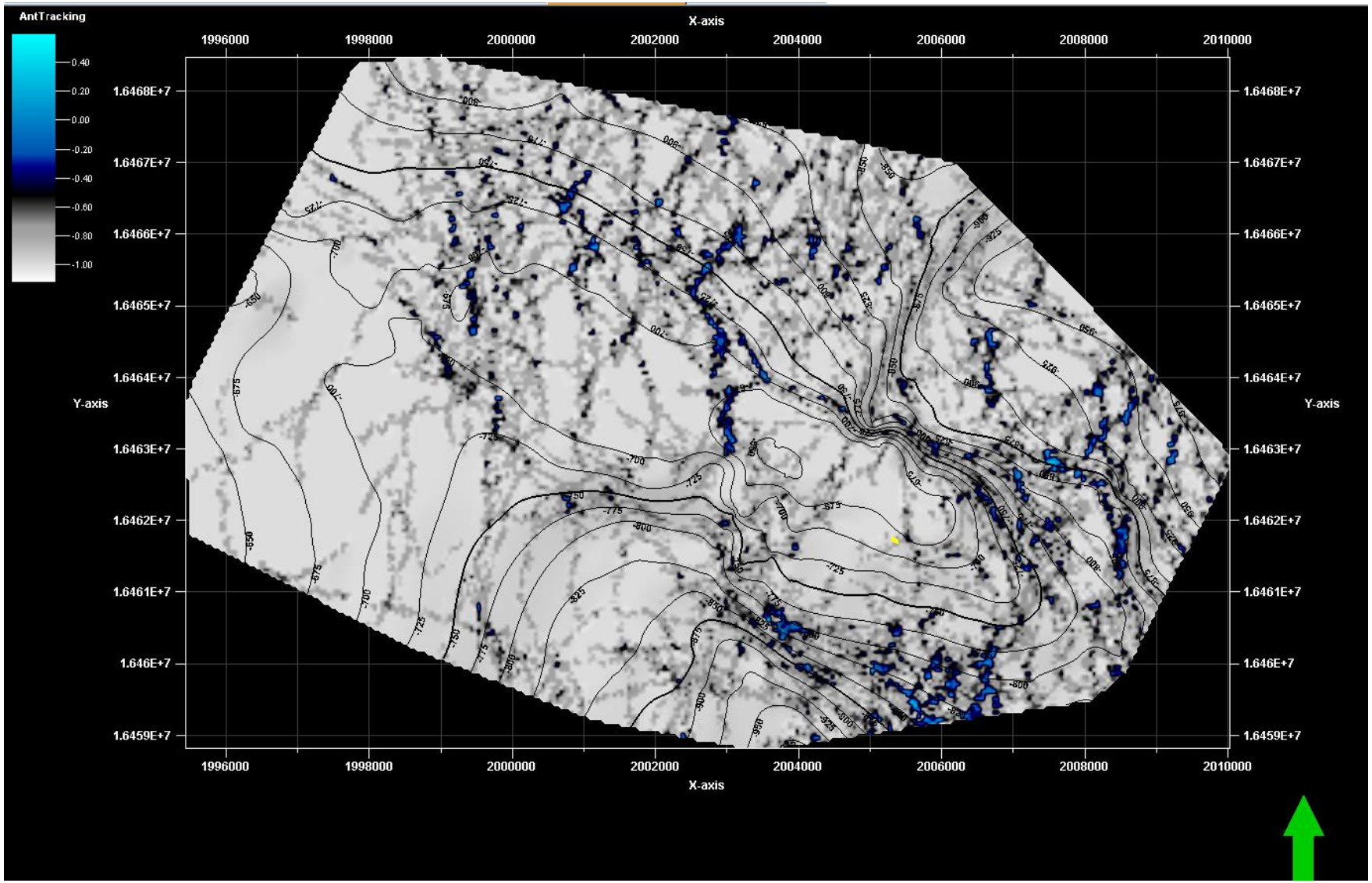

Figure 39. Curvature ant tracks extracted along the Fuson surface.

with major faults. Areas of faulting in the seismic data can make horizon picking more difficult and appear as false areas of thickening.

Lastly, Figure 42 shows a total thickness map for all four horizons, which shows little variation in thickness throughout the entire section of interest. This could mean that when planning new wells, stratigraphic variations may not be as important for targeting as structural variations. It could also suggest the vertical resolution of the seismic data (81.25 feet) is not small enough to detect subtle changes in thickness. In order to further investigate possible thickness variations, a spectral decomposition analysis was performed.

v. Spectral Decomposition

Spectral decomposition was completed by flattening a volume along two surfaces within the Greybull reservoir. A frequency spectrum was computed and dominant frequencies were detected at 24, 49, and 72 Hertz. Figure 43 shows the flattened Greybull reservoir at 590 ms, with red representing 24 Hz, green representing 40 Hz, and blue representing 60 Hz. There are no clear patterns or fluvial channels detected within this surface. There may be a possible thicker section shown in the southern part of the reservoir in red, but it does not look to be stratigraphically controlled. There is more red displayed on the northeastern side of the structure, which may suggest a slight thickening in that section. This could be due to an increase in deformation in this side of the structure.

Because the first surface didn't detect any channels, it was repeated on another horizon picked within the Greybull sandstone, this time at 710 ms. This figure also shows the flattened horizon with red displayed as 25 Hz, green with 35 Hz, and blue with 53 Hz.

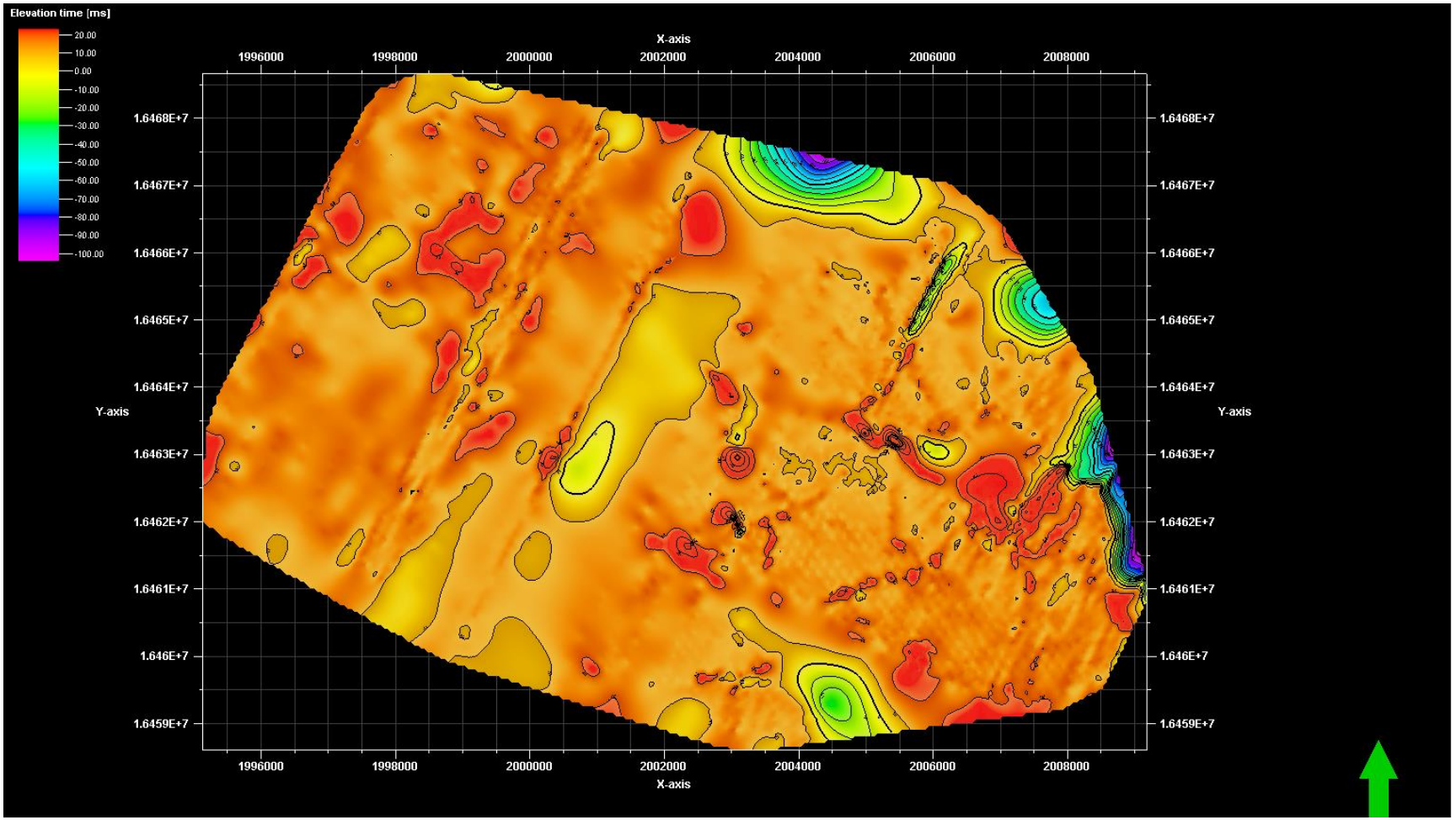

Figure 40. Greybull sandstone ispoach thickness map. Warmer colors represent thicker reservoir.

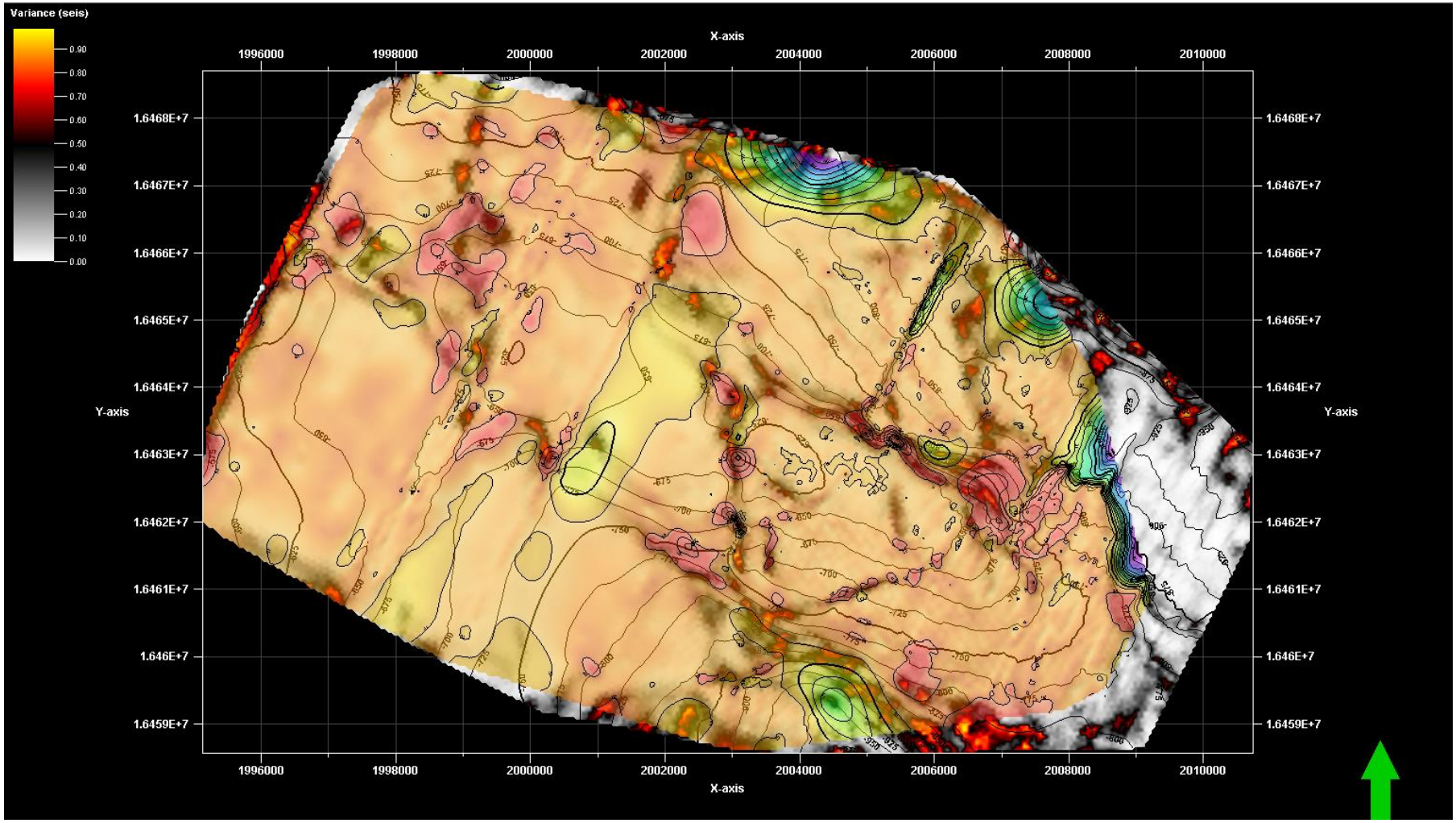

Figure 41. Greybull isopach thickness map (50% transparency) overlying the variance attribute showing major faults.

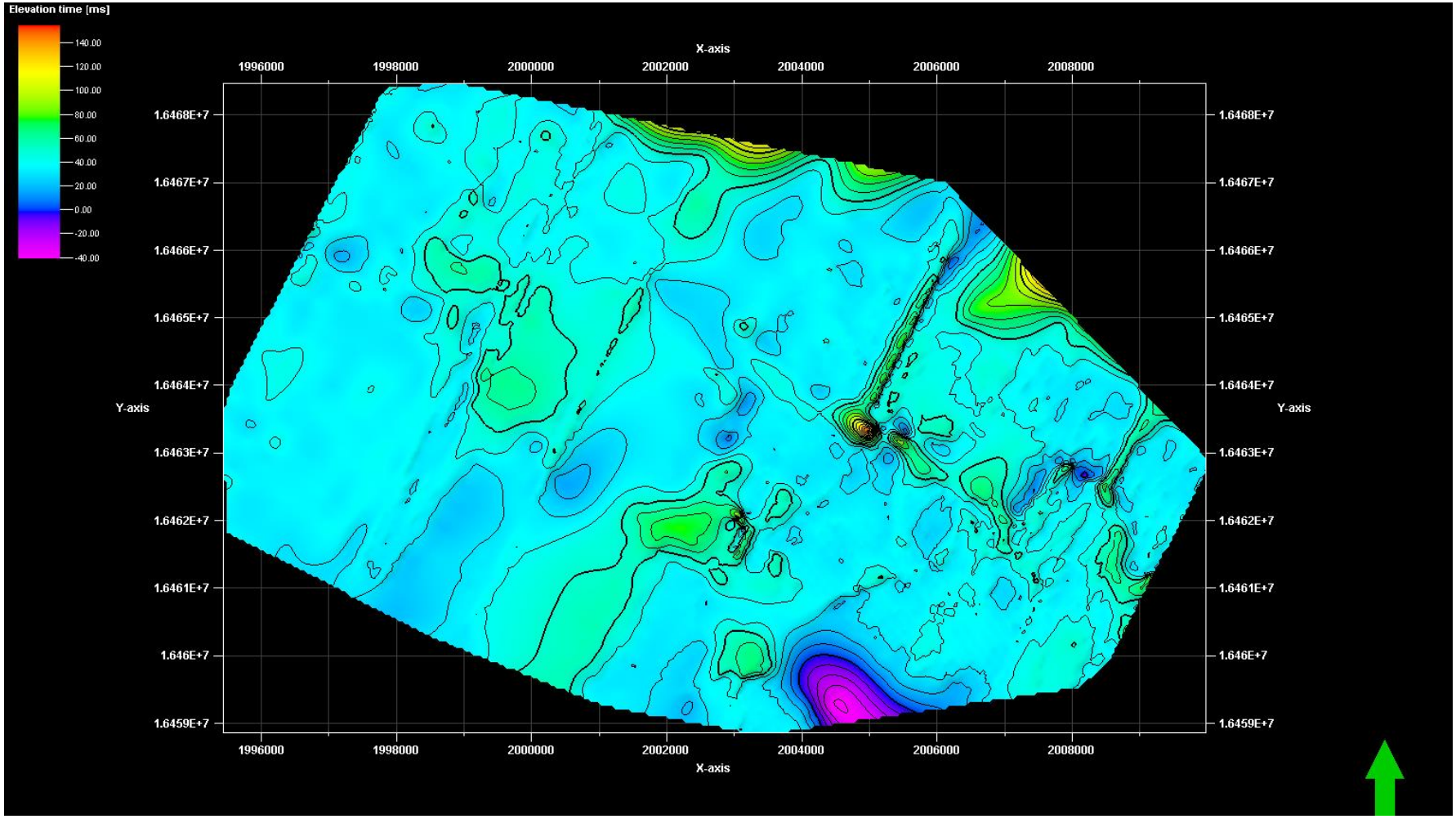

Figure 42. Total thickness map, from top of Greybull to top of Fuson.

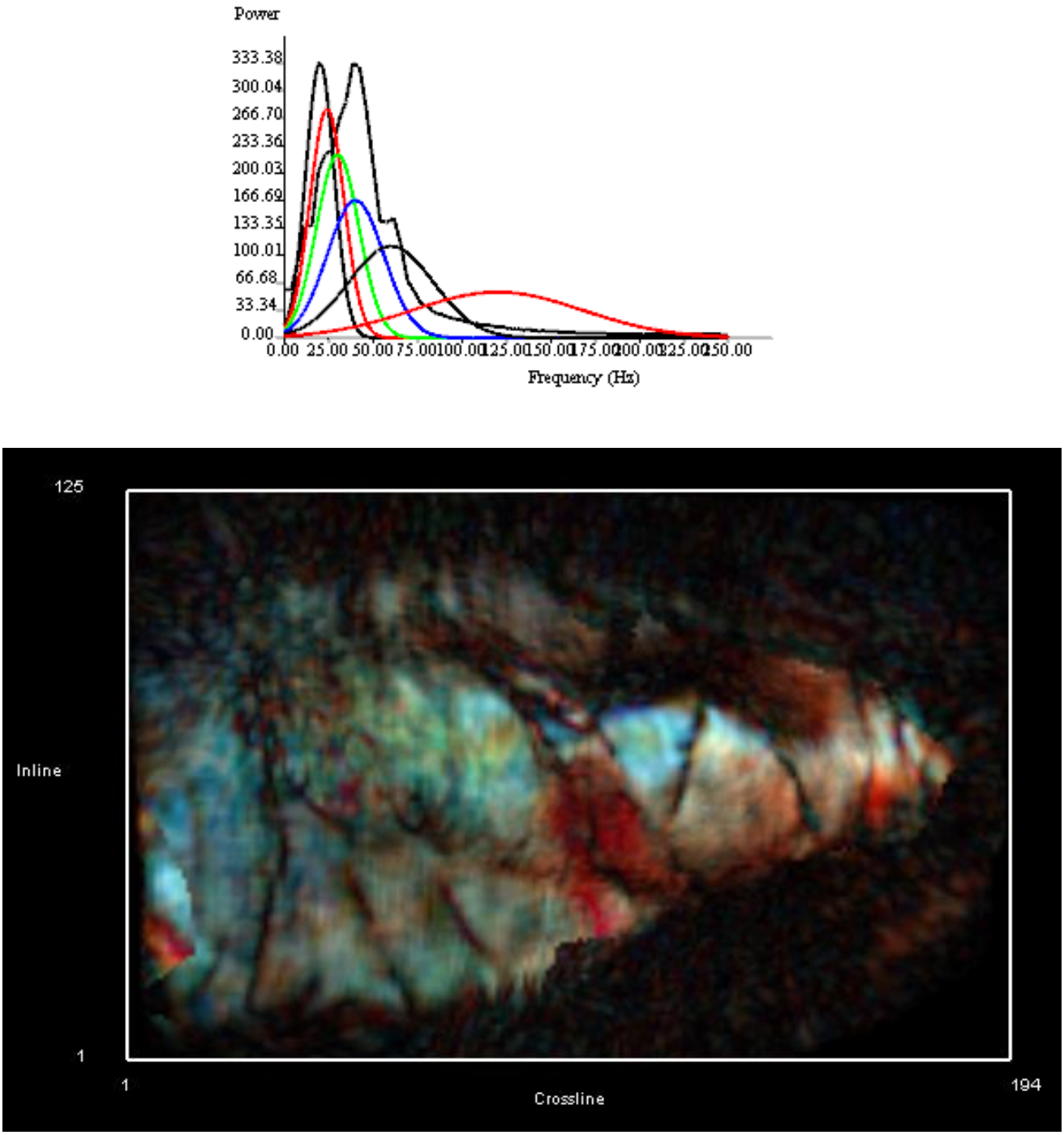

Figure 43 A. Frequency spectrum generated from seismic data.B. Spectral decomposition along Greybull surface, time=590 ms, Red=24Hz, Green=40 Hz, and Blue=60 Hz.

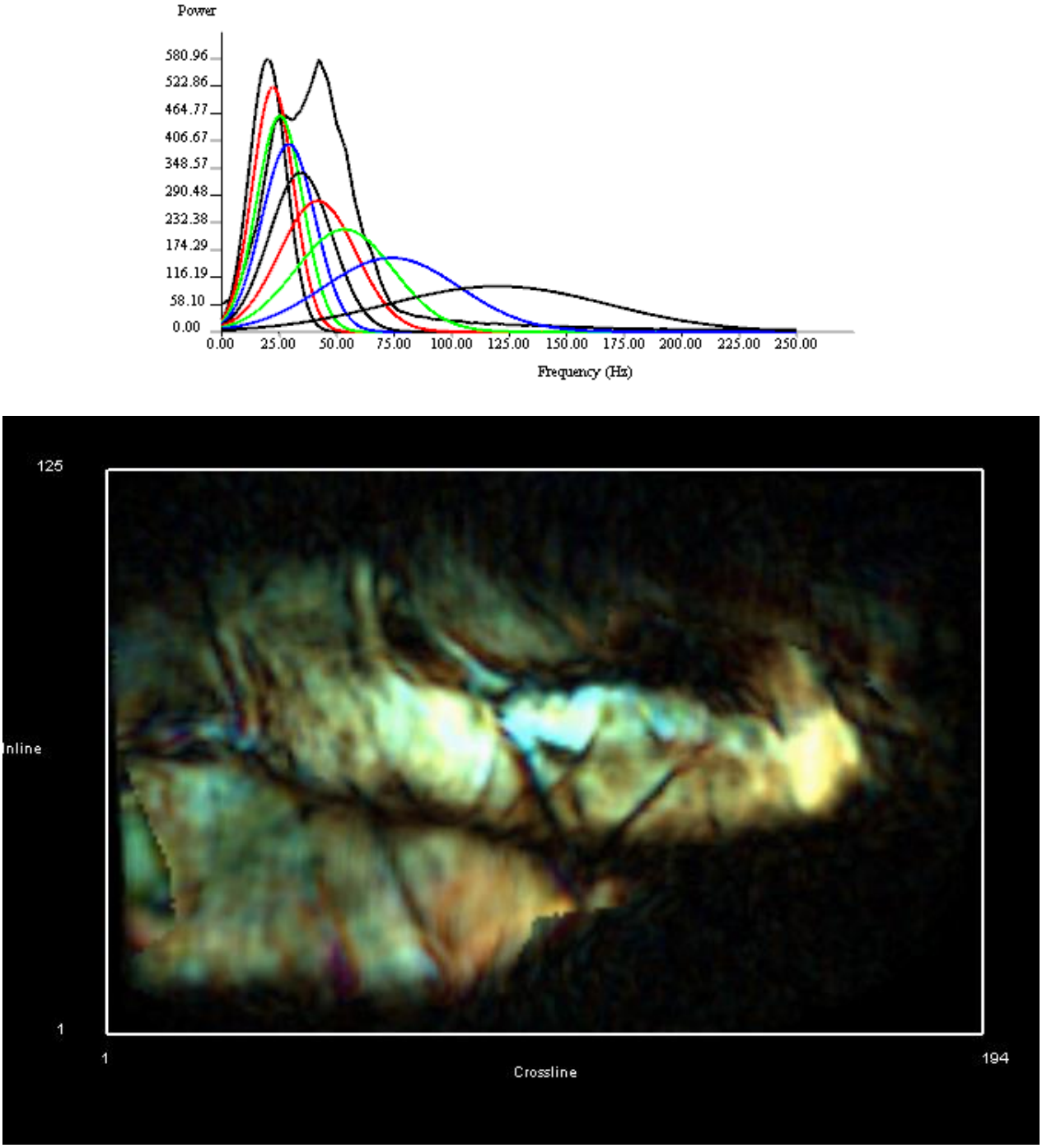

Figure 44. A. Frequency spectrum generated from seismic data. B. Spectral decomposition along Greybull surface, time=710 ms, Red=25 Hz, Green=35 Hz, and Blue=53 Hz.

This figure shows very little input from the 25 Hz component, which would be red, and represent thicker channel sands. There is no clear evidence for channels within this surface either. However, faults are clearly displayed as straight segmenting features.

In order to better observe changes in thickness within the Greybull reservoir, a spectral analysis was used. The ultimate goal of this analysis was to identify possible channel systems in the sandstone which may be cleaner, more porous rock for well targeting. Spectral decomposition was not effective in identifying channel extents within the reservoir as hoped, and this could be due to a number of reasons. The reservoir is very broken up, and it is possible that too much deformation has occurred to accurately restore this surface to a flattened one. Fault blocks may have also been rotated further complicating this restoration.

Although channels were not identified, spectral decomposition did highlight the faults along the flattened volume very clearly. Figure 45 is the spectral decomposition surface taken from Figure 44 with fault angles shown. It shows the northwest-southeast trending bounding faults as well as the segmenting faults. The segmenting faults are about 60° from one another. There is a smaller fault is not seen in the other attribute analyses, parallel to the northeast trending thrust fault that is only in this spectral decomposition attribute. The basin is speckled with Laramide deep basement thrusts, as well as Sevier detachments, that also could have caused local thrusting in the basin, unrelated to the formation of the dome.

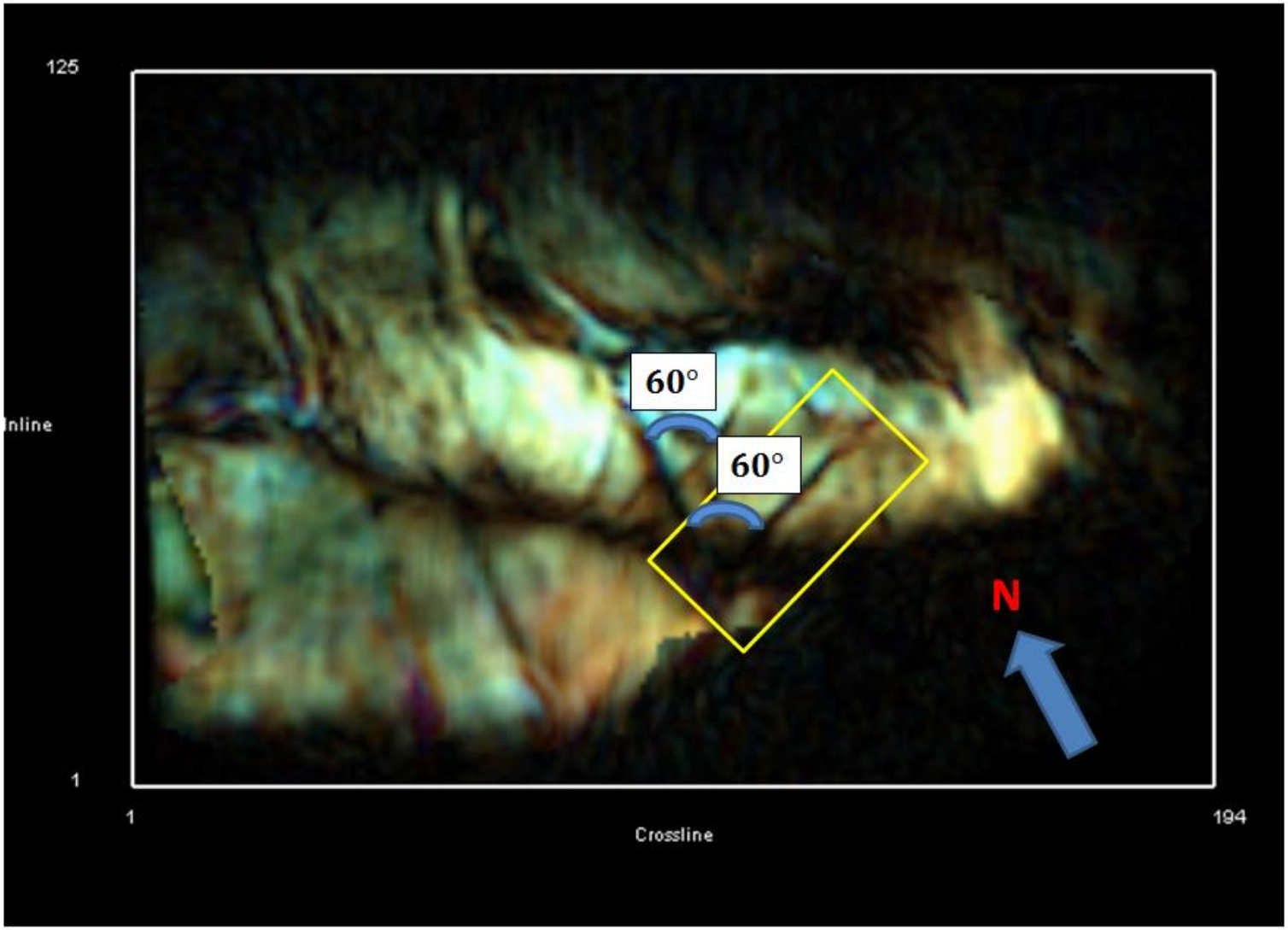

Figure 45. Spectral decomposition surface with segmenting fault highlighted in yellow box. An additional smaller fault is shown that is parallel to the segmenting fault and is also 60° from the nearest North-South trending fault.

d. Log Analysis

vi. Formation Water Resistivity and Salinity

In order to calculate Rw, the SP log for the well Foothills_13_12 was used, which is located on the eastern lobe of the structure. Figure 46 shows a map of the location of the wells mentioned in this study in relation to faults within the reservoir, highlighted by the variance attribute. The geothermal gradient was calculated from a nearby well, W_R_Mackay_#1, using the temperature log. The surface temperature was given as 68 degrees Fahrenheit, and the bottom hole temperature was 131 degrees. Knowing the depth was 5346, the formation temperature was found to be 113 degrees Fahrenheit. The resistivity of mud filtrate (R_{mf}) was given in the log header information for the surface temperature. The SP value was taken from drawing an average line for the Foothills_14_9 well, and found to be -30 mV. Using Petra's Rw from SP calculator tool, the resistivity of the formation water was found to be 4.392 at 113 degrees F (Figure 47). This would make the formation water within the Greybull sandstone a freshwater. The Greybull sandstone is a fluvial rock, and could still preserve its original formation salinity.

vii. Pickett Plots and Hydrocarbon Saturation

Understanding Archie's Equation as well as the Pickett plot can be crucial in determining pay zones and water zones within a reservoir. The Pickett plot is a quick way to display data and make interpretations when computing power is not available. It is a useful method in log interpretation because it does not require the water resistivity and constants that Archie's equation requires in order to derive water saturation within an interval.

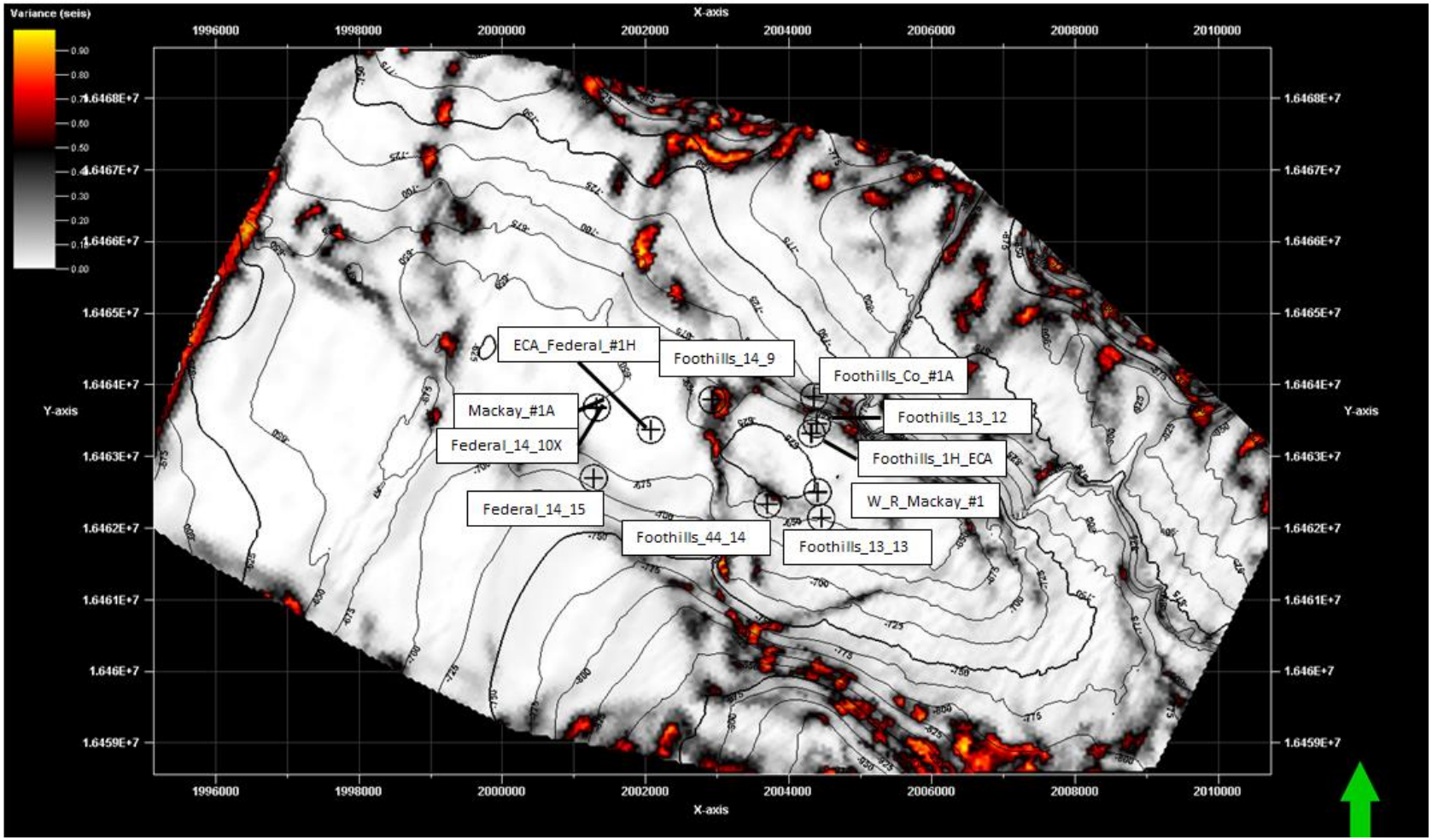

Figure 46. Location of wells in study over the Greybull variance attribute to highlight faults and compartments within the reservoir.

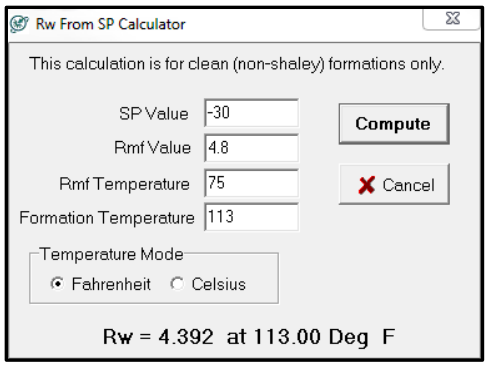

Figure 47. From well Foothills_14_9, Rw determination from SP log in Petra inputs and result.

Archie's Equation is used to determine water saturation from formation resistivity. Archie's Equation is formed from two equations, the first one being the relationship between the ratio of the resistivity of water in a rock to formation resistivity in the rock, to the porosity, as follows:

$$\frac{R_o}{R_w} = \frac{a}{\varphi^m}$$

Where, R_o =resistivity of a water saturated rock
R_w= formation water resistivity
a= constant
φ= fractional porosity
m= cementation factor

The second equation it is derived from consists of the ratio of the observed to expected resistivity, to the fractional water saturation, as follows:

$$\frac{R_t}{R_o} = \frac{1}{S_w^n}$$

Where R_t= expected resistivity
Sw= Water saturation
N= saturation exponent (usually 2)

Combining these two equations yields Archie's Equation, which is:

$$S_w = \left[\frac{a}{\varphi^m} * \frac{R_w}{R_t}\right]^{\frac{1}{n}}$$

The values for a, m, and n are usually unknown and may have to be derived from experience. The cementation factor, m, usually depends on rock texture, and n is usually just assumed to be 2. These values may change if the texture and porosity changes within a reservoir, so it is important to understand reservoir heterogeneity. Also, these equations are to be used in a clean, shale free formation. There are other corrections that can be applied to the Archie's Equation in order to account for shale presence.

The Pickett plot can be derived from the deep induction resistivity curve and porosity. It is based on Archie's equation when water resistivity and Archie's constants are unknown. It is a quick way to graphically display well data, and was developed to be used in the field for quick pattern recognition. The Pickett plot requires plotting porosity vs resistivity on a log-log scale. The 100% water saturation line can be determined by looking at the plot, and seeing where the lowest resistivity values plot. The slope of this line is –m, or the cementation factor which can be used in Archie's equation .

Once the 100% water saturation line is determined, any other water saturation line can be determined by using the equation:

$$I = \frac{1}{S_w^n}$$

For example, to determine the 50% water saturation line:

$$I = \frac{1}{S_w^n} = \frac{1}{.5^2} = 4$$

Because the value of I is 4, the 50% water saturation line will be drawn 4 ohm-m away from the 100% intercept, with the same slope of –m. This method can be repeated to find any water

saturation value. The Pickett plot can also be used to determine possible pay zones. Pay zones will show high resistivity but may differ in porosity.

First, average porosity logs were calculated for each well using the neutron density and density logs. Then the average porosity was crossplotted with deep induction resistivity on a log-log scale. All of the wells were plotted on the same graph in order to determine the 100% water saturation line (Figure 48). From this plot, the pay zone can be clearly seen and is highlighted. It consists of a high resistivity, low density zone. The points are shaded with gamma ray values with lower value sands respresented by warmer colors, and the pay zone consists of the lowest gamma ray values. This means the pay zone is in a very clean sandstone, which is expected. The cementation, saturation, and tortuosity exponents were found to be 2.150, 1.8, and .62, respectively. Water resistivity at formation temperature was found to be 1. Water saturation lines for 50% and 25% were also drawn. Figures 49-52 show all four wells plotted individually for reference. By looking at the Pickett plot for each individual well, clues about the reservoir quality can be unveiled.

Figure 49 shows the Pickett plot for Foothills#1H_ECA. At around the 12% porosity value, the resistivity increases. This indicates that there is an oil water contact in this well. Values plotted near the 100% water line indicate the well produces mostly water, but there are some hydrocarbons present. This well also consists of a shalier sandstone, represented by cooler colored points.

The Foothills 14_9 well is plotted in Figure 50, and shows that as porosity increases, resistivity decreases. This is a clean, well sorted sandstone represented by lower gamma ray values. Because the majority of points plot so close to the 100% Sw line, this well would appear

to produce almost completely water with little oil or gas. This well has successfully produced oil from 1980 through 1990, but has also produced excess amounts of water, which require costly disposal wells to be utilized.

Figure 51 shows the well Federal 14_10X, and may be the best well. Increases in porosity show an increase in resistivity. The points lie within the 100% to 25% Sw lines, which means there is a good amount of hydrocarbons present. The cleanest sand is represented by the warmer yellow colors, and represents the pay zone within this reservoir interval. The cooler colors may be shalier beds within the Greybull sandstone. This has been a productive well, as oil has been produced for a about a decade in the 1980's.

Figure 52 shows the Pickett plot for well 2509521275, ECA Federal #1H. This shows a very good pay zone, with some points containing less than 25% water saturation and low gamma ray values. The porosity in part of this reservoir is well over 50%, however, and this may be the result of a washout. This well has been extended to a horizontal well, which crosses though both the Western and Eastern lobes in order to drain a larger area of reservoir.

Lastly, Figure 53 shows the Pickett plot for well 2500921153, Foothills 13_12. This plot is very similar to the Federal 14_10X plot, which means there is a good amount of hydrocarbons present. The cleanest sand is represented by a yellow color, and there is as low as 20% water saturation. This particular well is very close to the Foothills_#1H_ECA well spatially(Figure 46), but has very different log characteristics. Even though the better Pickett plot (Foothills 13_12) is located structurally below Foothills_#1H_ECA, it shows a better reservoir interval. This may be stratigraphically controlled, as the Foothills_#1H_ECA well has a shalier sandstone interval and therefore has lower reservoir potential.

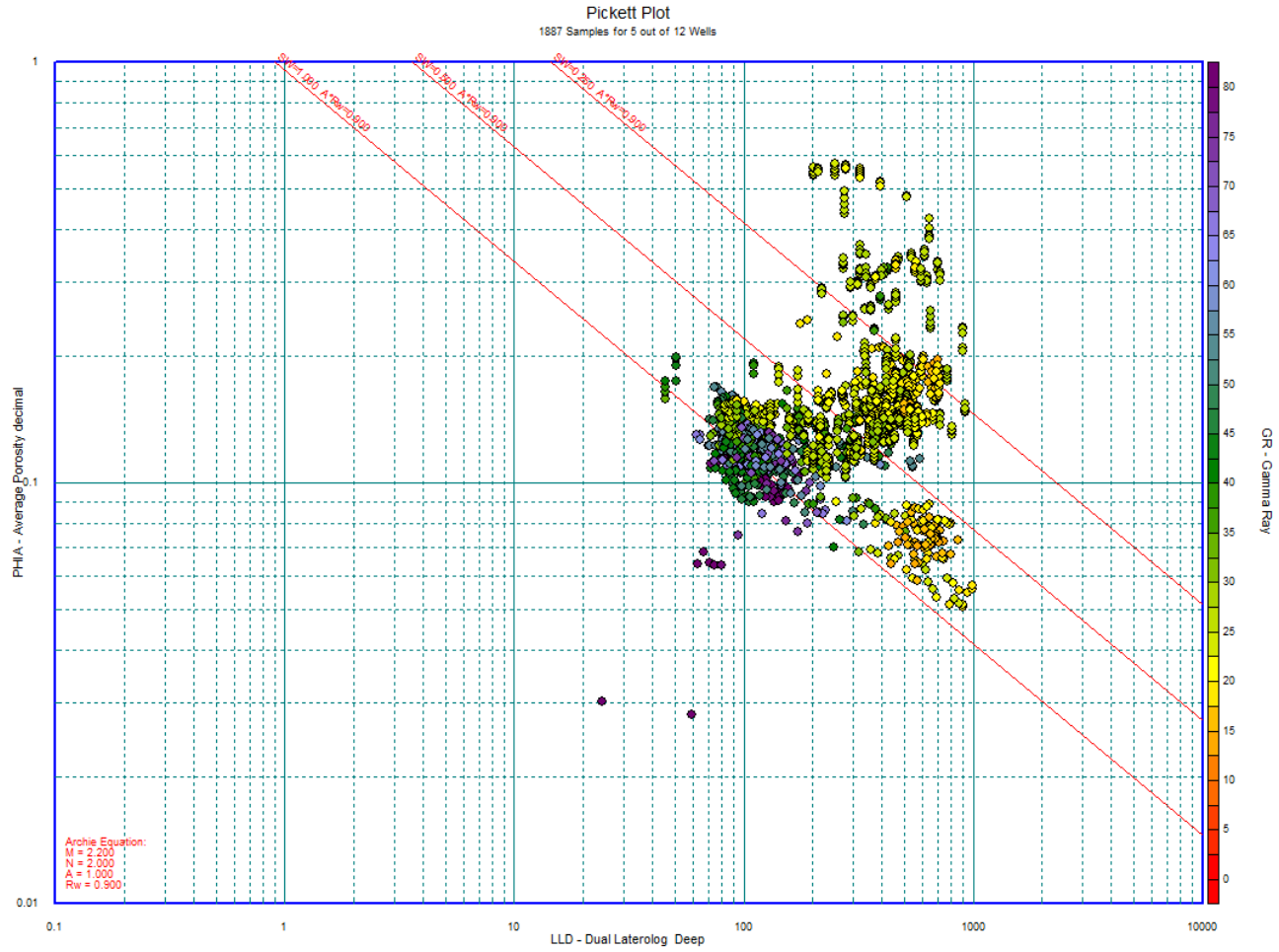

Figure 48. All wells combined for determination of water lines from Pickett plot. Warmer colors represent a lower gamma ray value, indicative of sands.

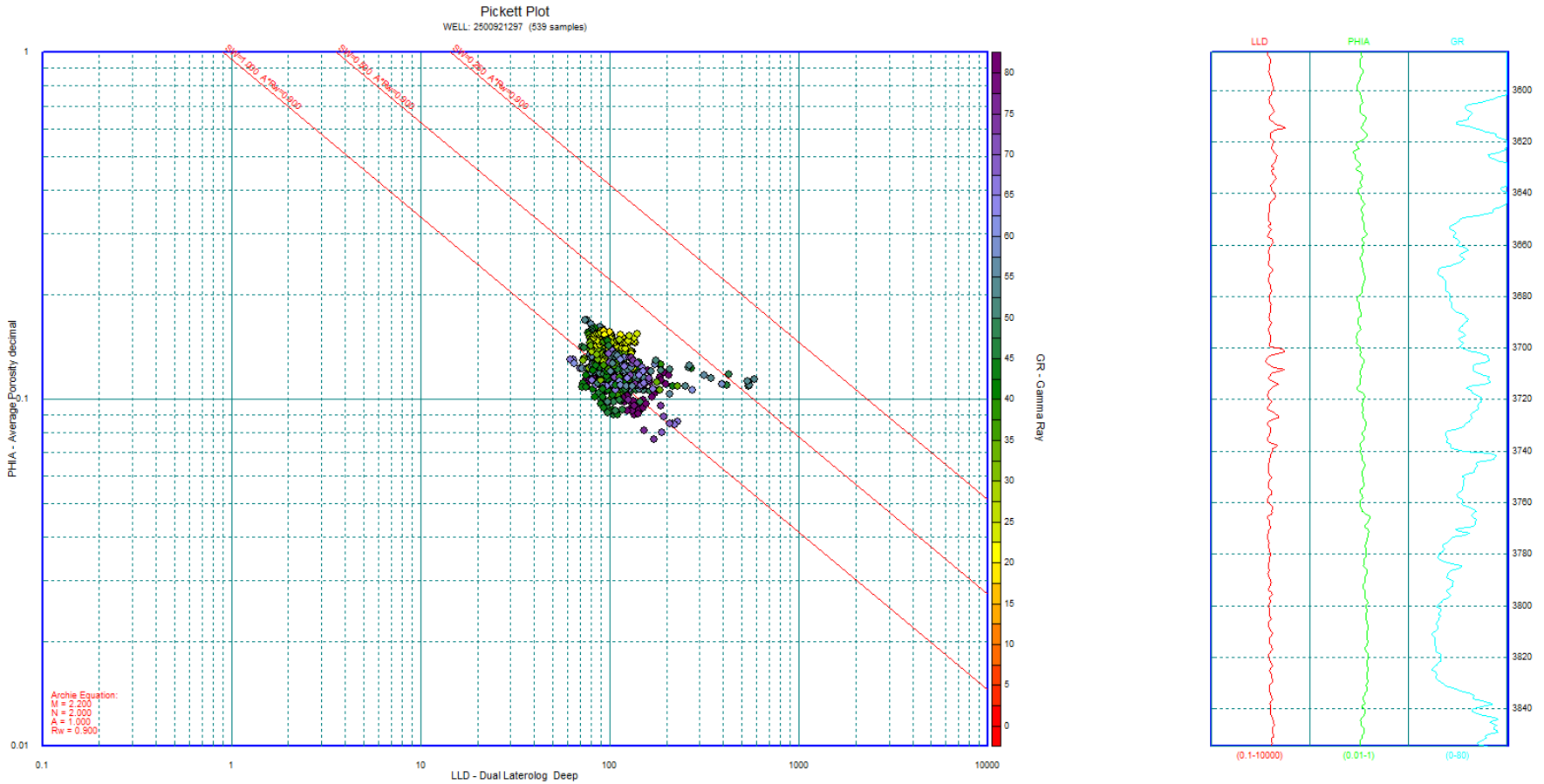

Figure 49. Pickett plot for well Foothills_#1H_ECA.

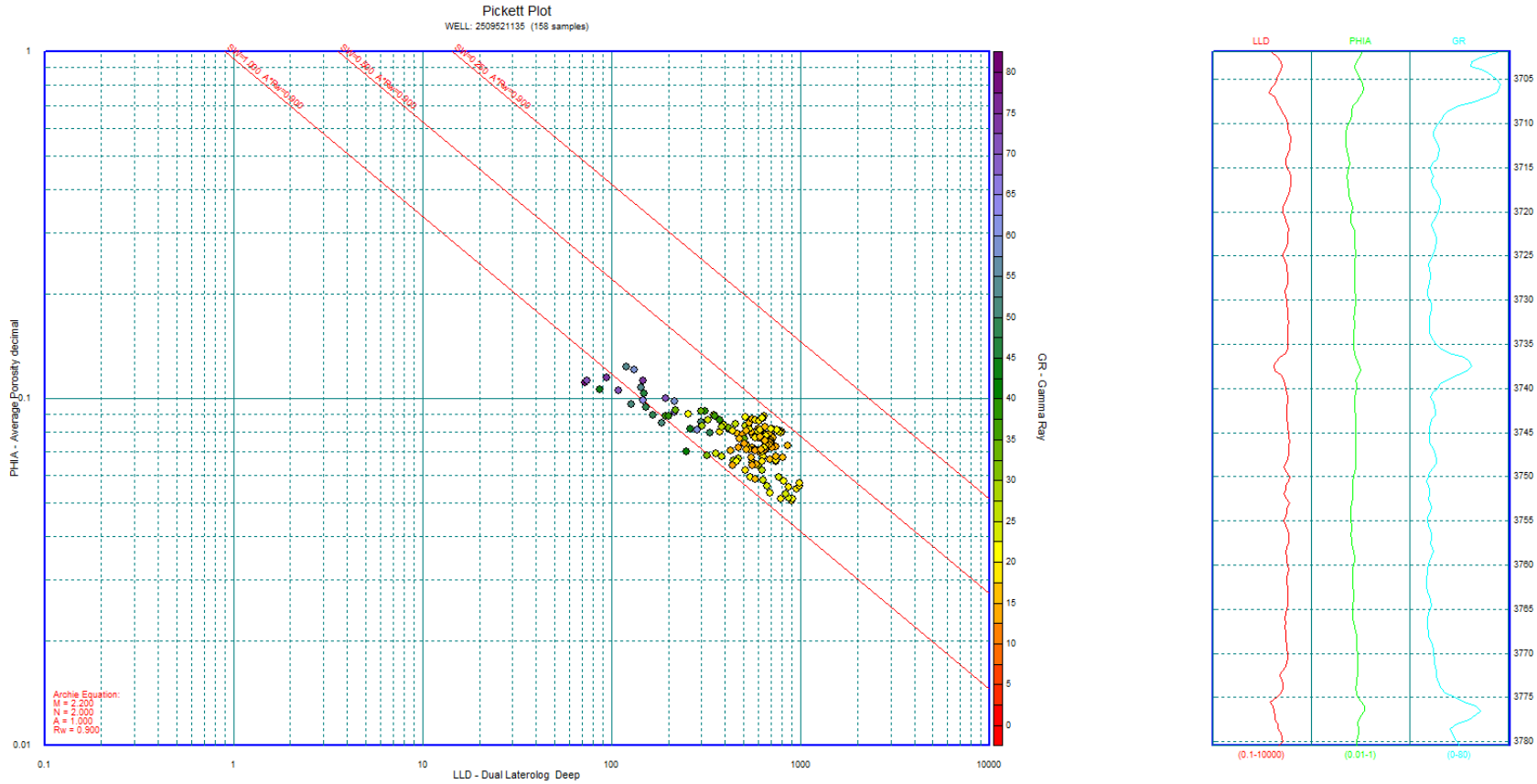

Figure 50. Pickett plot for well Foothills_14_9.

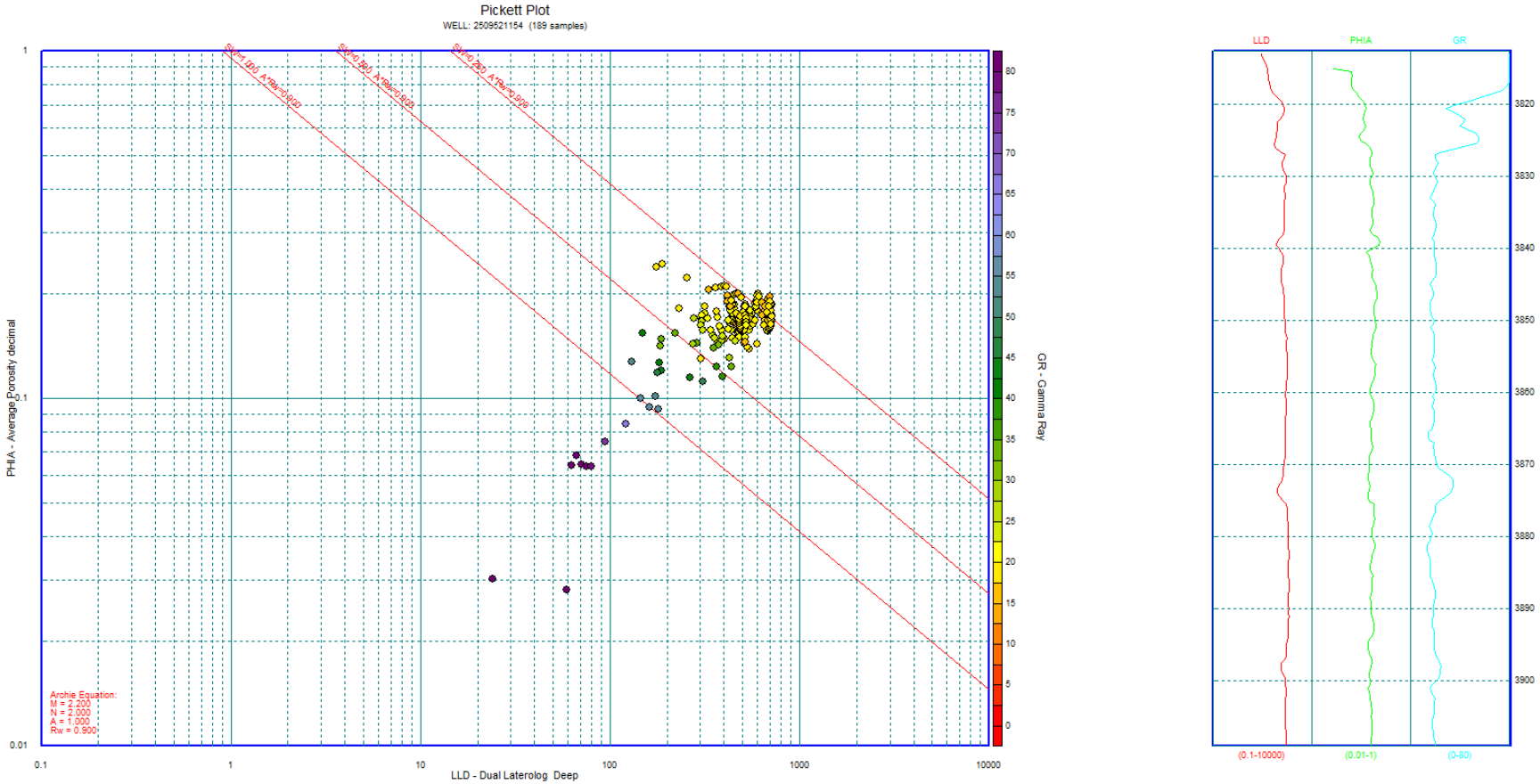

Figure 51. Pickett plot for well Federal 14_10X.

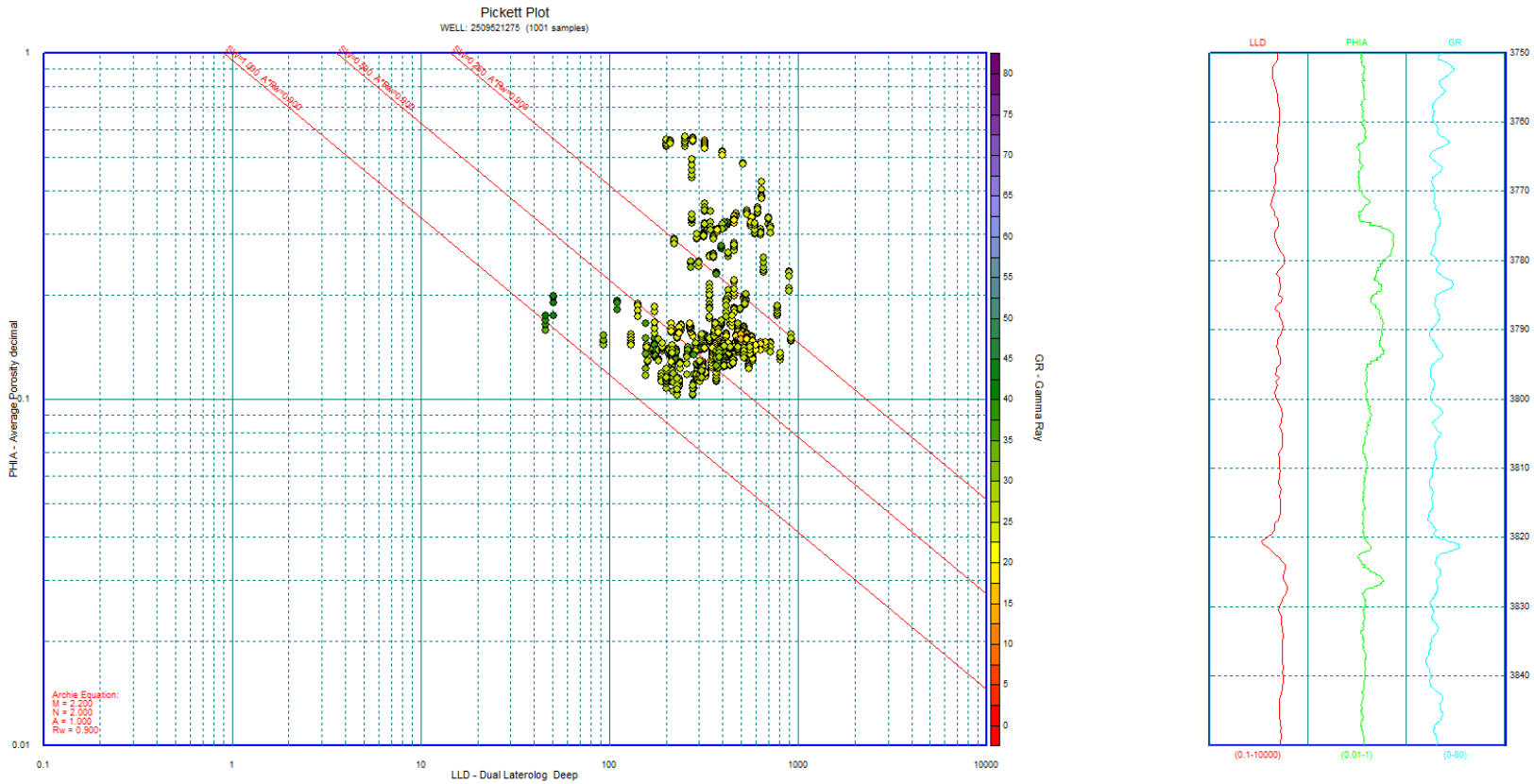

Figure 52. Pickett plot for well ECA_Federal_#1H.

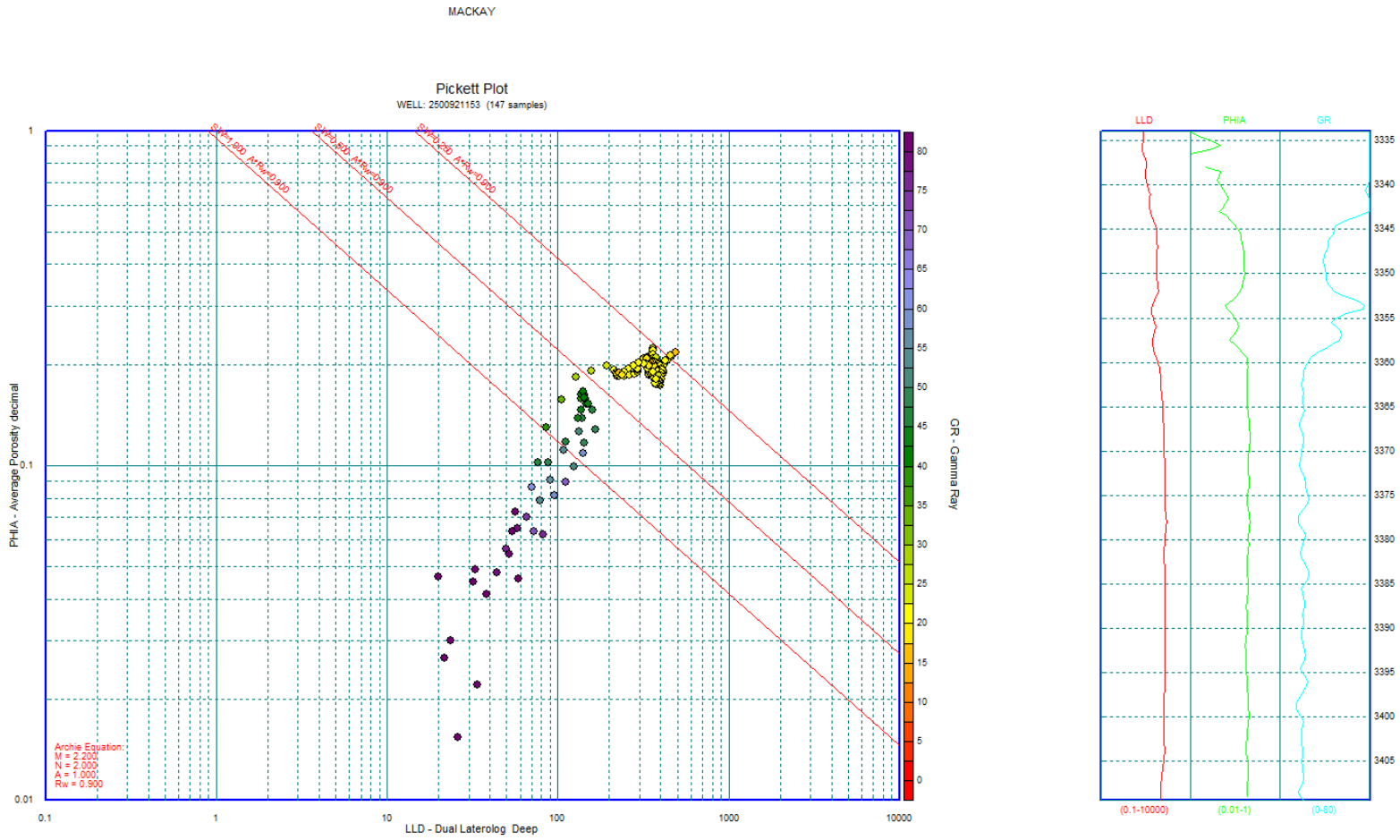

Figure 53. Pickett plot for well Foothills 13_12.

The three wells, 2500921153 (Foothills 13_12), 2500921297 (Foothills_#1H_ECA), and 2509521135 (Foothills 14_9), are plotted in Figure 54 and show the gamma ray in the left track, Sw curve in the middle track and the BVW and average decimal porosity (DPHI) on the right track. When bulk volume water (BVW) is less than porosity, the curve is shaded green. This is a good indication of hydrocarbon presence.

Well Foothills_13_12 is shown on the left in Figure 54, and there is good crossover between the BVW and porosity curves. The area shaded green shows a good hydrocarbon reservoir for the Greybull interval. The Pickett plot for this well (figure 53) suggested a good reservoir, with water saturation as low as 20%. Well Foothills#1H_ECA , is shown as the second log in Figure 54, and shows a lower hydrocarbon saturation. This section of the reservoir has a higher gamma ray response, and is shalier. The bottom of the Greybull interval shows some hydrocarbon saturation, and this is in the lower gamma ray interval. Although it is located adjacent to the Foothills 13_12 well on the eastern lobe and is structurally higher (Figure 46), it does not have good reservoir quality due to the higher shale content in the Greybull sandstone. Lastly, the Foothills 14_9, located on the western lobe, is shown as the last well in Figure 54, and shows an excellent low gamma ray sand with good hydrocarbon saturation. This well's Pickett plot in Figure 50 suggested a high water saturation, greater than 50%, but production data proved it was a good well. This BVW plot shows that the water saturation may be greater than 50%, but the porosity is very high, making it a good potential reservoir.

Federal_14_10X, ECA_Federal_#1H, and Foothills_14_9 are all on the Western lobe of the Mackay dome (Figure 46). They are close to major faults within this reservoir, and not drilled on structural highs. They appear to be within the same fault block of this reservoir, and prove that the Western lobe has good hydrocarbon saturation. The Foothills_14_9 well is drilled very

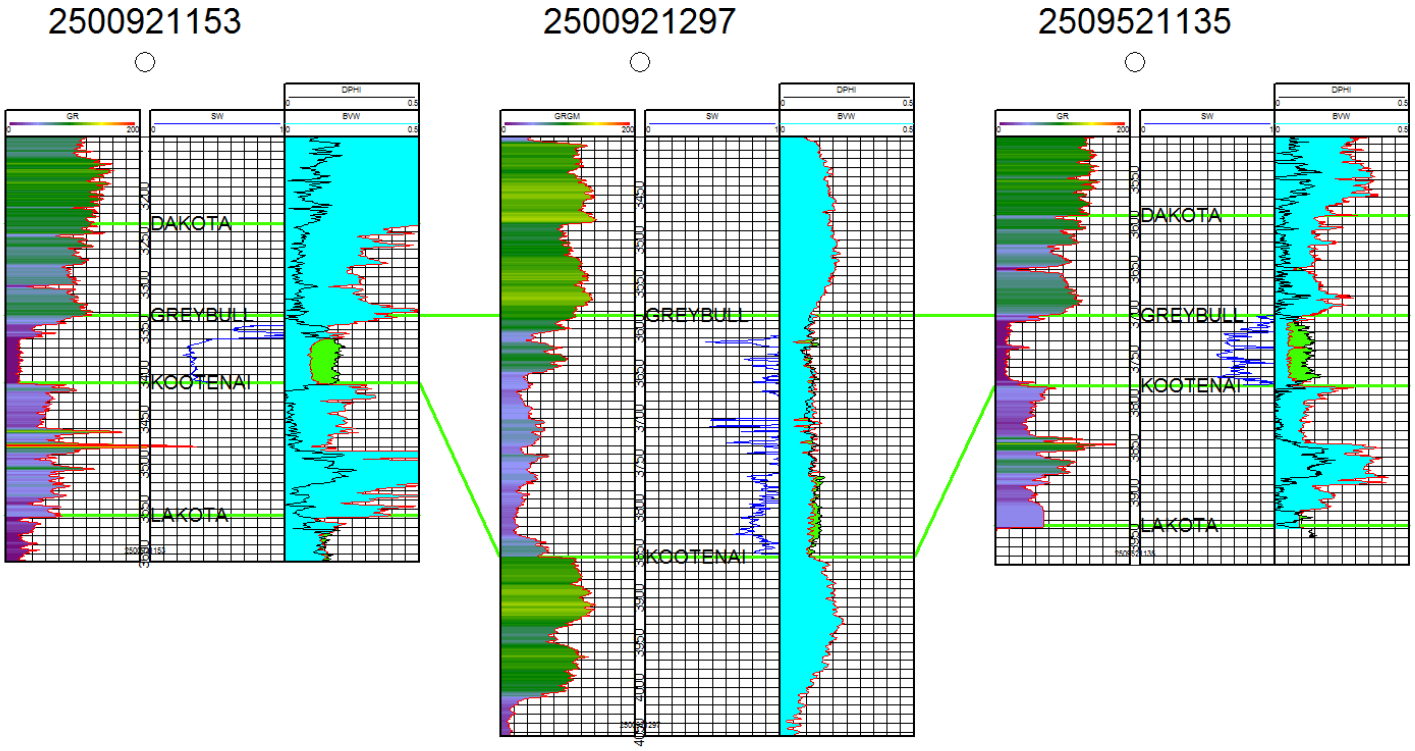

Figure 54. The three wells, Foothills_13_12 (2500921153), Foothills#1H_ECA (2500921297), and Foothills_14_9 (2509521135) are shown from left to right. Gamma ray is in the first track and water saturation for the Greybull reservoir is in the second track. Bulk volume water (BVW) is in the third track with average decimal porosity.

close to the north-south segmenting normal fault, and may be why it has high water saturation. The Federal_14_10X is structurally highest, and furthest to the west, and showed a very good pay zone. The structural high of this block is not drilled, and could be a good potential target in the future, as suggested by this trend. Foothills_13_12 and Foothills#1H_ECA are located on the eastern lobe, and show there are hydrocarbons present there as well. This shalier section is likely related to the deposition of the fluvial reservoir rock. Other wells have been drilled in this same compartment, close to the structural high. The well W_R_Mackay_#1 did produce gas, while the closest well, Foothills_13_13 did not. This makes a gas cap about 30 feet thick. Even though the highest point of the structure is not drilled, it is wise to stay away from the highest 30 feet of this lobe in order to extract heavy oil rather than less valuable natural gas. As oil is produced, the gas cap can expand and gas cap drive can help continue to produce oil.

7. Summary and Conclusions

In order to produce better wells in the Mackay dome oil and gas field, its structural geometry and history need to be better understood. The field consists of a complex transpressional flower structure with both small and large scale folding and faulting. Understanding the reservoir involves understanding both major and minor deformational structures. Large scale faults can be responsible for the overall flower structure, or provide major migration pathways from the source to the reservoir. Smaller scale faults can separate the reservoir into fault block compartments, which are important to recognize for targeting while drilling.

The flower structure consists of northwest-southeast trending transpressional bounding faults. In cross section, these faults are expressed as low amplitude fault zones that show structural changes on either side (Figures 21 and 23). The nose of the flower structure can be expressed as

an anticline that plunges to the southeast. It has good four way closure, as the structure is highest towards the center (Figure 17). The structure increases in deformation in the shallower region, where the transpressional faults within the flowers splay outward and decrease in dip. The beds on the top of the flower are steeper than in the deeper section, suggesting a detachment surface below the flower.

Mapping major cross structure faults and identifying orientation trends can help predict the style of subseismic fractures and faults that can be encountered while drilling. Figure 18 shows a generalized map of the three major fault sets found in this structure. Although the major faults found in this structure are compressional, strike-slip, or a transpressional hybrid, smaller extensional faults within small intervals may still be present. These extensional faults do not agree with the orientation of the left lateral major faults, and may be more localized fracture events. Because of the extreme deformation within this structure, fault block rotation may also have taken place.

Structural seismic attributes, including most extreme curvature, variance, and ant tracking, can assist in the detection of major and minor faults, both reservoir and cross structure scale. These attributes can be used as time slices for identifying major faults where amplitude pattern may not be clear, or extracted along surfaces to see how the surface expression relates to faulting. Attribute assisted fault detection can improve confidence for faults picked with just amplitude pattern, and aid in the detection of more small scale fractures. It is important when mapping faults to use all methods possible, including manual fault mapping and attribute assisted mapping to assure the most detailed story of structural deformation.

Two major compartments, the western and eastern lobes, have been identified previously by ECA. They are separated by a north-south trending normal fault that places the eastern block higher than the western side. This may be why the eastern side has a gas cap present. Because the fault that separates the two main lobes is normal, there may be potential for migration from the western lobe in to the eastern one. Figure 55 shows a crossline with the western and eastern lobes identified, separated by the large normal fault shown in yellow. The western lobe shows two possible smaller compartments. Block 1 is characterized by two bounding thrust faults. Although this block is on the down thrust side, it shows a higher amplitude expression than the strata to the northwest. The westernmost thrust fault must be a sealing fault that prevents the higher amplitude hydrocarbons from migrating northwestward out of the dome. Block two is bound by a thrust fault to the northwest and normal fault to the southeast. This block has been rotated vertically so that the northwest side is slightly higher. However, the boundary with the normal fault shows that some drag has occurred along the fault from friction, which may indicate a tight normal fault.

The eastern lobe can be broken into an additional three compartments. Block 3 is a fault block bound to the northwest by a normal fault and to the southeast by a thrust fault. This block has also rotated vertically so that the northwest side is slightly higher. There is evidence for smaller thrust faults within this block, but because there is little change in amplitude expression along these faults, the smaller blocks have been categorized into one larger. The amplitude pattern is very high in this block, which may be due to the presence of the gas cap previously discovered. Fault block 4 is bound on both sides by thrust faults. There is a large major fault that cuts across this block, represented by the dashed line. This fault aligns with the fault set 1 thrusts, and marks the boundary in the block 4 between higher amplitude to the northwest and

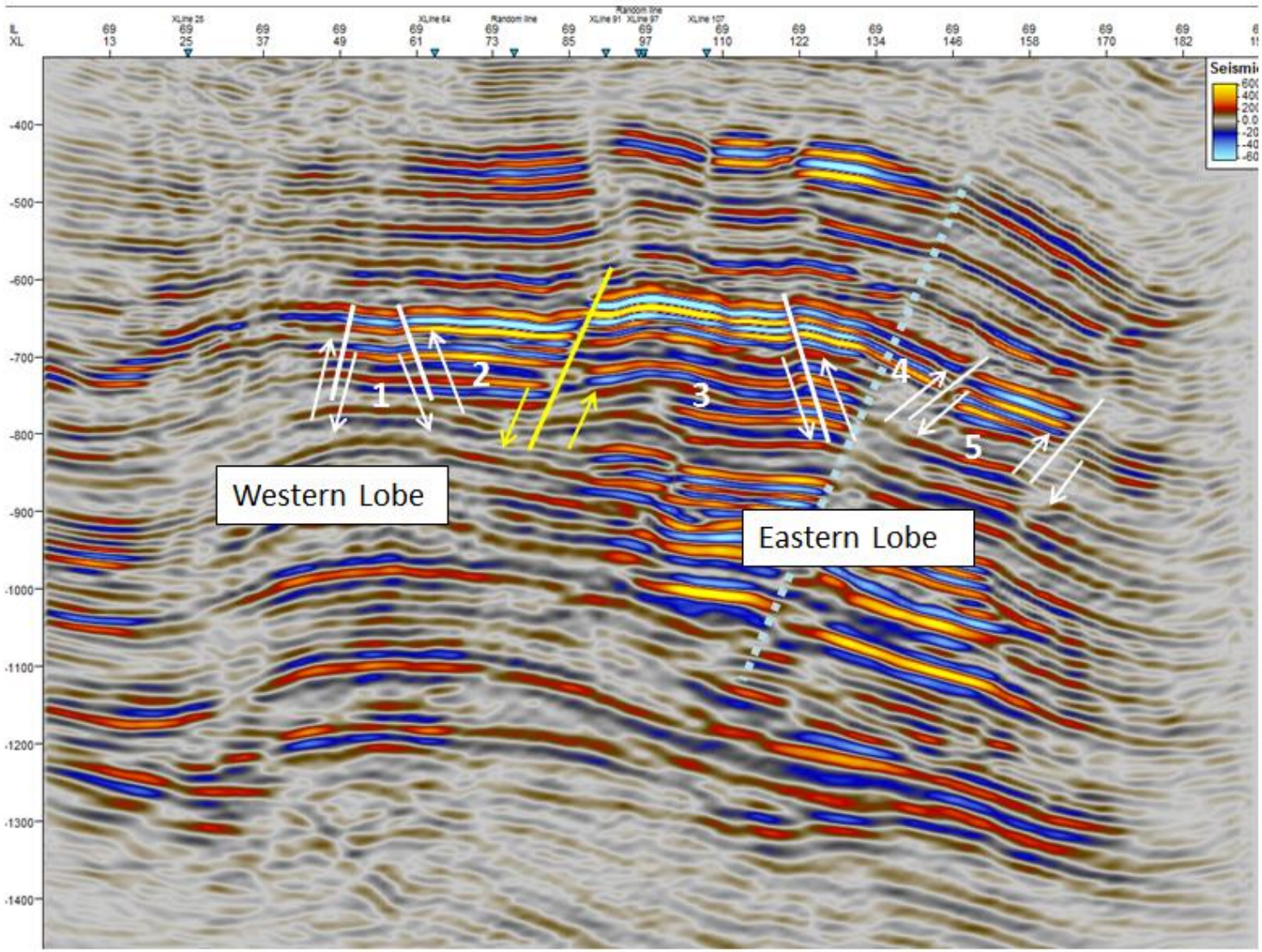

Figure 55. Inline 69 showing fault block orientations for reservoir compartmentalization. Left is northwest, right is southeast.

lower amplitude to the southeast. This fault may serve as a migration pathway that charges the upper Frontier sands, which are shown at the top of the seismic data as high amplitude anomalies. Fault block 5 is bound on both sides by thrust faults and shows a higher amplitude pattern than the strata immediately to the northwest of the thrust fault. Although this block is lower than block 4, it has a high amplitude pattern, which suggests that the thrust fault to its northwest is a sealing fault, preventing hydrocarbons from leaking up the major thrust fault.

Isopach maps of the reservoir suggest a continuous thickness across the reservoir. In order to better investigate small changes in wiggle trace frequency, a spectral decomposition analysis was used. The results show a relatively homogenous reservoir, that does not have original stratigraphic features such as channel deposits. However, Figure 45 shows an image that suggests thickening has occurred in the southeastern side of the reservoir. These thickness changes are bound by faults shown in the spectral decomposition frequency image, meaning thickness changes are a reflection of structural deformation rather than depositional artifacts. The increase in thickness to the southeast may be related to an increase in strain towards the nose of the anticline, where folds are most intense. Although reservoir rock may be thicker towards the southeast, the reservoir is structurally lowest, and may not have good hydrocarbon charge. Amplitude pattern shows bright spots in fault block 5, but due to the depth this target may be risky.

Using the log data, the reservoir formation water was determined to be a freshwater. This water may be the original formation water from the fluvial, terrestrial system. If it is original formation water, the Greybull sandstone is an excellent reservoir, because it has not been contaminated by saltwater from nearby marine rocks. Log data also provided a good way of identifying water and pay zones within the reservoir. Water zones lie along the 100% water line

determined from the Pickett plot. Pay zones occurred as high resistivity samples which varied in density porosity. Identifying the pay zone in logs can help to determine the amount of hydrocarbon in place, and where the oil water contact lies in the log.

Integrating the log data with seismic data is crucial in understanding reservoir behavior. Seismic data provides structural constraints for the reservoir, while log analysis can give more detailed stratigraphic variations. This study focused on seismic analysis, because of the high resolution data provided. Hand mapping surfaces and faults can give a good structural framework which can be strengthened by the addition of attribute analysis. Although the vertical resolution of the data is only 81.25 feet, often large scale structures reflect smaller scale, subseismic structures. By analyzing the seismic data in detail, a better understanding of large scale structural history and small scale reservoir compartmentalization can be obtained.

REFERENCES

Blakey, Ron., "Paleogeography and Geologic Evolution of North America", Paleogeography, March 2011. Web. 03 Dec 2013.

Brown, A.R., 1996, Seismic attributes and their classification: The Leading Edge, Society of Exploration Geophysicists, October, p. 1090.

Chopra S. and Marfurt K. J., 2007, Seismic Attributes for Prospect ID and Reservoir Characterization. Society of Exploration Geophysicists, ISBN 1-56080-141-7.

Chopra, S. and Marfurt, K. J., 2010,. Integration of coherence and volumetric curvature images. The Leading Edge, 29, 9, p. 1092-1107.

Cox, T., and Seitz, K., 2007, Ant tracking seismic volumes for automated fault interpretation. 2007 CSPG CSEG Convention, Let it Flow, p. 670-671.

Dickinson, W. R., and Snyder, W. S., 1978, Plate tectonics of the Laramide orogeny. Geological Society of America Memoir 151, ISBN 0-8137-1151-7, p. 355-366.

Donahoe, T., 2011, 3D seismic attribute-assisted subsurface interpretation in central Appalachian Basin: Master's Thesis, Morgantown, West Virginia University.

Finn, T.M., and Pawlewicz, M.J., 2007, New Vitrinite Reflectance Data for the Bighorn Basin, North-Central Wyoming and South-Central Montana: U.S. Geological Survey Open-File Report 2007-1246, 10 p.

Finn, T., Kirschbaum, M., Condon, S., Roberts, L., and Johnson, R., 2010, Cretaceous-Tertiary composite total petroleum system (501402), Bighorn Basin, Wyoming and Montana: U.S. Geological Survey Open-File Report.

Fox, J.E. & Dolton, G.L., 1995, Bighorn Basin Province (034). In: National Assessment of United States Oil and Gas Resources – Results, Methodology, and Supporting Data. (Ed. by D.L. Gauther, G.L. Dolton, K.I. Takahashi & K.L. Varnes) U.S. Geol. Surv. Digital Data Ser., 30, 1–22.

Gao, Dengliang, 2013, Integrating 3D seismic curvature and curvature gradient attributes for fracture characterization: Methodologies and interpretational implications, Geophjysics, 78, 2, p. 21-30.

Jolley, S., Fisher, Q., and Ainsworth, R., 2010, Reservoir compartmentalization: an introduction, Geological Society, London, Special Publications,347, p. 1-8.

Kauffman, E.G., 1977, Geological and biological overview—Western Interior Cretaceous Basin, in Kauffman, E.G., ed., Cretaceous facies, faunas, and paleoenvironments across the Western Interior Basin: The Mountain Geologist, 14, 3 and 4, p. 75–99.

Kirschbaum, M., and Roberts, Laura, N., 2005, Stratigraphic framework of the Cretaceous Mowry shale, Frontier formation and adjacent units, Southwestern Wyoming province, Wyoming, Colorado, and Utah: United States Geologic Survey Digital Data Series DDS-69-D, Ch. 15.

Lopez, D., 2000, Petroleum Potential of the Greybull Sandstone on the Northern Cheyenne Reservation, South-Central Montana: Montana Bureau of Mines and Geology Open File Report.

Maughan, E. K., 1975, Organic carbon in shale beds of the Permian Phosphoria Formation of Eastern Idaho and adjacent states: A summary report, Wyoming Geological Association, 27th Annual Field Conference Guidebook, p. 107-115.

Partyka, G. A., Gridley, J. M., and Lopez, J., 1999, Interpretational Applications of Spectral Decomposition in Reservoir Characterization, The Leading Edge, Society of Exploration Geophysicists, v. 18, No. 3, p. 353-360.

Roberts, Emily, 2013, Structure segmentation and transfer faults in the Marcellus shale, Clearfield county, Pennsylvania: Implications for gas recovery efficiency and risk assessment using 3D seismic attribute analysis: Master's Thesis, Morgantown, West Virginia University.

Taner, MT., 2001, Seismic attributes: Canadian Society of Exploration Geophysicists Recorder, September, p. 48-56.

Wilcox, R.E., Harding, T.P., and Steely, D.R., 1973, Basic wrench tectonics, American Association of Petroleum Geologists Bulletin, 57, p. 74-96.